CHARACTERIZING SOURCES AND DYNAMICS OF METALS AND METALLOIDS IN URBAN SOILS

by

Robert James Rossi

B.S. Pennsylvania State University, 2009

Submitted to the Graduate Faculty of the

Kenneth P. Dietrich School of Arts and Sciences in partial fulfillment

of the requirements for the degree of

Doctor of Philosophy

University of Pittsburgh

2016

UNIVERSITY OF PITTSBURGH

KENNETH P. DIETRICH SCHOOL OF ARTS AND SCIENCES

This dissertation was presented

by

Robert James Rossi

It was defended on

September 30, 2016

and approved by

Emily Elliott, Associate Professor, Geology and Environmental Science

William Harbert, Professor, Geology and Environmental Science

Darrel Jenerette, Associate Professor, Botany and Plant Sciences, University of California, Riverside

Josef Werne, Associate Professor, Geology and Environmental Science

Dissertation Advisor: Daniel Bain, Assistant Professor, Geology and Environmental Science

CHARACTERIZING SOURCES AND DYNAMICS OF METALS AND METALLOIDS IN URBAN SOILS

Robert J. Rossi, Ph.D.

University of Pittsburgh, 2016

During the latter 20th century, global urban areas, and by extension, road networks have rapidly expanded. Urban soils are often contaminated with potentially toxic trace metals due to multiple human activities, and the relatively high loadings of trace metals to urban ecosystems pose a significant risk to public and ecosystem health. However, metal dynamics in near-road areas are driven by the interactions of many processes, and consequently, few studies have comprehensively examined urban soil metal dynamics.

Examination of both anthropogenic and natural loadings of metals to urban areas and the interactions among processes (e.g., soil acidification, exchange reactions) reveal urban soil chemical dynamics. This dissertation documents findings resulting from a variety of approaches to clarify near-road and urban soil metal dynamics: 1) Soil acidification across regional gradients of road network density, climate, and geology in Southern California results in road construction material weathering (i.e., concrete) and significantly influences near-road soil metal dynamics. 2) Inputs of road material weathering offset calcium losses due to the flushing of soil exchange sites during road deicer pulses in Pittsburgh, Pennsylvania. Moreover, complicated soil water flowpaths documented in this transect create discontinuous and delayed down slope transport of sodium. 3) Two centuries of metal inputs to a Southwestern Pennsylvanian lake revealed an unexpectedly long period and complicated mix of trace metal

contamination, accumulated from a historical sequence of industrial transitions. 4) Synthesis of roadside soil phosphorus concentration data from both the Southern California dataset and the Pittsburgh transect indicate near-road soil phosphorus accumulation at magnitudes near estimated phosphorus accumulations in global agricultural soils, suggesting that vehicular emissions are a significant, yet under characterized component of the global phosphorus cycle.

This research documents roadside soil metal dynamics and the role of historical metal inputs and ultimately will contribute to more effective management of road networks and urbanization.

TABLE OF CONTENTS

LIST OF TABLES

LIST OF FIGURES

PREFACE

Funding for this research was provided by the University of Pittsburgh Dietrich School of Arts and Sciences, the University of Pittsburgh Office of Experimental Learning, the University of Pittsburgh Department of Geology and Environmental Science Henry Leighton Memorial Fellowship, the University of Pittsburgh Andrew Mellon Predoctoral Fellowship, the Heinz Foundations, University of California - Riverside, and the National Science Foundation (NSF# 0919006).

This work would not have been possible without the help from collaborators including, Mark Abbott (UPitt), Marion Divers (UPitt), Matthew Finkenbinder (WilkesU), Aubrey Hillman (UL Lafayette), Bridget O'Neill (UPitt), David Pompeani (UPitt), Lorraine Weller Clarke (UDC), and Kat Wilson (USGS).

I would like to thank all those at the University of Pittsburgh who helped with sample collection and analysis. This includes Alex Beatty, Bruk Berhanu, Katherine Colwell, Adam Olsen, Troy Ferland, and Dervla Kumar. Furthermore, I appreciate the support given to me by the members and alums of the Bain and Elliott lab groups who have assisted in field and laboratory work, provided feedback on manuscript drafts, presentations, fellowship applications, and more importantly, graciously dealt with my inane ramblings for the past five years. These members include Justin Coughlin, Marion Divers, Dave Felix, Kassia Groszewski, Kristina

Hopkins, Sarah Lavin, Erin Pfeil-McCullough, Katherine Redling, Lucy Rose, Melissa Sullivan, and Zhongjie Yu. Heartfelt thanks also goes to James Gardiner, Dominic Petrazio, and Kevin Reath, who in addition with helping with sample collection, generally kept me as close to sane over the past years as is possible.

I would also like to thank my committee members for their guidance and impressive expertise.

Thank you to my family, in particular my parents, who have supported me from the beginning. To my father, and the many hours you worked to make my undergraduate, and by extension, graduate education possible. To my mother, for encouraging my curiosity from an early age. To both, I am eternally grateful.

Lastly, and by no means least, immeasurable thanks to my advisor Daniel Bain. Over the past years you have provided me with an immeasurable amount of knowledge, guidance, and support. Without your astute, albeit often cryptic, feedback my success would not be possible. More importantly, your patience and flexibility provided me with the room to grow and broaden my skill set.

1.0 INTRODUCTION

Between 1970 and 2000, global urban land area has increased by over 50,000 km^2 (Seto *et al.*, 2011), and by 2050 the United Nations predicts that sixty-six percent of the Earth's population will reside in urban areas (United Nations, 2014). As a result, road networks, which are a defining characteristic of urban areas, are spatially extensive and thus impact large numbers of ecosystems (Forman and Alexander, 1998). Soils in urban areas often contain elevated concentrations of trace metals due to human activities, such as smelting and refining metals and ores (Nriagu and Pacyna, 1988; Nriagu *et al.*, 1996; Rabinowitz, 2005), waste incineration (Nriagu and Pacyna, 1988; Chillrud *et al.*, 1999), and vehicular emissions (Nriagu and Pacyna, 1988; Nriagu *et al.*, 1996; Mielke *et al.*, 1999; Fakayode and Olu-Owolabi, 2003; Nabulo *et al.*, 2006). Trace metals are toxic to a wide variety of biota including humans (Alexander and Delves, 1981; Mielke *et al.*, 1999), vegetation (Foy *et al.*, 1978), animals (Hammond and Aronson, 1964), and aquatic biota (Mance, 1987), thus the relatively high loadings of trace metals to urban ecosystems pose a significant risk to public and ecosystem health.

Challenges to urban management created by the expansion of urban areas, and by extension road networks, creates a critical need for the characterization of soil metal dynamics in road side soils. However, metal dynamics in near-road areas are complex and involve the

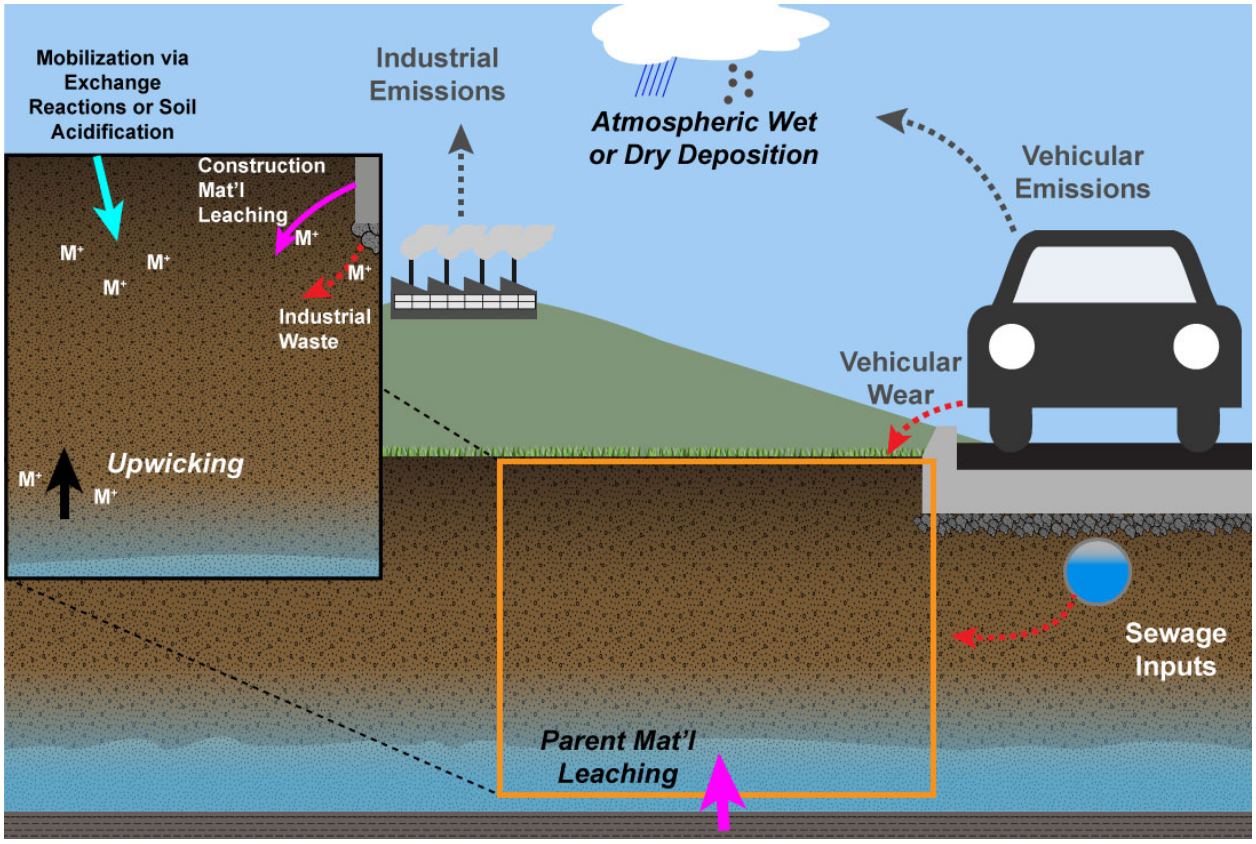

Figure 1-1. Conceptual model of fluxes of metals to urban soils, and processes that affect soil metal concentrations. Processes that potentially deplete soil cation pools are indicated by *turquoise arrows*. *Italicized titles* represent natural sources of metals. *Dashed dark grey arrows* signify metal-rich emissions. *Dashed red arrows* show direct anthropogenic inputs. *Solid black arrows* indicate inputs of metals that are driven by soil moisture status.

interactions of many processes (Figure 1-1). For example, roadside soils receive increased trace metal (Fakayode and Olu-Owolabi, 2003) and reactive nitrogen (N_r) loadings (Redling *et al.*, 2013). Interactions of deposited N_r with soil water can acidify roadside soils (Fenn *et al.*, 1996), subsequently mobilize trace metals (Kumpiene, 2010), and promote the leaching of major cations (e.g., Ca, Mg, K) which play a vital role in soil health (Fernandez *et al.*, 2003). Additionally, the flushing of soil exchange surfaces via road deicer pulses can also stimulate the mobilization of soil metals (Shanley, 1994; Granato *et al.*, 1995). While the effects of isolated

processes (i.e., considering only the impacts of soil acidification) have been explored, few studies have examined the metal dynamics in urban soils that result from the interaction of these different processes. This research examines anthropogenic loadings of metals to urban areas, and the dynamic interactions among processes (e.g., soil acidification, exchange reactions) that influence urban soil metal chemistry.

1.1 OBJECTIVE

The main objective of my dissertation is to characterize metal and metalloid dynamics in urban soils, specifically roadside soils, by examining patterns in soil and soil water metal chemistry. Specifically, this research addresses 1) the effects of soil acidification processes on roadside soil cation pools, 2) the flushing of roadside soil exchange surfaces by road deicer pulses, 3) trace metal loadings from changes in land use and industry in the 19th and 20th centuries, and 4) phosphorus loadings to roadside areas from exhaust deposition. The remainder of this chapter is organized around the four research topics, with an overview of the background of each topic and a brief literature review demonstrating key knowledge gaps.

1.2 ROADSIDE SOIL ACIDIFICATION IN THE LOS ANGELES, CA METROPOLITAN AREA

The Los Angeles (LA) Metropolitan Area is densely covered by roadways with high traffic volumes. This traffic creates significant amounts of atmospheric pollutants, including trace

metal-rich particulates (Singh *et al.*, 2002) and oxidized forms of nitrogen (Fenn *et al.*, 2000) that are deposited within the LA air basin. In particular, LA urban soils receive nitrogen loadings of up to 50 kg ha^{-1} yr^{-1} (Fenn and Bytnerowicz, 1997), which can occur through both dry and wet pathways; however dry deposition is likely the major source of N deposition in arid regions such as LA (Fenn *et al.*, 1996, 2000; Fenn and Bytnerowicz, 1997). Nitrogen compounds (e.g., NO_x) can react with soil or meteoric water, subsequently transforming into nitric acid (Reuss, 1977), potentially acidifying nearby soils or waters (Fenn *et al.*, 1996).

Impacts of soil acidification in forested and natural systems are extensively documented (Federer and Hornbeck, 1989; Huntington and Hooper, 2000; Fernandez *et al.*, 2003; Juice *et al.*, 2006). In particular, acidified soils retain fewer base cations during exchange reactions, which depletes base cation pools (Federer and Hornbeck, 1989; Huntington and Hooper, 2000; Fernandez *et al.*, 2003; Juice *et al.*, 2006; Green *et al.*, 2013). Exchange reactions resulting from soil acidification have caused notable base cation depletion, particularly Ca, in soils in the Northeastern United States (Likens *et al.*, 1996; Driscoll *et al.*, 2003; Fernandez *et al.*, 2003; Juice *et al.*, 2006), Europe (Veselý *et al.*, 1989; Katzensteiner and Glatzel, 1992; Jagoe *et al.*, 1993; Kirchner and Lydersen, 1995; Krám *et al.*, 1997; Navrátil, 2000), Asia (Larssen and Carmichael, 2000), and other regions of the United States (Ulrich *et al.*, 1980; Huntington and Hooper, 2000; Edwards *et al.*, 2002; Perakis *et al.*, 2013). Calcium is an essential plant nutrient, and depletion of soil Ca pools can reduce tree growth (Likens *et al.*, 1996; Huntington and Hooper, 2000; Juice *et al.*, 2006), increase the effects of stresses from pests and disease (Shortle and Bauch, 1986; Huntington and Hooper, 2000), lower drought and cold resistance (Shortle and Smith, 1988; Schaberg *et al.*, 2002), and alter forest evapotranspiration (Green et

al. 2013). In addition to mobilizing soil base cations, acidification increases the solubility, and by extension, export of aluminum (Cronan and Schofield, 1979; Driscoll, 1985; Hooper and Shoemaker, 1985; Cozzarelli *et al.*, 1987; Driscoll and Schecher, 1990; Lawrence *et al.*, 2007), beryllium (Veselý *et al.*, 1989; Jagoe *et al.*, 1993; Navrátil, 2000; Kaste *et al.*, 2002), and trace metals (Kumpiene, 2010), which can impact aquatic ecosystems (Mance, 1987).

While many studies have examined the effects of nitrogen deposition on forested regions in Southern California (Bytnerowicz and Fenn, 1996; Fenn *et al.*, 1996, 2000; Fenn and Bytnerowicz, 1997), few have characterized acidification processes in LA roadside soils, despite the large amount of N_r input to near-road soils (Cape *et al.*, 2004; Bettez *et al.*, 2013; Redling *et al.*, 2013). Additionally, while Ca depletion has been widely observed in acidified forest soils, the prevalence of Ca-rich road construction materials (e.g., concrete) likely significantly affects soil Ca dynamics in acidified soils. Although several studies have considered the effects of concrete weathering on stream water (Davies *et al.*, 2010; Kaushal *et al.*, 2013), and riparian sediment (Bain *et al.*, 2012) chemistry, little attention has been given to the interaction of concrete weathering and soil acidification processes. Thus, the extent of road network coverage and resulting amplified trace metal inputs to roadside soils (Mielke *et al.*, 2010; Clarke *et al.*, 2015), widespread impervious surface coverage (61%) (McPherson *et al.*, 2011), and heavy Nr loadings (50 kg ha^{-1} per year) (Fenn and Bytnerowicz, 1997) to the LA region make acidification and subsequent mobilization of LA roadside soil metals likely (Figure 1-1). Additionally, roadways in the LA region do not receive inputs of road deicers, as winter frosts are brief due to the region's Mediterranean climate (Bytnerowicz and Fenn, 1996). Consequently, the confounding factor of the dissolution of road salt, and resulting exchange reactions with salt-

rich runoff does not exist in the LA region, and can thus be ignored when examining roadside soil cation pool dynamics in this region. Therefore, these characteristics make Southern California an idea study site to examine the impacts of soil acidification on roadside soil cation pools.

1.3 THE FLUSHING OF ROADSIDE SOIL EXCHANGE SURFACES VIA ROAD DEICER PULSES IN THE NINE MILE RUN WATERSHED, PITTSBURGH, PA

Nine Mile Run (NMR) is an urban stream draining 15.7 km^2 of eastern Pittsburgh (PGH) (Environmental Resources Reseach Institute, 2014). The prevalence of urban infrastructure (38% of the watershed is covered with asphalt or roofs) (Homer *et al.*, 2004), roadways (15.5 km km^{-2}, including I-376, a major interstate that parallels and crosses the stream), and historical industrial activities within the watershed make soil enrichment in trace metals likely. Historically, urbanization and industry have heavily impacted the NMR watershed, as a significant portion of the stream was buried (McElwaine, 2005), and 18 million tonnes of trace metal-rich steel by-products (i.e., slag) were disposed within the watershed (Koryak and Stafford, 2002). In particular, the percolation of groundwater through this slag pile has significantly altered NMR stream water chemistry, including alkalization of lower reach stream waters (Koryak and Stafford, 2002), and relatively increased trace metal loadings to stream waters (ONeill *et al.*, 2013). Additionally, the PGH region receives moderate amounts of snowfall (41.4 cm yr^{-1}) (National Weather Service, 2014), and as a consequence, more than 762,000 tonnes of road salt (sodium chloride), were applied to Pennsylvanian roadways

between 2009 and 2014 (PennDOT, 2014). These characteristics therefore make NMR an ideal site to examine the interactions of salt-rich solutions and soil metals.

The dissolution of sodium chloride (NaCl) in highway runoff creates waters with high total dissolved solids (TDS), that can mobilize soil metals through soil cation exchange reactions (Shanley, 1994; Granato *et al.*, 1995). Additionally, relatively large inputs of Cl, supplied by the dissolution of road deicers, promote the formation of metal Cl complexes (Bäckström *et al.*, 2004), which are relatively mobile in the soil solution (Chaney, 2010). Lastly, increased loadings of Na to soil waters can negatively impact soil structure, decrease soil permeability and exacerbate soil erosion (Amrhein *et al.*, 1992),and therefore promote the physical transport of both soluble and sorbed metals to surface waters. While several studies have detailed increased metal loadings to surface waters due to interactions of soils and high TDS solutions (Kunkle, 1972; Amrhein *et al.*, 1992; Shanley, 1994; Mason *et al.*, 1999; Koryak and Stafford, 2001; Kaushal *et al.*, 2005; Kelly *et al.*, 2008; Cooper *et al.*, 2014), less attention has been given to the impacts of high TDS solutions on near-road soils.

Studies that have examined roadside areas (Amrhein *et al.*, 1992; Bauske and Goetz, 1993; Norrström and Bergstedt, 2001) largely focus on cation exchange reactions driven by Na-rich roadway runoff. However, these studies do not discuss impacts on soil metal dynamics via the weathering of road construction materials (e.g., concrete and slag fill), that could significantly affect patterns of cation mobilization in roadside soils. Furthermore, given the significant loadings of N_r (Cape *et al.*, 2004; Bettez *et al.*, 2013; Redling *et al.*, 2013) and road deicers (Buttle and Labadia, 1999) to near-road soils, soil acidification processes could interact with and likely exacerbate cation exchange reactions by high TDS runoff. Interactions between

these processes potentially mobilizes roadside soil cations in unexpected ways, such as affecting the speciation (e.g., promoting the formation of metal chloride complexes) and by extension, toxicity of dissolved trace metal mixtures. Lastly, existing studies underappreciate the impact that aging highway infrastructure has on near road soil moisture regimes. As drainage infrastructures age, they have an increased chance of leaking (Davies *et al.*, 2001), and subsequently recharging local ground water with highway runoff (Lerner, 1986). Relatively direct inputs of runoff to local ground water remove the ability of soil to filter pollutants (Kabir *et al.*, 2014), and could possibly increase the size of areas affected by vehicular metal deposition. A clearer documentation of these processes is essential to understanding metal dynamics in urban and near-road environments.

1.4 RECONSTRUCTING LEGACY TRACE METAL LOADINGS IN SOUTHWESTERN PENNSYLVANIA

The Southwestern Pennsylvania (USA) region has a long industrial history, and industrial activities have included, but are not limited to, iron manufacturing (Albert, 1882; Muller and Tarr, 2005), coal and coke works (Albert, 1882), steel production (Warren, 1987), and Zn smelting (Ingalls, 1916; Bleiwas and DiFrancesco, 2010), which occurred during the 19th and 20th centuries. Many of these industries altered local air (Eatough *et al.*, 2007) and water (Davis III and Jacknow, 1975) chemistry through trace metal-rich emissions. While trace metal loadings from conventional, modern sources (e.g., metallurgical facilities) are reasonably characterized (Van Alphen, 1999; Vermillion *et al.*, 2005; Mattielli *et al.*, 2009), trace metal loadings from

relatively undercharacterized sources (i.e., early and pre-industrial activities) are not.

While studies have acknowledged the use of trace metals in early human activities (Bintliff *et al.*, 1990; Nriagu, 2001; Borkow and Gabbay, 2009), the trace metal loadings from early and pre-industrial activities are poorly characterized. Consequently, the magnitude and distribution of contamination associated with these activities is often unknown. Moreover, the sequential input of trace metal contamination from multiple industries (e.g., leather tanneries, metallurgical facilities) likely results in unpredictable biogeochemical interactions, and presumably, an accumulation of contamination. Accordingly, elevated trace metal loadings likely stretch beyond the lifespan of a single pollution source, resulting in a significant amount of trace metal contamination that is relatively unknown.

Because sediments deposited in alluvial and lacustrine environments can accumulate trace metals (Mielke *et al.*, 2000; Bain and Brush, 2005; Rhoades *et al.*, 2009), they can also record periods of significant trace metal contamination (Graney *et al.*, 1995; Spliethoff and Hemond, 1996; Mahler *et al.*, 2006; Hillman *et al.*, 2015). While this accumulation allows for reconstruction of temporal sequences of trace metal loadings, it can also result in a reservoir of contaminants with a strong potential to remobilize, particularly by physical disturbances (Axtmann and Luoma, 1991; Spliethoff and Hemond, 1996; Steding *et al.*, 2000; Tao *et al.*, 2005; Pizzuto, 2014). As potential changes in global precipitation patterns will increase the probability of extreme precipitation events (Palmer and Räisänen, 2002), and by extension, flood events (Jongman *et al.*, 2012), changes to global climate likely will increase likelihood of the mobilization of contaminated alluvial sediments. Therefore, effective risk assessment will require a characterization of legacy trace metal contamination in many regions with an

industrial legacy and subject to climate change.

1.5 PHOSPHORUS ACCUMULATION IN ROADSIDE SOILS

Phosphorus is an essential element to all lifeforms (Ashley *et al.*, 2011) and subsequently P is relatively tightly cycled by biota (Ryan, 2014). As a result, P is a major component of fertilizers (Jasinski, 2013). With the onset of industrial agricultural fertilization in the mid-20th century, application rates of P to agricultural soils greatly increased (Crop Reporting Board, 1966). Consequently, human activities have greatly altered the global P cycle (Filippelli, 2008; Ashley *et al.*, 2011). For example, the mobilization of P from agricultural soils have increased loadings of P to surface waters (Wilcock, 1986; Vighi and Chiaudani, 1987; Ward *et al.*, 1990; Uunk, 1991). Because P is generally a limiting nutrient in aquatic ecosystems (Correll, 1999), larger inputs of P increase the incidence of eutrophication events (Anderson *et al.*, 2002), that can deplete dissolved oxygen in the water column, shift species composition, and cause fish kills (Smith, 1998). While agricultural and natural P sources (e.g., guano, phosphate minerals) are well characterized, knowledge gaps still exist in the global P cycle (Stoddard *et al.*, 2016).

Although previous studies have examined the atmospheric deposition of P due to the combustion of multiple types of fuels (e.g., Mahowald *et al.*, 2008; Wang *et al.*, 2014), loadings of P to near-road areas are poorly understood, despite the widespread use of P in vehicular fuels and lubricants. Specifically, diesel (Pierson and Brachaczek, 1982; Spencer *et al.*, 2006) and both leaded (Pierson and Brachaczek, 1982) and unleaded (Pierson and Brachaczek, 1982;

Spencer *et al.*, 2006) gasolines contain varying P contents. Moreover, lubricating oils contain P-based additives (Pierson and Brachaczek, 1982; Nicholls *et al.*, 2005; Spencer *et al.*, 2006; McDonald, 2009), namely zinc dialkyl dithiophosphate (ZDDP) (McDonald, 2009), which was patented in 1944 (Freuler, 1944). Because the P content of P-based additives in lubricating oils was unregulated for 45 years (Spikes, 2004), roadside soils have likely received substantial P inputs, and by extension, accumulated a significant amount of P due to the deposition of vehicular exhaust. Road networks are known to increase both rates of soil erosion (Forman and Alexander, 1998; Jones *et al.*, 2000), and runoff (Dunne and Leopold, 1978), and soil P losses occur primarily during erosional and runoff events (Sharpley *et al.*, 1992). Thus the accumulation of P in roadside soils creates a P pool with a high propensity to be mobilized, and has important implications for surrounding natural systems.

1.6 DISSERTATION FORMAT

This doctoral dissertation comprises a collection of six chapters, of which four chapters represent individual papers to submit for publication in peer reviewed journals. The first and second chapters have already been published in the peer-reviewed scientific journals *Biogeochemistry* and *Hydrological Processes*, respectively. The third chapter has been submitted to the peer-reviewed scientific journal *Environmental Science & Technology* and is currently being revised to respond to the comments of three anonymous reviewers. The fourth chapter will shortly be submitted to a peer-reviewed scientific journal. The final chapter summarizes the major results and conclusions of each chapter.

2.0 RESPONSES OF ROADSIDE SOIL CATION POOLS TO VEHICULAR EMISSION DEPOSITION IN SOUTHERN CALIFORNIA

2.1 INTRODUCTION

Roadside soils generally contain elevated concentrations of trace metals (Garcia-Miragaya *et al.*, 1981; Amrhein *et al.*, 1992; Fakayode and Olu-Owolabi, 2003; Nabulo *et al.*, 2006) and receive increased loadings of reactive nitrogen (N_r) (Bettez *et al.*, 2013; Redling *et al.*, 2013). This N_r is sourced from vehicular exhaust, which is deposited close to roads and transforms to nitric acid (HNO_3) (e.g., a majority of exhaust N_r is deposited within 10 meters of roads, Figure 2-1) (Cape *et al.*, 2004; Redling *et al.*, 2013). Additionally, impermeable surfaces (e.g., roadway, sidewalks) in the near-road environment can create nitrogen hotspots in roadside soils (Göransson *et al.*, 2014). Deposition of reactive nitrogen can occur via both dry and wet pathways; however dry deposition is likely the major source of N deposition in arid regions such as Los Angeles (Fenn *et al.*, 1996, 2000; Fenn and Bytnerowicz, 1997). The excess reactive N deposited in roadside soils can acidify these soils (Fenn *et al.*, 1996), and potentially influence roadside metal contamination.

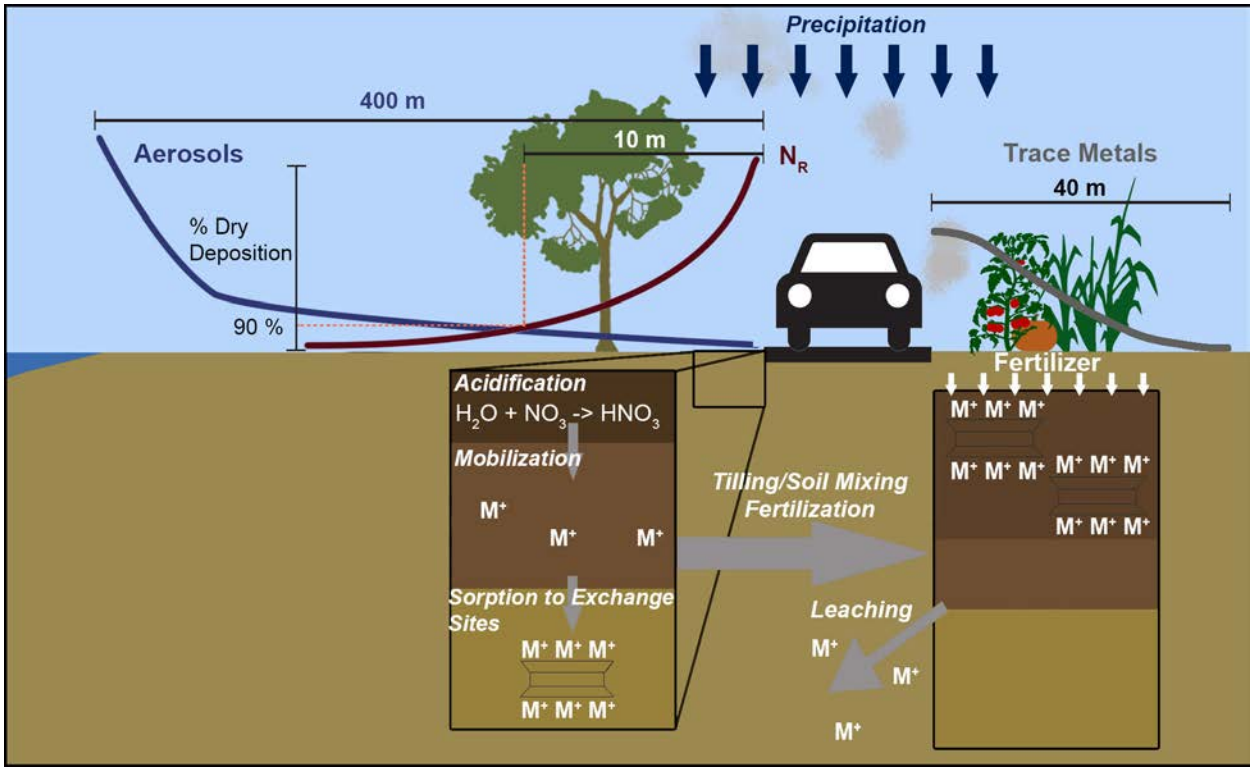

Figure 2-1. Conceptual model of vehicular exhaust (Cape *et al.*, 2004; Redling *et al.*, 2013)**, oceanic aerosols** (Feliu *et al.*, 1999)**, and trace metal depositional patterns** (Fakayode and Olu-Owolabi, 2003; Nabulo *et al.*, 2006)**. The left inset box details the acidification of soil water, mobilization of soil metals to lower horizons, and sorption of metals to clay minerals. The right inset box illustrates processes in gardens such as fertilization and mixing resulting from soil tilling.**

Impacts of soil acidification in forested soils are well documented (e.g., Federer and Hornbeck, 1989; Likens *et al.*, 1996; Huntington and Hooper, 2000; Fernandez *et al.*, 2003; Juice *et al.*, 2006) however soil acidification is poorly characterized in roadside soils. In particular, acidified soils retain fewer base cations during exchange reactions, promoting the depletion of base cation pools (Federer and Hornbeck, 1989; Huntington and Hooper, 2000; Fernandez *et al.*, 2003; Juice *et al.*, 2006; Green *et al.*, 2013). Base cations are essential plant nutrients and their depletion can impair vegetation health (Federer and Hornbeck, 1989; Huntington and Hooper, 2000; Fernandez *et al.*, 2003; Juice *et al.*, 2006; Green *et al.*, 2013). Likewise, soil

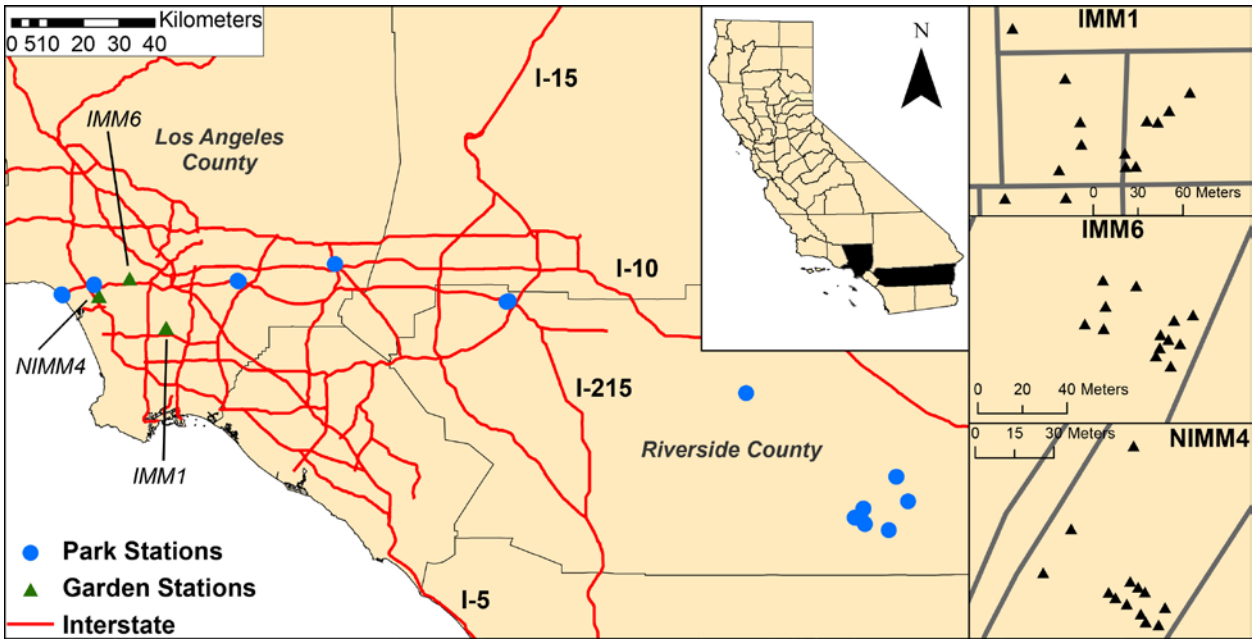

Figure 2-2. Locations of the sampled stations within Los Angeles and Riverside Counties in Southern California. The three urban gardens sampled and surrounding roads are detailed in the insets.

acidification also can increase the mobility of trace metals (Kumpiene, 2010). Given the substantial loads of N_r to roadside soils, we hypothesize that the acidification of roadside soils mobilizes exchangeable cations from these soils, depleting soil cation pools. In addition, we hypothesize that other material inputs to roadside soils, particularly weathering products of local lithology and human-made materials, can replenish metal losses to mobilization and affect observed patterns of metal concentration.

To evaluate these hypotheses about the acidification of roadside soils and near-road soil metal mobility, we compared 1) road network characteristics, 2) modeled, annual nitrogen deposition, and 3) soil metal concentrations. Furthermore, to determine the influence of local geology and construction materials on patterns in soil metal concentrations, we applied mixing models to identify the principal sources of cations in soil cation pools. Thus, this study

characterizes the interaction of vehicular exhaust with roadside soil cation pools in the local geochemical context.

2.2 METHODS

2.2.1 Study Region

Fifty-eight samples were collected from park (i.e., city, state, or wildland reserves) or urban garden plot soils in regions of Los Angeles and Riverside County that lie within the Los Angeles, California air basin (Figure 2-2). Park samples are a composite of six samples that were equally distributed between canopy and non-canopy areas. Garden samples, originally collected to examine legacy trace metal contamination (Clarke *et al.*, 2015a), were gathered as separate samples from urban community garden plots (IMM1, IMM6, and NIMM4) in the Los Angeles metropolitan area. Due to the contrast in sampling design, the garden plot samples exhibit much greater variability than the variability in composited soils across the regional gradients the soils straddle (Figure 2-3). This creates data clouds challenging to compare with samples collected from the broader spatial extent, sampled to represent average park soils. Therefore, for these regional analyses, the median values of all samples taken within each community garden (i.e., “garden samples”) were compared as a single value with the park samples in analysis (Figure 2-3).

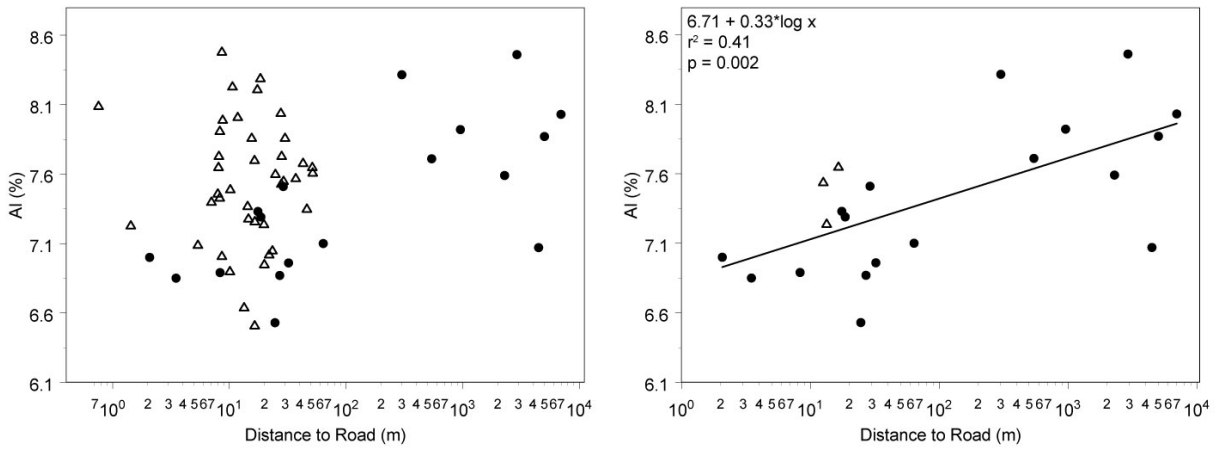

Figure 2-3. Example of the high variance in garden samples and the resulting data cloud (a). For regional analyses the median values of all samples taken within each community garden were used (b). Park samples are represented by solid shapes, whereas garden samples are represented by hollow shapes.

2.2.2 Field Sampling & Chemical Analysis

Park samples were collected in July 2008, and garden plot samples were taken in July 2011. The top 5 cm of soil materials were collected, dried, and subsamples for metals analysis powdered in a ball mill (tungsten carbide bomb). Total metal concentrations in powdered samples were measured via four acid (perchloric, nitric, hydrofluoric, and hydrochloric) digestion (Procedure ME-MS61) by ALS Chemex. Soil pH values were measured using a 5:2 water to soil solution. Soil clay content was determined for park sites using the hydrometer method. Loss on ignition (LOI) was determined by drying the soil at 105 °C for 24 hours, and then combusting the dried sample in a muffle furnace at 550 °C for 4 hours. Percent organic matter was then inferred by mass difference. Metal input sources (e.g., concrete, parent material) were determined via standard mixing model analysis (Faure and Mensing, 2005).

2.2.3 Spatial and Statistical Analysis

Geographical analysis was conducted in ArcGIS 10. Road coverage data for Los Angeles and Riverside counties were obtained from county governments, and used to determine road proximity and density (Los Angeles County GIS Data Portal, 2012; Riverside County Transportation & Land Management Agency, 2012). Road densities were calculated as the total length of roadways within a 1 km radius circular buffer around each sampling station. Influence of traffic densities was not considered in this study as average annual daily traffic rates for the sampled areas were not available. Annual precipitation amounts for each soil sampling station were determined from long-term mean precipitation data (800m resolution) (PRISM Climate Group Oregon State University, 2004a). Total annual N deposition was determined from modeling data (Center for Conservation Biology at the University of California - Riverside, 2006). Lastly, data analysis and multiple linear least squares regressions, used to determine the association between site variables (e.g., road density, road proximity) and soil metal concentrations, were performed in Tibco Spotfire S+ 8.2.0.

Table 2-1. Latitude, longitude, road density, distance from road, distance from ocean and average annual precipitation for each sampling station and each community garden sampled.

Station	Latitude	Longitude	Road Density (km km^{-2})	Distance to Nearest Road (m)	Distance to Ocean (km)	Average Annual Precipitation (mm)
AGH	33.633333	-116.40000	3.65	301	60.1	235
BDC	33.581944	-116.37111	0.00	5031	57.0	379
FG1	34.077056	-117.81183	9.84	63.9	44.3	464
FG2	34.077169	-117.81109	9.57	17.6	44.3	464
FP1	33.999642	-117.37445	12.1	27.1	59.8	283
FP2	33.998103	-117.37978	8.62	8.3	59.4	284
JR	33.808333	-116.77778	1.91	543	70.5	676
PF	33.566667	-116.48333	2.60	957	49.8	420
PP1	34.011389	-118.49543	17.2	3.5	0.34	351
PP2	34.013731	-118.49819	17.3	32.3	0.29	355
PRP1	34.032953	-118.41711	17.3	18.7	7.40	380
PRP2	34.034217	-118.41702	17.0	2.1	7.48	380
SR5	33.547750	-116.50494	5.69	2295	47.0	482
SR6	33.544861	-116.49019	3.87	2921	47.4	582
SR7	33.533944	-116.47897	3.87	4482	46.9	612
SR8	33.521222	-116.41975	0.00	6975	48.9	666
WN1	34.040589	-118.05389	11.6	29.1	31.1	394
WN2	34.042600	-118.05668	12.7	24.7	31.3	393
IMM1	33.943525	-118.235941	16.4	12.6	17.7	370
IMM6	34.046265	-118.327962	13.4	16.5	14.6	376
NIMM4	34.010451	-118.404832	18.0	13.4	6.67	358

2.3 RESULTS

2.3.1 Regional Patterns in Roads and Geophysical Characteristics

Geographical analysis highlighted the wide variance of road densities (0 to 18.0 km km^{-2}) (Los Angeles County GIS Data Portal, 2012; Riverside County Transportation & Land Management Agency, 2012), road proximities (0.002 to 7.0 km) (Los Angeles County GIS Data Portal, 2012; Riverside County Transportation & Land Management Agency, 2012), annual precipitation rates (235 to 676 mm yr^{-1}) (PRISM Climate Group Oregon State University, 2004a), and distances from the ocean (0.29 to 71 km) (Metropolitan Transportation Commission, 2004) observed by this study (Table 2-1). Likewise, parent material and soil type of the sampled stations varied widely (Table 2-2). In particular, bedrock geology underlying sample locations consists primarily of Quaternary alluvial deposits and Mesozoic granitic intrusives, with some outcrops of shale, metasedimentary, sedimentary, and paralic deposits (California Geological Survey, 2012).

Linear regression analysis revealed the varying influence of each of these spatial metrics on individual cationic species (Table 2-3). Despite the observed regional heterogeneity, we observe overarching patterns in cation chemistry that transcend bedrock geochemistry and soil type (Table 2-2, Table 2-4, & Table 2-5). In particular, patterns of soil metal depletion are independent of the underlying bedrock geology. Similarly, underlying bedrock appears to minimally influence pH in roadside soils (Figure 2-4a).

Table 2-2. Parent rock (California Geological Survey, 2012) **and soil type of the sampling stations** (National Cooperative Soil Characterization Database, 2012)**. Soil surveys are not available for the City of Los Angeles.**

Station	Parent Rock	Soil Type
AGH	Granitic	Data not available
FP1	Alluvium	Metz loamy fine sand, 0 to 2 percent slopes
FP2	Alluvium	Metz loamy fine sand, 0 to 2 percent slopes
JR	Granitic	Green Bluff-Brader families association
PF	Granitic	Trigo family-Lithic Xerorthents, warm complex
SR5	Granitic	Lithic Xerorthents, warm-Rock outcrop complex
SR6	Sedimentary	Osito-Modesto families association
SR7	Metasedimentary	Lithic Xerorthents, warm-Rock outcrop complex
SR8	Granitic	Crouch rocky sandy loam
FG1	Shale	Data not available
FG2	Shale	Data not available
BDC	Granitic	Rock Outcrop
PP1	Alluvium	Data not available
PP2	Alluvium	Data not available
PRP1	Paralic	Data not available
PRP2	Paralic	Data not available
WN1	Alluvium	Data not available
WN2	Alluvium	Data not available
IMM1	Alluvium	Data not available
IMM6	Alluvium	Data not available
NIMM4	Alluvium	Data not available

Table 2-3. R^2 and p-values for multiple regression analysis.

	r^2	p-value	r^2	p-value	r^2	p-value	r^2	p-value	r^2	p-value	r^2	p-value
Road Density (RD)	0.41	*0.002*	0.44	*0.001*	5.1E-04	*0.92*	0.10	*0.17*	7.1E-04	*0.91*	0.01	*0.75*
Road Proximity (RP)	0.41	*0.002*	0.50	*<0.001*	0.08	*0.23*	0.26	*0.02*	0.03	*0.48*	1.3E-05	*0.99*
Distance to Ocean (O)	0.16	*0.08*	0.29	*0.01*	0.07	*0.28*	0.03	*0.46*	0.01	*0.67*	0.02	*0.60*
Annual Precipitation (P)	0.10	*0.16*	0.08	*0.22*	0.42	*0.002*	0.04	*0.42*	0.42	*0.002*	0.02	*0.60*
RD+RP	0.43	*0.006*	0.51	*0.002*	0.31	*0.04*	0.33	*0.04*	0.09	*0.43*	0.02	*0.84*
RD+O	0.49	*0.002*	0.44	*0.006*	0.29	*0.06*	0.14	*0.27*	0.05	*0.60*	0.02	*0.84*
RD+P	0.41	*0.009*	0.44	*0.005*	0.57	*0.0008*	0.10	*0.39*	0.56	*0.0006*	0.02	*0.87*
RP+O	0.41	*0.008*	0.52	*0.001*	0.38	*0.02*	0.30	*0.05*	0.09	*0.42*	0.02	*0.81*
RP+P	0.43	*0.007*	0.55	*<0.001*	0.45	*0.006*	0.27	*0.07*	0.51	*0.002*	0.02	*0.83*
O+P	0.20	*0.14*	0.30	*0.04*	0.65	*0.0001*	0.05	*0.63*	0.51	*0.002*	0.02	*0.81*
RD+RP+P	0.45	*0.02*	0.55	*0.003*	0.65	*0.0007*	0.34	*0.08*	0.56	*0.003*	0.04	*0.86*
RD+O+P	0.51	*0.006*	0.45	*0.01*	0.65	*0.0006*	0.14	*0.46*	0.56	*0.003*	0.04	*0.88*
RP+O+P	0.43	*0.02*	0.56	*0.003*	0.67	*0.0004*	0.31	*0.10*	0.54	*0.004*	0.05	*0.83*
RD+RP+O	0.49	*0.008*	0.52	*0.005*	0.38	*0.05*	0.33	*0.09*	0.10	*0.62*	0.02	*0.94*
RD+RP+O+P	0.51	*0.02*	0.56	*0.008*	0.68	*0.001*	0.34	*0.15*	0.5	*0.008*	0.05	*0.93*

Table 2-4. Soil pH, clay content, and loss on ignition (LOI) for each sampled station. Clay content was not measured in garden samples. Additionally, LOI and soil pH were not analyzed for IMM6 and NIMM4 garden samples.

Station	pH	Clay (%)	LOI (%)	Station	pH	Clay (%)	LOI (%)
AGH	7.07	2.14	2.47	WN1	7.70	9.16	8.78
BDC	7.96	2.35	1.75	WN2	7.88	9.36	20.15
FG1	5.68	8.46	6.74	IMM1-1	7.20	--	10.07
FG2	7.96	6.66	7.07	IMM1-2	7.69	--	5.93
FP1	7.22	6.87	11.96	IMM1-6	6.77	--	11.93
FP2	7.59	7.70	22.17	IMM1-7	7.45	--	7.82
JR	5.72	6.51	6.94	IMM1-13	7.09	--	6.88
PF	7.44	4.93	2.20	IMM1-15	7.09	--	10.88
PP1	7.61	13.7	13.97	IMM1-19	6.94	--	16.28
PP2	7.29	12.3	10.22	IMM1-22	7.29	--	7.51
PRP1	6.40	12.3	13.91	IMM1-28	6.96	--	10.71
PRP2	6.50	8.74	13.90	IMM1-32	6.96	--	9.21
SR5	6.66	1.90	5.03	IMM1-OUT1	7.53	--	6.44
SR6	6.52	3.77	4.95	IMM1-OUT2	--	--	--
SR7	6.18	0.47	4.32	IMM1-OUT3	--	--	--
SR8	5.80	1.19	7.89				

Table 2-5. Soil metal concentrations (g kg^{-1}) for each sampling station.

Station	Al	Ca	K	Mg	Na	Be	Sr	Ti	Station	Al	Ca	K	Mg	Na	Be	Sr	Ti
AGH	83.2	32.4	19.9	14.7	20.7	2.07	0.45	5.82	IMM1-OUT1	74.6	31.5	18.3	9.0	24.6	1.36	0.64	3.91
BDC	78.7	28.8	21.1	13.7	19.1	1.61	0.37	5.56	IMM1-OUT2	76.5	33.2	18.5	9.9	24.9	1.34	0.64	4.43
FG1	71.0	18.7	17.1	4.7	18.4	1.45	0.41	3.84	IMM1-OUT3	74.9	32.1	18.9	11.5	22.4	1.20	0.53	3.99
FG2	73.3	24.1	18.2	8.5	17.3	1.40	0.34	3.74	NIMM4-1	77.3	23.0	20.9	8.1	22.9	1.51	0.46	4.97
FP1	68.7	28.6	22.3	10.5	19.6	1.64	0.37	3.48	NIMM4-2	76.0	23.2	20.8	7.7	22.6	1.46	0.45	5.01
FP2	68.9	40.9	16.3	11.4	18.8	1.15	0.38	3.66	NIMM4-4	69.5	25.8	20.7	7.4	21.1	1.31	0.45	3.79
JR	77.1	21.0	20.0	4.5	21.0	1.49	0.42	2.92	NIMM4-6	66.4	24.4	18.7	6.5	19.5	1.13	0.45	4.16
PF	79.2	27.4	21.1	6.2	21.7	1.58	0.45	3.51	NIMM4-8	70.9	24.3	20.1	6.9	21.1	1.14	0.44	4.51
PP1	68.5	19.8	20.6	7.9	18.5	1.27	0.35	3.41	NIMM4-10	74.0	23.0	21.0	7.0	22.5	1.45	0.46	4.76
PP2	69.6	18.4	20.6	8.2	19.9	1.31	0.36	3.38	NIMM4-13	65.1	27.7	19.1	7.3	19.1	1.21	0.44	4.01
PRP1	72.9	20.4	16.4	7.6	19.7	1.21	0.38	4.24	NIMM4-14	72.4	23.6	21.2	6.7	21.6	1.27	0.46	4.45
PRP2	70.0	21.7	15.6	7.9	19.4	1.11	0.38	4.51	NIMM4-15	70.5	25.4	20.1	7.2	21.0	1.34	0.45	4.34
SR5	75.9	26.1	20.5	8.6	19.3	1.76	0.40	4.03	NIMM4-OUT1	77.3	25.3	20.5	12.4	23.0	1.78	0.46	4.54
SR6	84.6	15.9	19.3	6.4	18.8	2.22	0.24	3.56	NIMM4-OUT2	79.1	25.0	20.3	11.7	24.7	1.61	0.48	4.12
SR7	70.7	16.3	24.3	3.4	18.7	1.42	0.22	2.18	NIMM4-OUT3	80.1	26.5	20.8	13.3	22.3	2.00	0.47	5.02
SR8	80.3	15.8	14.9	8.2	10.6	1.83	0.24	5.22	NIMM4-P12	69.0	26.3	20.7	7.0	20.8	1.18	0.45	3.97
WN1	75.1	32.9	20.0	12.3	21.0	1.39	0.46	4.00	IMM6-1	73.7	25.7	20.4	7.9	20.1	1.41	0.43	3.97
WN2	65.3	72.6	17.6	12.7	16.2	1.31	0.53	3.53	IMM6-2	82.9	25.5	23.2	8.1	23.0	1.75	0.48	4.44
IMM1-5	75.3	29.5	20.1	10.9	22.0	1.39	0.53	3.83	IMM6-6	77.0	26.5	21.6	8.3	21.2	1.53	0.48	3.99
IMM1-25	82.1	31.9	20.7	11.9	23.9	1.47	0.57	4.21	IMM6-7	72.6	21.5	20.3	7.6	19.7	1.36	0.41	3.89
IMM1-28	75.5	33.1	20.2	11.1	23.1	1.34	0.57	3.91	IMM6-13	76.8	24.1	20.5	7.4	21.9	1.41	0.44	4.12
IMM1-45	70.2	33.4	21.2	10.5	20.7	1.27	0.54	3.48	IMM6-15	76.5	24.3	21.3	7.9	21.3	1.47	0.44	4.05
IMM1-46	72.8	33.3	19.0	9.5	22.7	1.33	0.56	3.38	IMM6-19	73.5	24.7	19.9	7.6	20.2	1.14	0.42	3.80
IMM1-52	78.6	33.0	19.7	12.3	22.4	1.48	0.55	4.15	IMM6-22	76.1	24.4	20.6	8.3	21.1	1.49	0.44	4.17
IMM1-83	80.4	29.2	19.2	11.5	22.9	1.43	0.56	4.21	IMM6-28	75.7	26.5	21.1	8.2	21.0	1.49	0.45	4.06
IMM1-95	80.9	25.4	20.6	10.0	23.7	1.32	0.57	3.82	IMM6-32	78.6	23.2	21.3	8.0	21.4	1.57	0.44	4.28
IMM1-109	74.3	30.2	19.3	10.0	22.3	1.41	0.54	3.75	IMM6-OUT1	84.8	21.3	21.5	8.8	22.1	1.62	0.44	4.80
IMM1-110	72.3	30.0	18.8	10.2	21.5	1.27	0.52	3.56	IMM6-OUT2	79.9	22.1	21.1	8.1	21.9	1.51	0.44	4.45
IMM1-115	82.3	28.7	19.9	11.2	24.2	1.38	0.55	4.12	IMM6-OUT3	70.1	22.5	18.4	6.6	21.0	1.29	0.44	3.87

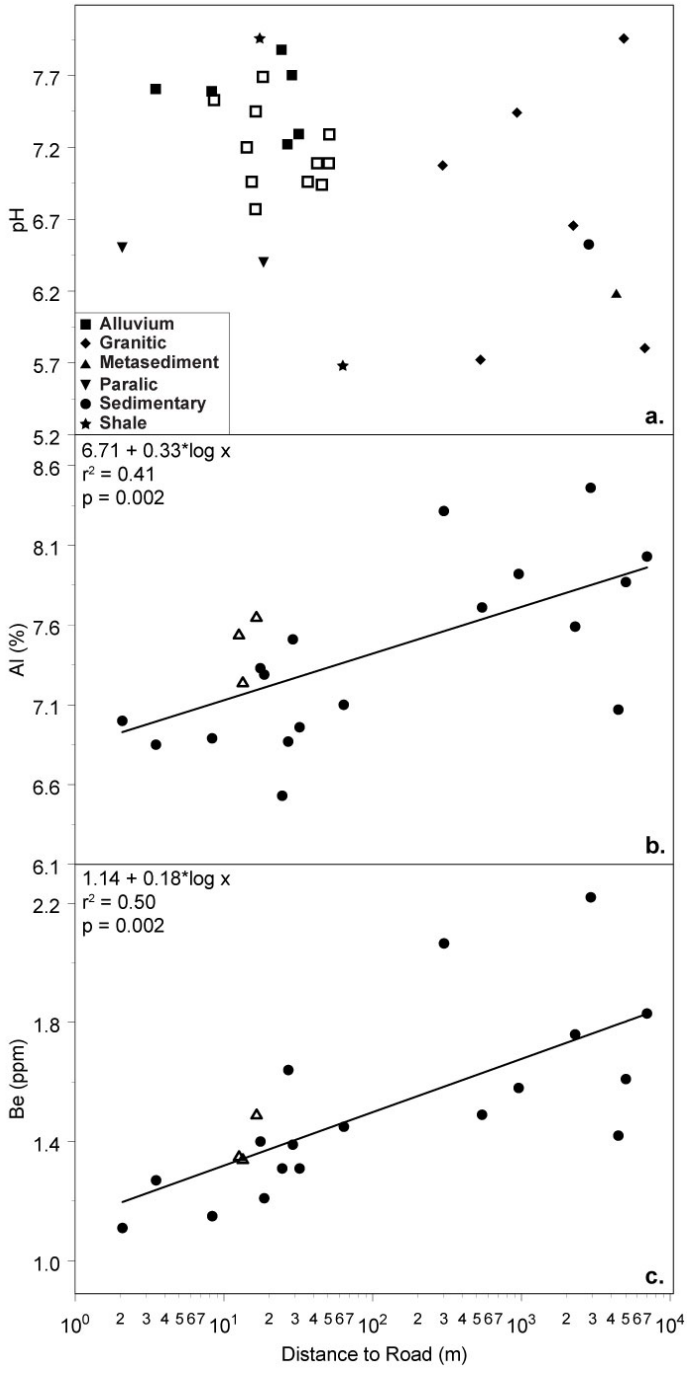

Figure 2-4. Soil pH (a), soil aluminum concentrations (b), and soil beryllium concentrations (c) vs. the log transformed distance from the roadside. In frame a bedrock is indicated by symbol shape. Park samples are represented by solid shapes, whereas garden samples are represented by open shapes. The relatively low pH in samples far from the road likely reflects granitic parent material. Soil pH was not measured for IMM6 and NIMM4 garden samples. Relatively elevated aluminum concentrations observed in the garden medians likely results from tilling of the garden soils, which mixes clays from deeper horizons with the topsoil

2.3.2 Roadside Soil Cation Depletion

In our samples, soil Al decreases in near-road soils (Figure 2-4b), and soil Al concentrations were most strongly associated with road density and road proximity (r^2 = 0.41 for both). Additionally, transportation networks also appear to affect soil Be concentrations, as sampled near-road soils are also depleted in Be (r^2 = 0.50) (Figure 2-4c). Furthermore, in the sampled soils, K concentrations are also influenced by road proximity (r^2 = 0.26), with soil K concentrations decreasing in near-road soils (Figure 2-5c). In contrast however, near-road soils have higher clay-sized particle contents (r^2 = 0.71) (Figure 2-5a) and higher LOI (a proxy for SOM) (r^2 = 0.21) (Figure 2-5b, Table 2-4).

2.3.3 Roadside Soil Calcium and Magnesium Trends

Although several metals (Al, Be, K) are relatively depleted in the sampled roadside soils, soil Ca and Mg concentrations appear unaffected by road density and road proximity. In particular, in our samples there is a weak relationship (r^2 = 0.08 and 0.03, respectively) between both soil Ca and Mg concentrations and road proximity (Figure 2-6a). Instead, precipitation fluxes influence soil Ca and Mg concentrations, as soil Ca and Mg are most strongly associated with mean annual precipitation (r^2 = 0.42 for both) (Figure 2-6b, c).

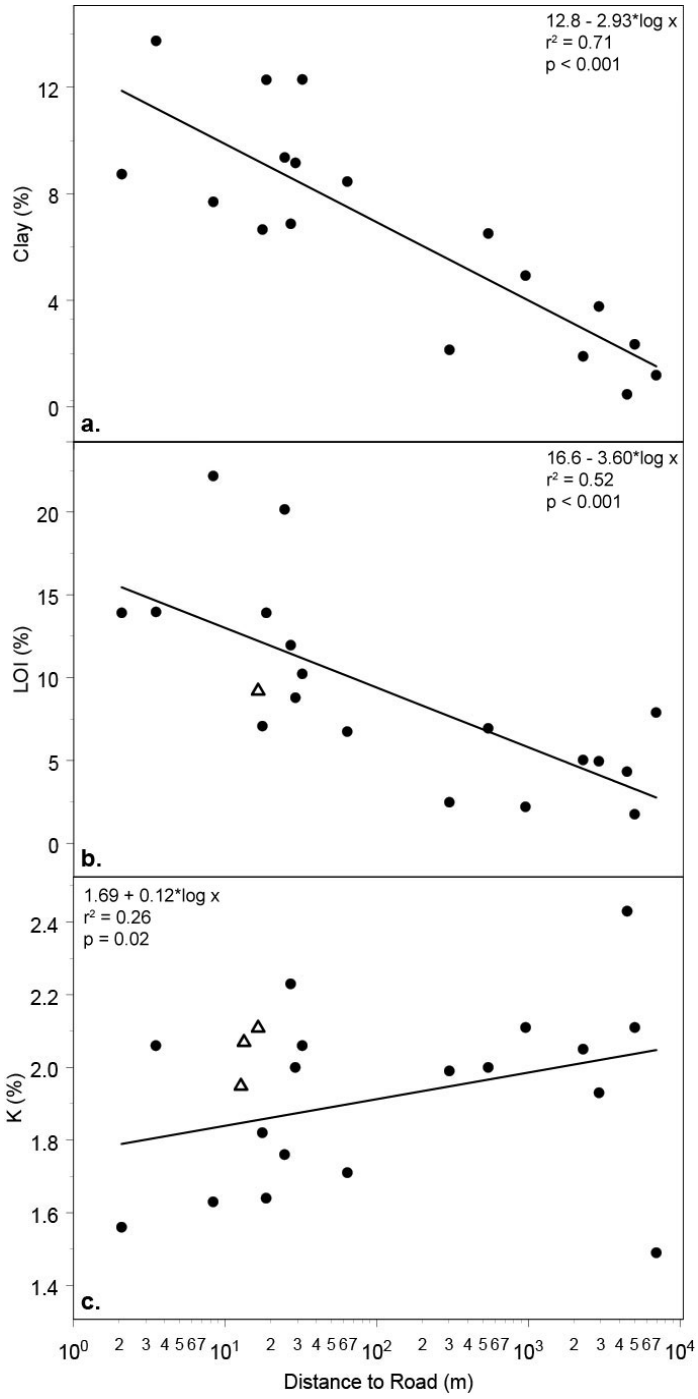

Figure 2-5. Soil clay content (a), soil organic matter (LOI) (b), and soil potassium concentrations (c) versus distance from roadside. The outlying potassium concentration (lower right) occurs in an area with low potassium parent rock (Gromet and Silver, 1987)**. Park samples are represented by *circles*, whereas garden samples are represented by *triangles*. Clay content was not measured for garden samples, and loss on ignition was not performed on two of the gardens.**

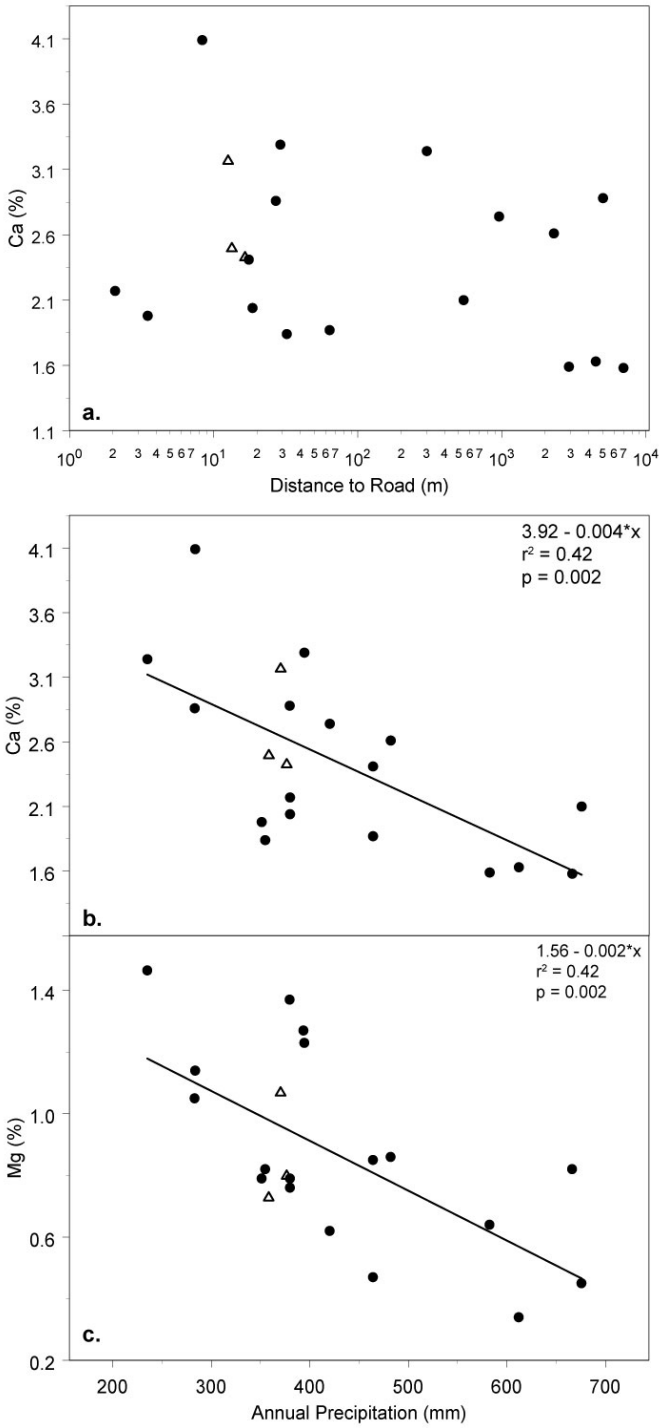

Figure 2-6. Although soil calcium concentrations are unresponsive to road proximity (a), soil calcium (b) and magnesium (c) concentrations are influenced by annual precipitation. Park samples are represented by *circles*, whereas garden medians are represented by *triangles*. One outlying calcium concentration (7.26%, not shown, 24.7 meters from the road) likely reflects fertilizer inputs.

2.4 DISCUSSION

2.4.1 Regional Approach to Roadside Soil Metal Patterns

Studies of soil metal concentrations in roadside soils often utilize a transect-based approach to analyze patterns in near-road areas. However, this study relies on the leveraging of archived samples collected as parts of other efforts. This design allows comparison of samples with both gradients of road proximity and density. While this does not capture the local spatial detail of road-side transects, it does allow examination of soils across a wide variety of road densities, road proximities, annual precipitation rates, and distances from the ocean (Table 2-1). Our approach thus considers drivers distinct from that in road transect designs, revealing the influences of factors such as precipitation, oceanic aerosols, and parent material (Table 2-2 & Table 2-3).

2.4.2 Near-Road Soils and Element Mobilization

Near-road soils in the Los Angeles area should experience acidification effects due to the deposition of N_r from vehicular exhaust (Fenn *et al.*, 1996). In general, as proton loadings increase, soil pH decreases (McFee *et al.*, 1977). However, there is no clear relationship between soil pH and road proximity in our samples (Figure 2-4a). Further, when soil pHs are examined within specific geologic substrates, relationships between soil pH and bedrock

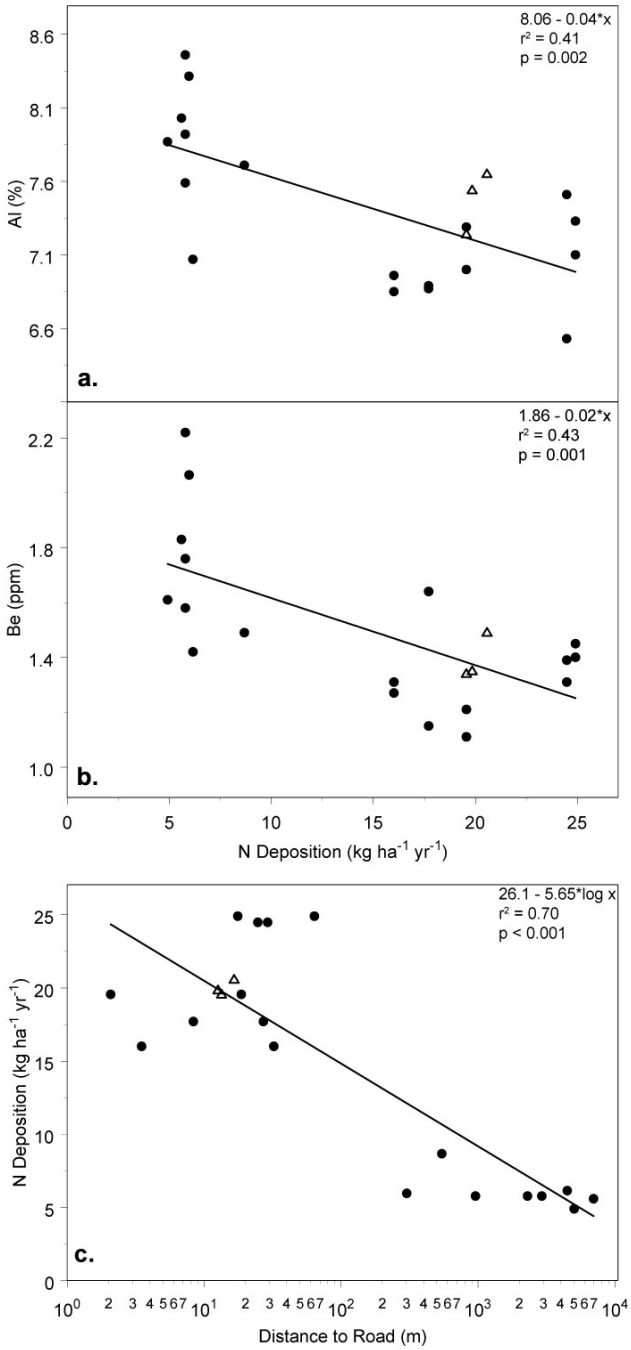

Figure 2-7. Total annual nitrogen deposition based on the Community Multiscale Air Quality Model (Center for Conservation Biology at the University of California - Riverside 2006; Fenn et al. 2010) vs. soil aluminum (a) and beryllium (b) concentrations. Panel c details the relationship between total annual nitrogen deposition and distance from the roadside. Park samples are represented by *solid* shapes, whereas garden samples are represented by *open* shapes

geology do not emerge, so underlying geology does not seem to confound our observations. The absence of a relationship between soil pH and road proximity could mean that soil acidification is not occurring in these roadside soils. However, the depletion of multiple elements from shallow soils across these same gradients (Figure 2-4b, Figure 2-4c, & Figure 2-5c), suggests major cations are being mobilized from these soils despite the lack of patterns in soil pH.

Soil Al is notably sensitive to soil acidification (Driscoll and Schecher, 1990). In particular, decreases in soil pH increase Al solubility, mobilizing labile Al to deeper soil horizons (Cronan and Schofield, 1979; Cozzarelli *et al.*, 1987). The observed mobilization of soil Al that occurs in areas that experience concentrated exhaust deposition (i.e., roadsides) suggests the deposition of vehicular exhaust is acidifying these soils. This suggestion is confirmed by the relationship between soil Al concentrations and N deposition (r^2 = 0.41) (Figure 2-7a), and also the relationship between N deposition and road proximity (Figure 2-7c). Not only does N deposition increase in roadside environments, but soil Al concentrations also decrease in these same environments. As only surface soils were sampled, accumulation of Al at depth cannot be confirmed. However, the relatively higher Al concentrations in the garden samples likely is influenced by this accumulation, as tilling would mix deeper Al-rich soils with the topsoil (Figure 1-1). Thus the behavior of Al in these surface roadside soils seems to be indicative of Al dynamics in acidified soils.

In addition to Al, soil Be concentration patterns also imply that soil acidification occurs in near-road soils. In our samples, transportation networks also affect soil Be concentrations, as the depletion of Be occurs in soils that receive increased N loadings (r^2 = 0.43) (Figure 2-7b).

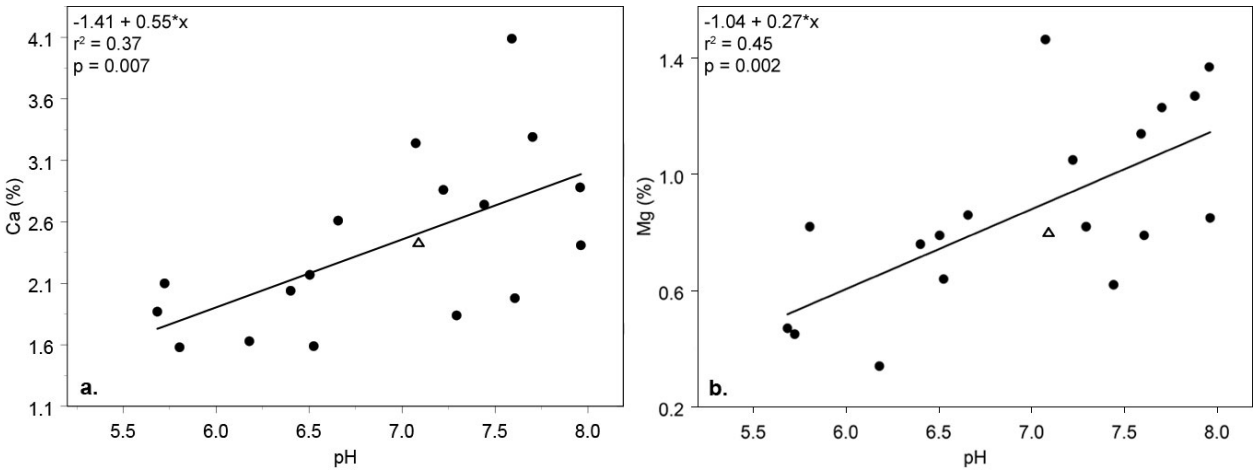

Figure 2-8. Soil calcium (a) and magnesium (b) concentrations versus soil pH. Park samples are represented by circles, whereas garden medians are represented by triangles. Soil pH was not measured for IMM6 and NIMM4 garden samples

This is a parallel relationship consistent with soil acidification, as Al and Be are chemically similar and thus behave similarly in acidic environments (Jagoe *et al.*, 1993). Any acidification of roadside soils should accelerate chemical weathering rates, including the production of clay and clay-sized particles.

Soil exchange capacity is a primary control on soil metal concentrations, with clay-sized minerals and soil organic matter providing the majority of the exchange sites in a soil column (Appelo and Postma, 2005). In our samples, the increased amount of clay-sized particle contents (Figure 2-5a), and higher LOI (Figure 2-5b, Table 2-4) found in near-road soils should result in increased exchange capacity in near road soils and therefore relative metal enrichment in these soils. However, contrary to this expectation, K, a major soil nutrient metal, is depleted in roadside soils (Figure 2-5c). Although this relationship is unexpected given the inferred patterns in exchange capacity (Figure 2-5a & b), it is consistent with soil acidification. Potassium

mobilized from exchange sites by protons is likely transported through the soil column, thereby depleting K^+ pools in surface near-road soils.

Precipitation fluxes are also important to metal mobilization and concentrations for several cations, including Ca and Mg which are associated with mean annual precipitation (Figure 2-6b & c). These relationships, diminished concentrations with increased precipitation, suggest that Ca and Mg transport in the soil profile is transport limited. However, other processes, particularly weathering of road building materials also influence Ca and Mg concentrations in these near road environments.

2.4.3 Road Material Inputs

The weathering of concrete (primarily of CaO) produces $CaCO_3$-rich materials (Papadakis *et al.*, 1992) which can influence both calcium and proton concentrations in near-road soils. This weathering seems to mask expected relationships between soil pH and road proximity, as $CaCO_3$ inputs can buffer soil pH (Papadakis *et al.*, 1992), thus explaining in part the lack of soil pH patterns. Even a small amount of CaO (e.g., 101 or 162 g) can provide enough $CaCO_3$ to raise a square meter of soil's pH by one standard unit (4.5 to 5.5 and 5.5 to 6.5 respectively) (Vossen, 2006). In our samples, Ca concentrations are related to soil pH (r^2=0.37), suggesting roadside soils receive contributions from weathering concrete road components (Figure 2-8a). Therefore the weathering of concrete road materials likely influences patterns in soil pH and roadside soil cation pools.

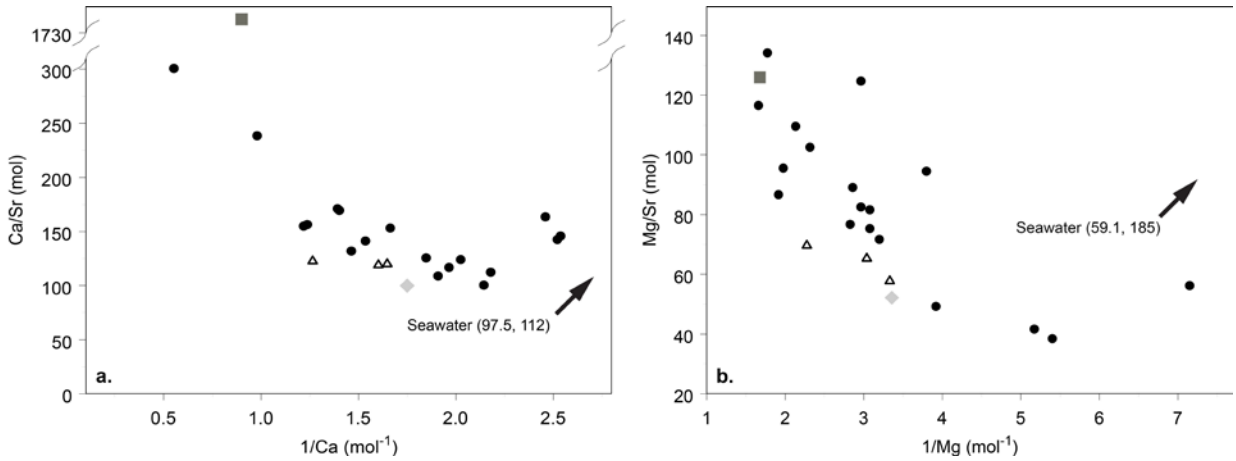

Figure 2-9. Soil calcium (a) and magnesium (b) concentrations normalized with soil strontium concentrations. Park samples are represented by circles, whereas garden medians are represented by triangles. The square represents typical values for cement (Diamond, 1955; Bouzoubaa and Zhang, 1997; Idriss *et al.*, 2009) **and the diamond represents values typical of southern Californian granite** (Dodge, 1972)**. The arrow denotes the position of typical seawater values.**

In addition to influencing soil pH, concrete weathering inputs affect responses to soil acidification. The weak relationship (r^2 = 0.08 & 0.03 respectively) between both soil Ca and Mg concentrations and road proximity (Figure 2-6a) suggests that soil Ca^{2+} and Mg^{2+} pools are not subject to processes driving Al and K pools in the near-road environment. Instead, roadside pools of these cations seem to be replenished. To evaluate the contributions of various Ca and Mg sources we utilize mixing models based on Ca/Sr and Mg/Sr ratios.

Mixing model analysis suggests that primary Ca and Mg source end members are parent material and concrete road materials (e.g., roadways, road drains, curbs, etc.) (Figure 2-9). Ca^{2+} and Mg^{2+} pools with relatively low ratios are dominated by bedrock sources, in particular granitic parent material (Dodge, 1972), whereas the weathering of concrete road materials is the predominant source to samples with relatively high ratios (Diamond, 1955; Bouzoubaa and Zhang, 1997; Idriss *et al.*, 2009). Oceanic aerosols appear to only influence soil Ca concentrations in near-ocean localities, as Ca/Sr ratios in coastal samples are at or near values

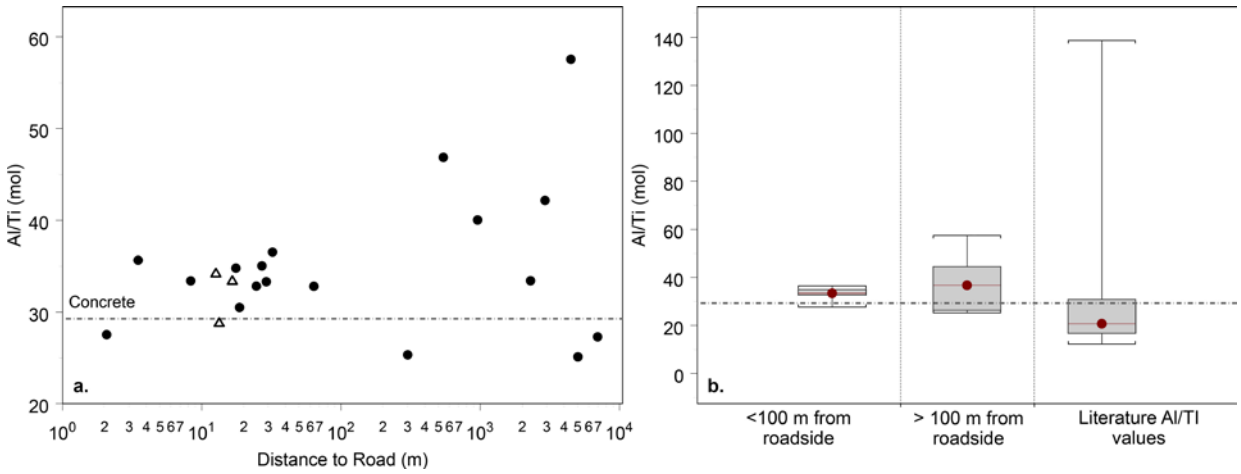

Figure 2-10. Soil aluminum concentrations normalized with soil titanium concentrations versus distance from roadside (a). Park samples are represented by circles, whereas garden medians are represented by triangles. The dashed line represents the Al/Ti typical of Southern Californian concrete dust (Hildemann, 1991). The variability of values in samples collected further from roads likely represents concentration variability in bedrock, as ratios cover a wider range (~12 to 139 n = 511) similar to that found in local granitic intrusives (Piwinskii, 1968; Dodge and Ross, 1971; Dodge, 1972; Baird and Miesch, 1984)**.**

typical of seawater (112) but sample values quickly move away from this ratio as distance from the ocean increases. Annual precipitation is not a significant source of Ca or Mg replenishment, as there is no discernible relationship between annual precipitation and Ca/Sr and Mg/Sr ratios. While several points on the plot suggest another, relatively low Ca, low Sr source, source rock geochemical data is limited, precluding identification of this apparent source.

Observed patterns of other elemental ratios in these soil chemistries are consistent with near road areas being dominated by road inputs. Al/Ti ratios in near-road environments are close to values (29.6) measured in road dusts, sourced via the attrition of road surfaces, in southern California (Figure 2-10) (Hildemann, 1991). Samples collected further from roads increasingly vary across ranges found in local bedrock, including local granitic parent material whose Al/Ti ratios range from ~12 to 139 (Piwinskii, 1968; Dodge and Ross, 1971; Dodge, 1972; Baird and

Miesch, 1984). That is, as one moves closer to the road, Al/Ti ratios converge on values typical of road dust.

While soil Ca^{2+} and Mg^{2+} pools seem to be replenished by concrete and bedrock weathering, the depletion of roadside soil K^{+} pools is not replenished by inputs of weathering products. The low concentration of K in road building materials (<1% by mass in cement) is insufficient to replenish soil pools during concrete weathering (Bouzoubaa and Zhang, 1997; Idriss *et al.*, 2009). Further, K-rich minerals are relatively more resistant to weathering than Ca-rich minerals (Essington, 2004), and local granitic intrusives typically contain relatively lower amounts of K than Ca (Gromet and Silver, 1987). Thus, replenishment of soil K^{+} pools via parent material weathering likely occurs over longer time scales than soil Ca^{2+} or Mg^{2+} pools.

2.5 CONCLUSIONS AND IMPLICATIONS

Patterns observed in roadside soil Al, Be, and K concentrations support the hypothesis that acidification of roadside soils deplete roadside soil cation pools. In particular, the persistence of these patterns, regardless of underlying gradients in bedrock geochemistry, emphasizes the dominance of road inputs on soil chemistry. Soil cation content patterns, driven by roadside exhaust deposition, suggest shifts in fundamental soil chemistry in the roadside environment. While roadside soil K^{+} pools appear to be depleted, in contrast, inputs from road material weathering seem to diminish soil Ca^{2+} pools sensitivity to soil acidification. For example, the average soil Ca concentration in all of the samples (26.8 g kg^{-1}) is higher than the average value recorded in southern Californian soils (23.0 g kg^{-1}) (Shacklette and Boerngen,

1984), despite the depleted concentrations observed in other metals. The insensitivity of calcium and magnesium concentrations to roadside acidification and the source signatures indicated by mixing models confirms that cation depletion in roadside soils is heavily influenced by local geochemistry and human activities.

In particular, the mobilization of major cationic species from near road soils with higher LOI and clay content suggests that trace metals in similar geochemical pools should also be mobilized. Urban soils contain higher concentrations of trace metals (e.g., Bain *et al.*, 2012), and in particular trace metals are heavily deposited at the immediate roadside (Figure 1-1) (Fakayode and Olu-Owolabi, 2003; Nabulo *et al.*, 2006; Clarke *et al.*, 2015a). The mobilization of these metal inputs from roadside soils would exacerbate potential impacts to surrounding biota.

Further, the increased LOI in road side soils suggests that these soils are fertilized via reactive nitrogen inputs. Such fertilization can affect species composition, as N saturation is known to promote the dominance of exotic grass species in coastal sage scrub shrublands (Cione *et al.*, 2002). These alterations can interact to increase wildfire susceptibility (Cione *et al.*, 2002), thereby increasing risks to a variety of coupled systems (Meixner *et al.*, 2006). While the effects of N saturation are well addressed (Aber *et al.*, 1989; Bytnerowicz and Fenn, 1996), little attention has been given to the interaction of soil ecosystem nitrogen status with metal dynamics in near-road ecosystems.

As population centers grow, expanding urban areas (Kabir *et al.*, 2014), and therefore transportation networks, will affect more ecosystems. While metal dynamics resulting from vehicular inputs are reasonably understood, the interaction of these inputs and soil acidification

is not well characterized. This research demonstrates the potential for unexpected interactions potentially detrimental to associated systems. Thus, accounting for the influences of soil acidification on near-road soils seems fundamental to the management and understanding of complicated urban systems.

3.0 HILLSLOPE SOIL WATER FLOWPATHS AND THE DYNAMICS OF ROADSIDE SOIL CATION POOLS INFLUENCED BY ROAD DEICERS

3.1 INTRODUCTION

Over the past sixty years, road deicers (i.e., road salt) have been applied to roadways to improve traffic safety in winter weather (Kelly *et al.*, 2008). In particular, more than 762,000 tonnes of road salt (sodium chloride), have been applied to Pennsylvanian roadways between 2009 and 2014 (PennDOT, 2014). The dissolution of these road deicers in highway runoff creates waters with high total dissolved solids (TDS), which can mobilize roadside soil metals via soil cation exchange reactions (Granato *et al.*, 1995). Additionally, increased loadings of sodium to soil waters can negatively impact soil structure, decreasing soil permeability and exacerbating soil erosion (Amrhein *et al.*, 1992).

While several studies have detailed interactions of high TDS solutions and surface waters (Amrhein *et al.*, 1992; Mason *et al.*, 1999), less attention is given to the impacts of high TDS solutions on near-road soils. As roadways are commonly sited near streams, particularly in valley floors (Jones *et al.*, 2000; Blanton and Marcus, 2009), stresses to roadside ecosystems can also directly or indirectly impair riparian areas. In particular, the mobilization of soil cations via interactions with high TDS solutions (Shanley, 1994; Norrström and Bergstedt, 2001;

Bäckström *et al.*, 2004b) can affect soil cation pools, potentially impacting roadside vegetative communities (Fernandez *et al.*, 2003; Juice *et al.*, 2006; Green *et al.*, 2013) and promote shifts in the species composition of roadside vegetative communities (Bobbink *et al.*, 1998). Stresses to roadside biota can subsequently affect several processes that occur between the road and stream, such as the filtration of chemical pollutants, reduction of erosion, and the lengthening of flowpath.

This study evaluates the flushing of soil exchange sites by road deicer pulses, and the influence of local hydrologic flowpaths on soil cation dynamics. We analyze patterns in soil moisture content and soil water chemistry along a roadside transect and identify likely soil water flowpaths. Additionally, we evaluate roadside soil cation dynamics along the hillslope by examining temporal patterns in soil and soil water chemistry in samples collected between October 2013 and November 2014. In particular, insight from elemental mixing model analysis based on road deicers, soil parent material, and construction materials suggests the influence of these end-members on soil solutions. This study documents roadside salt impacts in the fundamental context of complicated hillslope hydrology, emphasizing the importance of the local hydrologic setting on seasonal cation dynamics in urban ecosystems.

3.2 METHODS

3.2.1 Field Site

Nine Mile Run (NMR) is an urban stream draining 15.7 km^2 of eastern Pittsburgh, PA, USA (Environmental Resources Reseach Institute, 2014) (Figure 3-1). Geology underlying the NMR catchment consists of cyclic sequences of Pennsylvanian age limestone, siltstone, shale, and sandstone (Leighton, 1927). Transect soils are Ultic Hapludalfs (Urban land-Culleoka complex), consisting of silt loams, channery silt loams, and flaggy clay loams (Soil Survey Staff *et al.*, 2013), and range from 74 to 83 cm deep (Figure S3). The long term (1981-2010) mean annual temperature (Arguez *et al.*, 2010) and precipitation (PRISM Climate Group Oregon State University, 2004b) of the NMR watershed are 11 °C and 959 mm respectively. Historically, urbanization has heavily impacted the NMR watershed, as a significant portion of NMR was buried during the 20^{th} century (McElwaine, 2005), and 38% of the watershed is covered with asphalt or roofs (Homer *et al.*, 2004). Because an interstate (I-376) parallels and crosses the stream (Figure 3-1), NMR is an excellent site to examine the interactions of high TDS (road salt) solutions and soil metals.

Sodium chloride, either applied directly to roadways or as a 23.3% brine, is the only road deicer applied to roadways within our study area (Angelo Pampina, PennDOT, personal communication, 2014). The drainage system of the reach of I-376 perpendicular to the study transect appears to be comprised of primarily surface storm drain inlets (Figure 3-2a), and thus most surface water from the roadway does not reach study transect soils (Figure 3-2b).

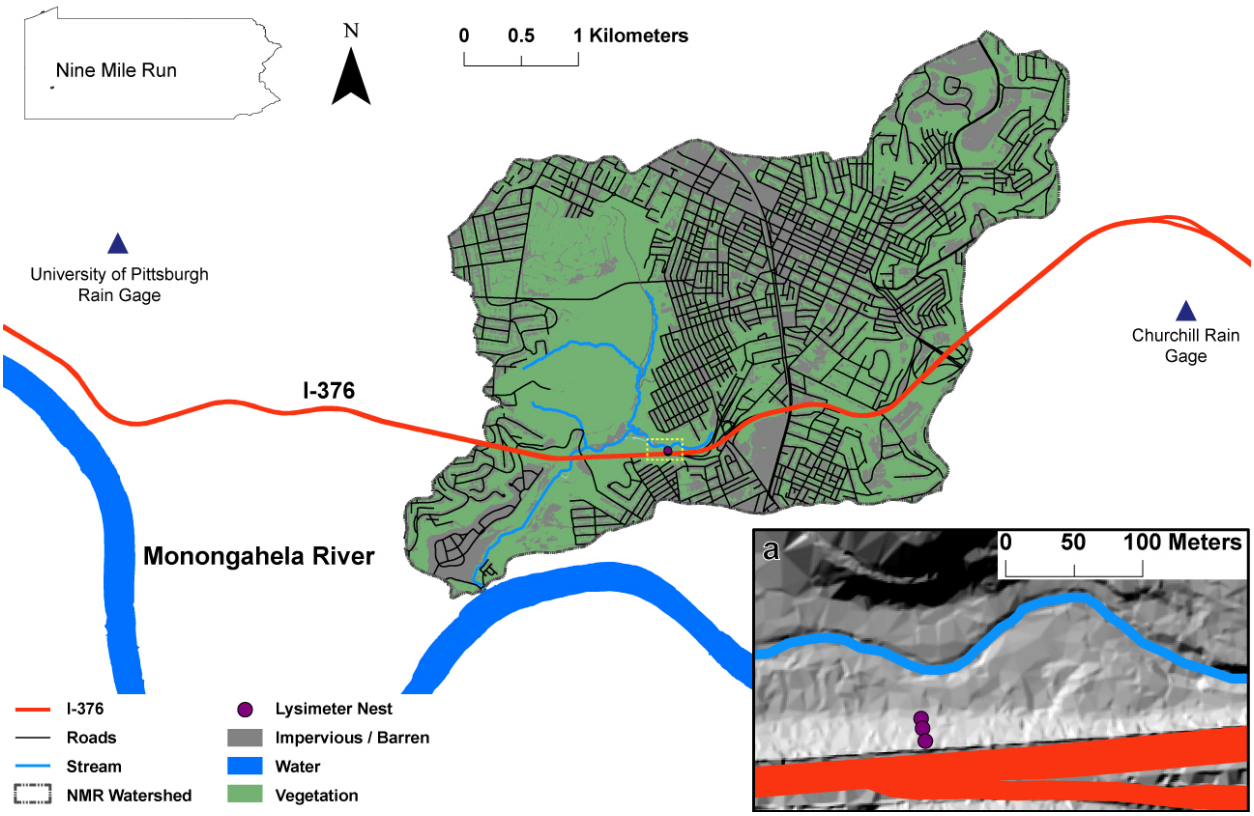

Figure 3-1. Map of the Nine Mile Run watershed which drains 17.4 km^2 of eastern Pittsburgh, and major roads contained within the watershed. Additionally, impervious (urban) and vegetated surfaces are shown (Homer *et al.*, 2004). Inset (a) provides hillshaded LiDAR terrain (1 m resolution) (PAMAP Program PA Department of Conservation and Natural Resources Bureau of Topographic and Geologic Survey, 2006) and details the roadside lysimeter sampling transect, its orientation relative to I-376 (Allegheny County Division of Computer Services Geographic Information Systems Group, 2006) and Nine Mile Run, and locations of soil water sampling nests.

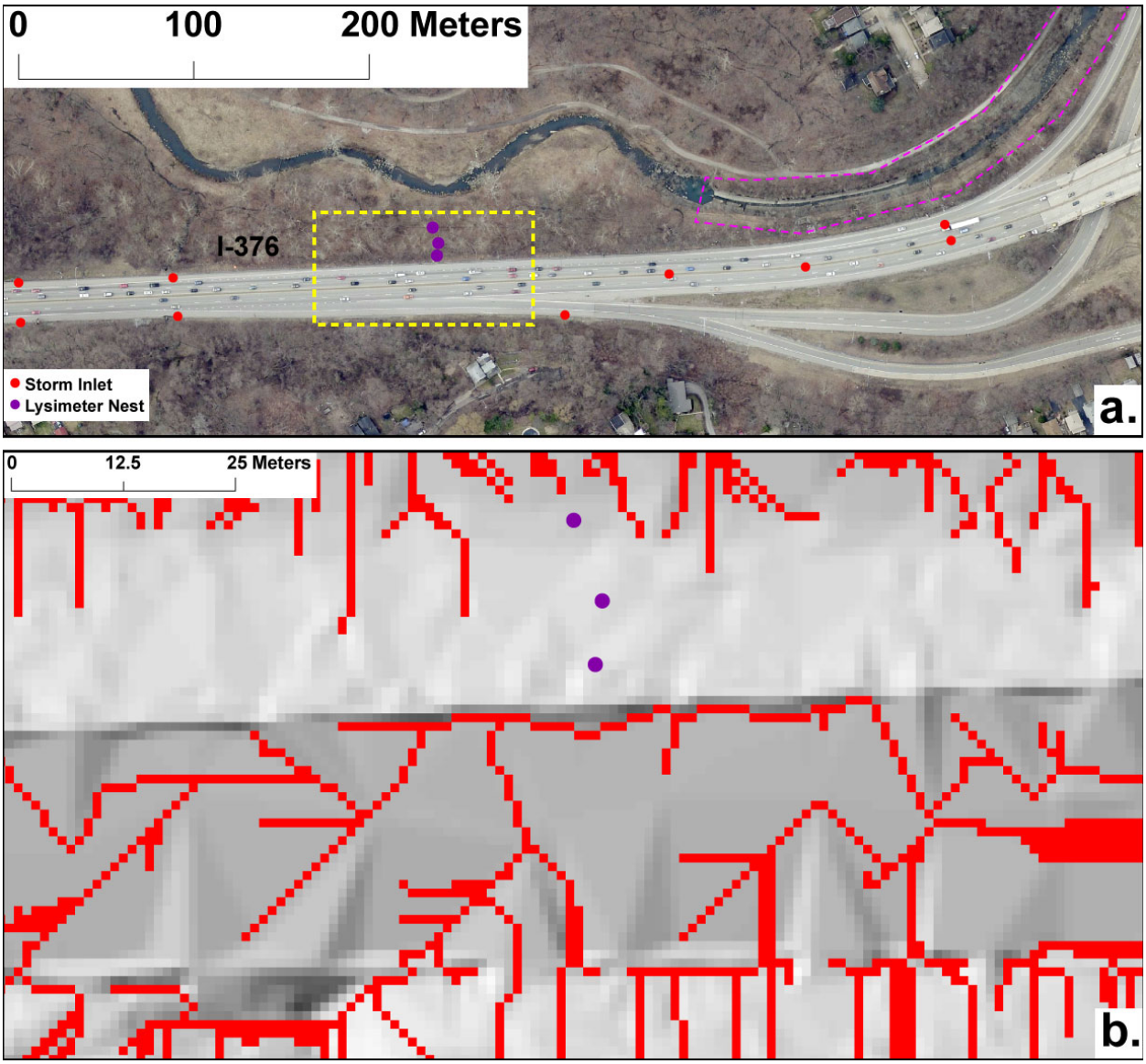

Figure 3-2. In panel a, the *red dots* indicate the location of storm drain inlets located along the reach of I-376 near the study transect (*purple dots*). The *dashed purple box* highlights the portion of Nine Mile Run where numerous sewer out falls are located. Panel b shows surface water flow paths within the *dashed yellow box* in panel a derived from a 1 meter LiDAR DEM (PAMAP Program PA Department of Conservation and Natural Resources Bureau of Topographic and Geologic Survey, 2006).

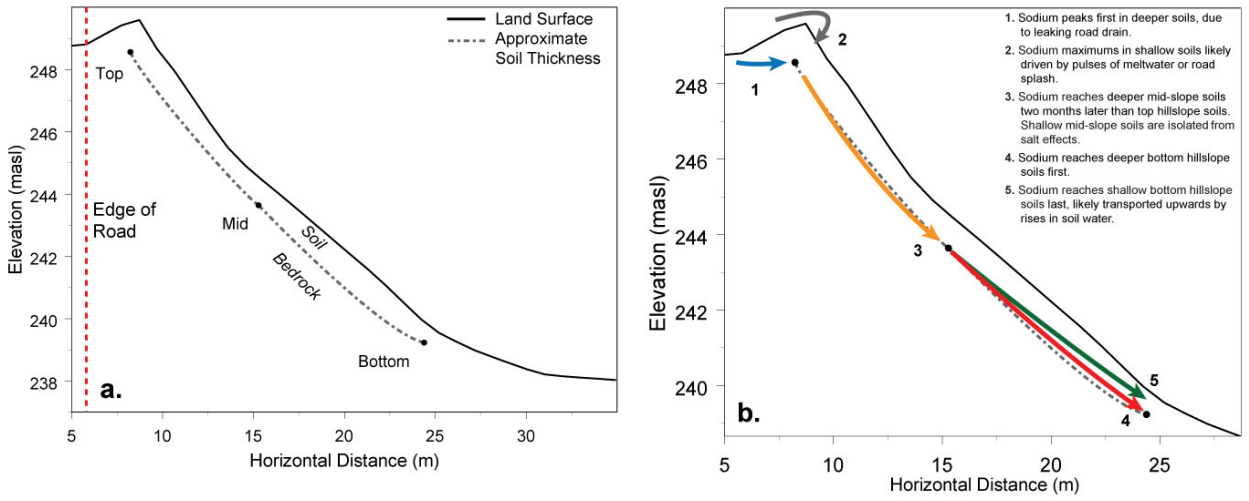

Figure 3-3. Elevation profile of the sampling transect,(PAMAP Program PA Department of Conservation and Natural Resources Bureau of Topographic and Geologic Survey, 2006) and approximate soil thickness of the hillslope (a). The relatively thicker soils at the top and mid slope nests likely reflect hillslope cutting and subsequent filling during the roadbed grading for I-376. Panel b provides a conceptual model summarizing the multiple hillslope soil water flow paths and how they affect hillslope sodium transport. The *numbers* and *colors* indicate the relative timing of the flowpaths.

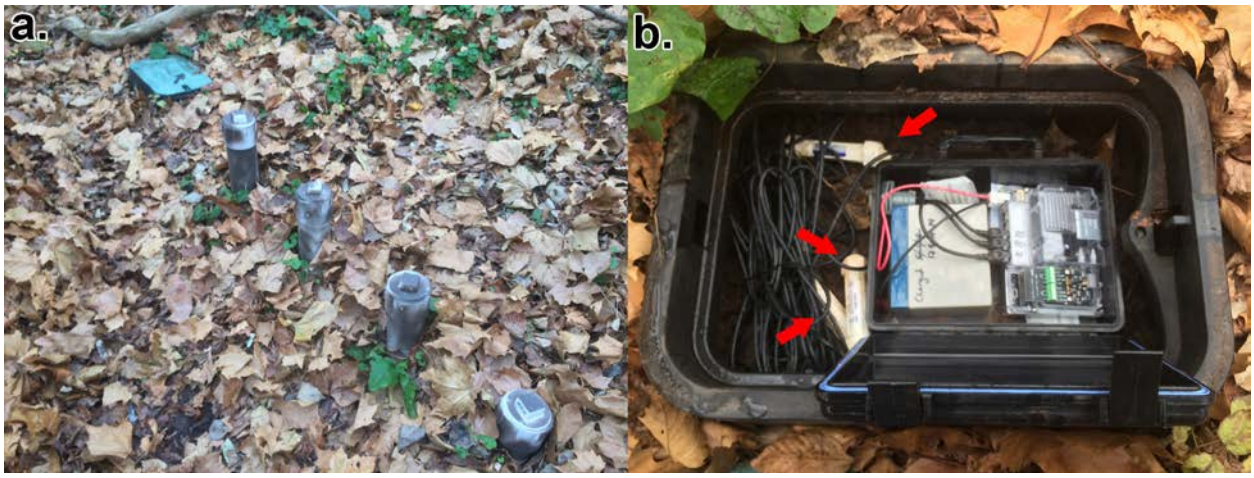

Figure 3-4. Detail of a soil moisture sampler nest (a) and soil moisture array (b)

Table 3-1. Depths of equipment installation, and the distance of soil moisture arrays and lysimeter nests from the edge of the highway.

Depth (cm)	Distance From Road (m)	Depth (cm)	Distance From Road (m)
Top-Slope Lysimeter Nest		*Mid-Slope Soil Moisture Probe Array*	
14	8.24	21	11.9
39	8.24	41	11.9
61	8.24	65	11.9
83	8.24	*Bottom-Slope Moisture Probe Array*	
Mid-Slope Lysimeter Nest		20	24.4
19	15.3	40	24.4
28	15.3	62.5	24.4
49	15.3		
80	15.3		
Bottom-Slope Lysimeter Nest			
19	24.4		
28	24.4		
53	24.4		
74	24.4		

3.2.2 Equipment Installation

The sampling transect, consisting of three porous cup suction lysimeter "nests" (Figure 3-3, Figure 3-4a), and two soil moisture monitoring "arrays" (Figure 3-4b) was installed during July and August of 2013. Each nest contains four soil water samplers (suction cup lysimeters, Soil Moisture Corp), which sample soil water at roughly 20, 40, 60, and 80 cm depths along a hill slope perpendicular to I-376 (Table 3-1). Similarly, each array (HOBO U30 data logger; Onset S-SMC-M005 Soil Moisture Sampler) measures soil moisture at roughly 20, 40, and 60 cm depths (Table 3-1). Prior to installation, suction cup lysimeters were soaked for 24 hours in 1 N HCl and rinsed three times with 18 mΩ water to clean potential adsorption sites in the ceramic cups

(Grover and Lamborn, 1970).

Soil water samplers (suction cup lysimeters, Soil Moisture Corp) were installed in July and August of 2013. The location of the sampling transect was selected due to the ease of access to I-376, and the proximity to the continued examination of biogeochemical processes in the Nine Mile Run watershed. Bore holes were created with a 2 inch bucket auger. During installation, soil samples were collected from excavated material in 10 – 20 cm increments. Excavated material was stored and used as backfill in the order that it was removed. Material from the bottom of the bore hole was sieved to 2 mm and backfilled to ensure adequate hydraulic conductivity between the ceramic cup and soil. Lysimeters were given approximately two months to equilibrate with local soil. During this period, soil solution samples were drawn and discarded every other week, to flush ceramic cups. After all lysimeters were "flushed" at least three times, samples were analyzed for metal chemistry.

Soil moisture arrays (HOBO U30 data logger; Onset S-SMC-M005 Soil Moisture Sampler) were installed in a similar manner. Bore holes were created with a 4 inch bucket auger, and moisture probes were inserted perpendicularly to the borehole wall at 20, 40, and 60 cm depth increments. Prior to installation, the functionality of soil moisture sensors was ensured by measuring air and 18 mΩ water (Onset, 2014). Smart sensor adapters (Figure S4b, *arrows*), were sealed with marine epoxy to ensure they were waterproof. Data loggers were housed in modified dry boxes (Underwater Kinetics 309 Dry Box), which were filled with silica desiccant pouches.

To protect against elemental damage (e.g., UV damage to plastic tubing) and vandalism, the above ground portions of suction cup lysimeters were housed in 4 inch PVC pipe (Figure

3-4a) (Crabtree and Seaman, 2006). Likewise, soil moisture data loggers were housed in irrigation boxes (Figure 3-4b).

3.2.3 Sample Collection

To characterize the chemistry of the local soil, soil samples were collected at roughly 10 cm depth increments during lysimeter installation. Likewise, samples of bedrock collected from the bottom of the soil auger hole (n = 10) were collected during soil moisture probe installation to characterize the chemical composition of local parent material. PennDOT road salt samples (n = 2) were collected from a PennDOT District 11 stockpile in Pittsburgh, PA. Soil water samples (n = 124), were collected approximately monthly between Oct 2013 and Nov 2014. In some cases (during frozen or dry periods) water was not present during collection. Soil water samples were stored in 60-mL HDPE bottles, acidified with nitric acid, and refrigerated. Sampling frequency during the salting season (i.e., November – April) was controlled by the occurrence of thaw events. Thus, soil water samples during this time period capture the flushing of soil exchange sites via road runoff, as thaw events produce pulses of high TDS meltwaters which can infiltrate roadside soils (Fay and Shi, 2012).

3.2.4 Laboratory Analysis

Soil samples, collected during equipment installation, were dried at 50 °C for 48 hours, divided, and a portion powdered in a ball mill (tungsten carbide). Soil fine particle grain size (0.75 – 995.6 μm) distribution was measured in non-powdered samples using a laser particle

counter (Microtrac S3500). Calculated surface (CS) of the non-powdered samples was determined using the Microtrac FLEX software (Plantz, 2009). Soil organic matter was measured via LOI (Loss On Ignition), determined by combusting the dried sample in a muffle furnace at 550 °C for 4 hours. Parent material samples (powdered in a ball mill) and PennDOT road salt samples were totally digested in aqua regia (3:1, vol/vol, concentrated, sub-boil distilled hydrochloric and nitric acid) to determine total metal concentrations. Sorbed and exchangeable metal concentrations in soil samples were measured using a weak acid extraction (10% nitric acid). Soil water samples were analyzed for cation (Ca^{2+}, K^{+}, Li^{+}, Mg^{2+}, Na^{+}, Rb^{+}, Si^{4+}, Sr^{2+}) concentrations (Perkin-Elmer Nexion ICP-MS) and Cl^{-} concentrations (Dionex ICS2000 Ion chromatograph). One improbable soil water chloride concentration data point was identified and removed, because it could not be checked as all remaining sample had been acidified. Cation source provenance was determined via mixing model analysis (Faure and Mensing, 2005). In mixing model analysis, elemental ratios are compared amongst collected samples and endmembers to evaluate the influence of endmembers on observed water and soil chemistry.

The influence of subsurface flowpaths on soil water sodium concentration patterns was determined by comparing soil water silicon and sodium concentrations. Specifically, ground waters contain relatively increased silicon concentrations, due to increased contact time between waters and geologic materials. Thus soil water silicon concentrations are used as a proxy for the contribution of groundwater to the samples (Uhlenbrook *et al.*, 2000; Uchida *et al.*, 2003; Rodgers *et al.*, 2004).

3.2.5 Soil Moisture and Precipitation Event Analysis

Precipitation amounts (mm) were measured at 15 minute intervals at rain gages located 5.35 and 4.50 km from the sampling transect (Three Rivers Wet Weather, 2014) (Figure 3-1). Precipitation data from the "University of Pittsburgh" rain gage was primarily used, however between 26 November 2013 and 5 December 2013 the "University of Pittsburgh" rain gage appeared to be malfunctioning, thus precipitation data from the "Churchill" gage was used to fill the data gap. Air temperature (°C) was logged at hourly intervals at the Allegheny County Airport, located 8.64 km from the sampling transect (NOAA National Climatic Data Center, 2014). The salting season was defined as beginning on the first day the overnight air temperate remained below 0°C for at least 8 hours and ending on the last day the overnight air temperate remained below 0°C for at least 8 hours. The growing season was defined as the period between the first and last hard frosts (i.e., 4 consecutive hours where the air temperature is below −3.89°C). Soil moisture content was logged in 5 minute intervals. However, at several points the soil moisture record is not continuous for various reasons (e.g., cold temperatures draining the data logger batteries). Relative saturation (Θ_{rel}, in %) was determined by normalizing the average daily soil moisture value for the day of sample collection by the maximum soil moisture value recorded for each probe over the entire sampling period (1).

$$SMC_{max} \div \overline{SMC}_{daily} \quad \textbf{(1)}$$

Discreet precipitation events were determined with the hydromad R package (Andrews *et al.*, 2011), and classified using natural breaks analysis into low, medium, and high precipitation volume events. The change in soil water storage (ΔSWS) was defined as the

change in soil moisture content during a storm event multiplied by the depth of the soil moisture sensor (2), and used to determine the influence of precipitation events on soil moisture status (Zhu *et al.*, 2014).

$$\Delta SWS_{S1} = (\Theta_{S1max} - \Theta_{S1ant}) \times h_1$$
$$\Delta SWS_{S2} = [(\Theta_{S2max} - \Theta_{S2ant}) \times h_2] + \Delta SWS_{S1} \quad \textbf{(2)}$$
$$\Delta SWS_{S3} = [(\Theta_{S3max} - \Theta_{S3ant}) \times h_3] + \Delta SWS_{S2}$$

Additionally, the lag in soil moisture response to precipitation events (t_{lag}) was determined by comparing the timing of precipitation events and periods of elevated soil moisture content (Figure 3-6). The duration of elevated soil moisture (t_{dur}), determined by the hydromad R package, was defined as the difference between the time when the instantaneous slope of the soil moisture content changed by 10% or more, and the time when changes in the instantaneous slope of the soil moisture content were less than 10%. Soil moisture events that preceded the start of precipitation events by 15 minutes (i.e., t_{lag} = -15 min) were assumed to result from the difference in soil moisture and precipitation data logging intervals (5 and 15

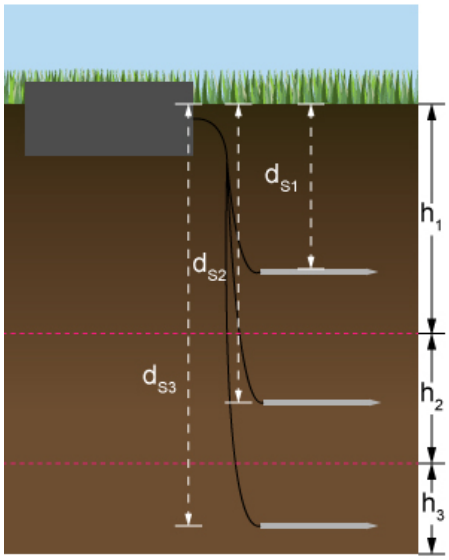

Figure 3-5. Determination of the thickness (h) of soil each probe is considered to represent.

minutes respectively) and set equal to zero.

Storms events began when measured precipitation exceeded 0.1 mm. Two hours was selected as the minimum amount of time between separate storm events, if any more precipitation events occurred within this 2 hour gap they were summed into the surrounding event. Similarly, a 2 hour buffer was attached to the end of each storm event, and if any subsequent events intersected this buffer, they were merged into the preceding event.

The duration of each soil moisture event was determined by the hydromad package.

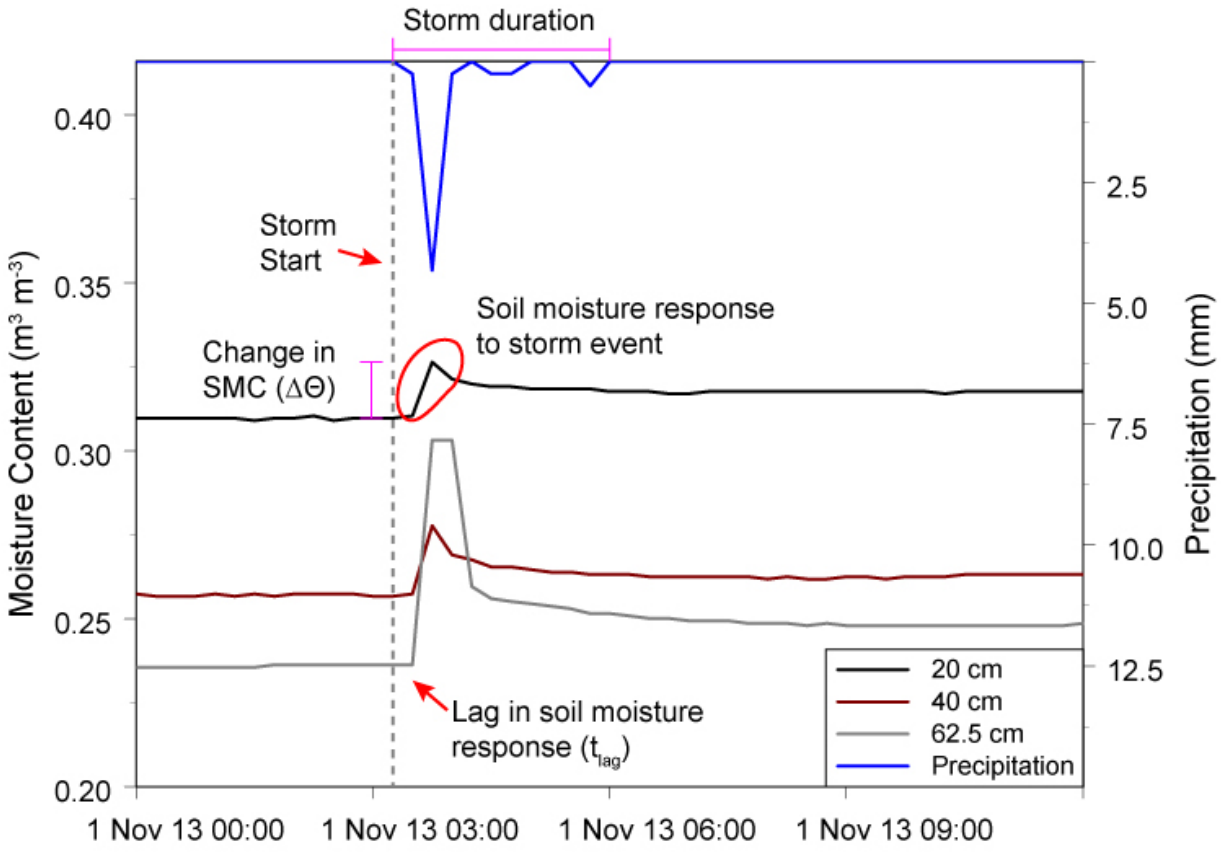

Figure 3-6. Example of a storm event, the subsequent soil moisture response to the storm event (*circled*), and the soil moisture metrics measured during each storm event. The change in soil moisture content (SMC, or ΔΘ) was determined by subtracting the antecedent soil moisture from the maximum soil moisture content recorded during the storm event.

Specifically, events began when the instantaneous slope of the soil moisture content changed by 10% or more, and events ended when changes in the instantaneous slope of the soil moisture content were less than 10%. The difference between these two times was defined as the duration of elevated soil moisture (t_{dur}).

3.3 RESULTS

3.3.1 Soil Physical Characteristics

In general, soils collected from the mid-slope station have the highest organic matter content, and soils from the bottom slope station have the lowest organic matter content (Figure 3-7a). Soil organic matter content spikes at approximately 30 cm depth in the mid-slope soils, however this spike is largely absent in top and bottom slope soils. Soil particle calculated

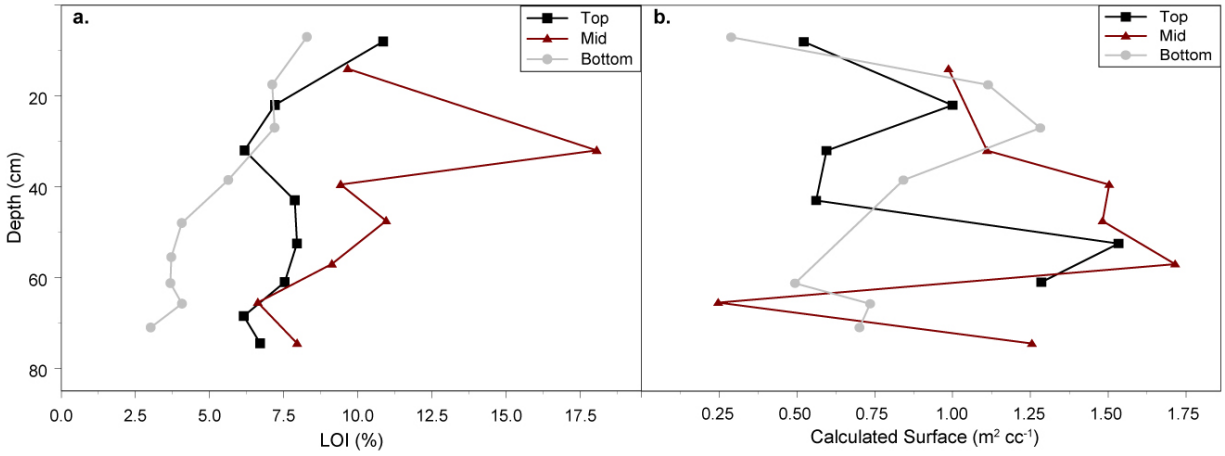

Figure 3-7. Soil organic matter (LOI) (a) and soil particle calculated surface (CS) (b) versus depth. Calculated surface was not measured in some samples because these samples were completely powdered in preparation for trace metal analysis.

surface (CS) also is the highest, in general, at the mid slope nest (Figure 3-7b).

3.3.2 Soil Moisture Response to Precipitation Events

During the period of record there were a total of 184 precipitation events, which were classified into low (0.10-0.76 mm, n = 46), medium (0.76-10.2 mm, n = 95), and high (10.2-57.4 mm, n = 38) precipitation events. Of these events, 27 occurred during subzero air temperatures, and were thus considered to be primarily snowfall events. Soil moisture events detected decreased with sensor depth, with the maximum number of soil moisture events (59) occurring in the shallow (21 cm depth) mid-slope soil soils (Table 3-2). Of the 38 soil moisture events observed in the 65 cm depth mid-slope soils, four events occurred without associated events in shallower, overlying soil layers. At the bottom slope soil moisture probe array, 41 soil moisture events were detected at both 20 and 40 cm depths (Table 3-2). The 62.5 cm depth bottom slope soil moisture probe malfunctioned throughout the sampling period.

Table 3-2. Summary of soil moisture response to storm events.

Depth (cm)	Events	Mean t_{lag} (min)	Min t_{lag} (min)	Med t_{lag} (min)	Max t_{lag} (min)	Mean t_{dur} (min)	Min t_{dur} (min)	Med t_{dur} (min)	Max t_{dur} (min)	ΔSWS>P	ΔSWS<P
Mid-Slope Moisture Probe Array											
21	59	486	-90	165	3915	231	135	210	735	21	**38**
41	42	417	-30	188	4020	235	135	195	495	14	**28**
65	39	900	-150	360	7335	212	150	195	450	**24**	15
Bottom-Slope Soil Moisture Probe Array											
20	42	236	-300	120	1770	294	135	255	660	3	**39**
40	42	421	-150	217	2490	249	135	195	675	19	**23**
*62.5**	N/A	N/A	N/A	N/A	N/A	N/A	N/A	N/A	N/A	N/A	N/A

*data from this probe was not included in analysis due to equipment malfunction

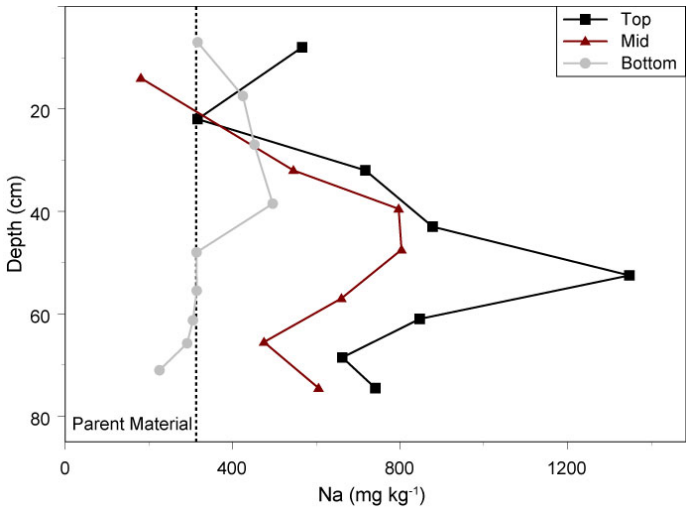

Figure 3-8. Soil sodium concentrations versus depth for the top (*boxes*), mid (*triangles*), and bottom (*circles*) slope stations. The *dashed line* is the average sodium concentration in parent material samples.

In general, periods of elevated soil moisture in the mid-slope soils persist the longest at 41 cm depth, and the shortest at 65 cm depth (Table 3-2). This relationship (i.e., the duration of wet periods decreasing with soil depth) is also observed in the bottom slope soils, as the average duration of soil moisture events is the longest at 20 cm depth (Table 3-2). During soil moisture events at all stations, precipitation inputs exceed soil water storage (SWS) in the shallow and mid depth soils (Table 3-2). However, in the deep (65 cm depth) mid-slope soils SWS exceeds precipitation inputs (Table 3-2).

3.3.3 Sodium and Chloride Concentration Patterns

Because sodium chloride is the only road deicer applied to roadways within our study area (Angelo Pampina, PennDOT, personal communication, 2014), we expect soil sodium (Na)

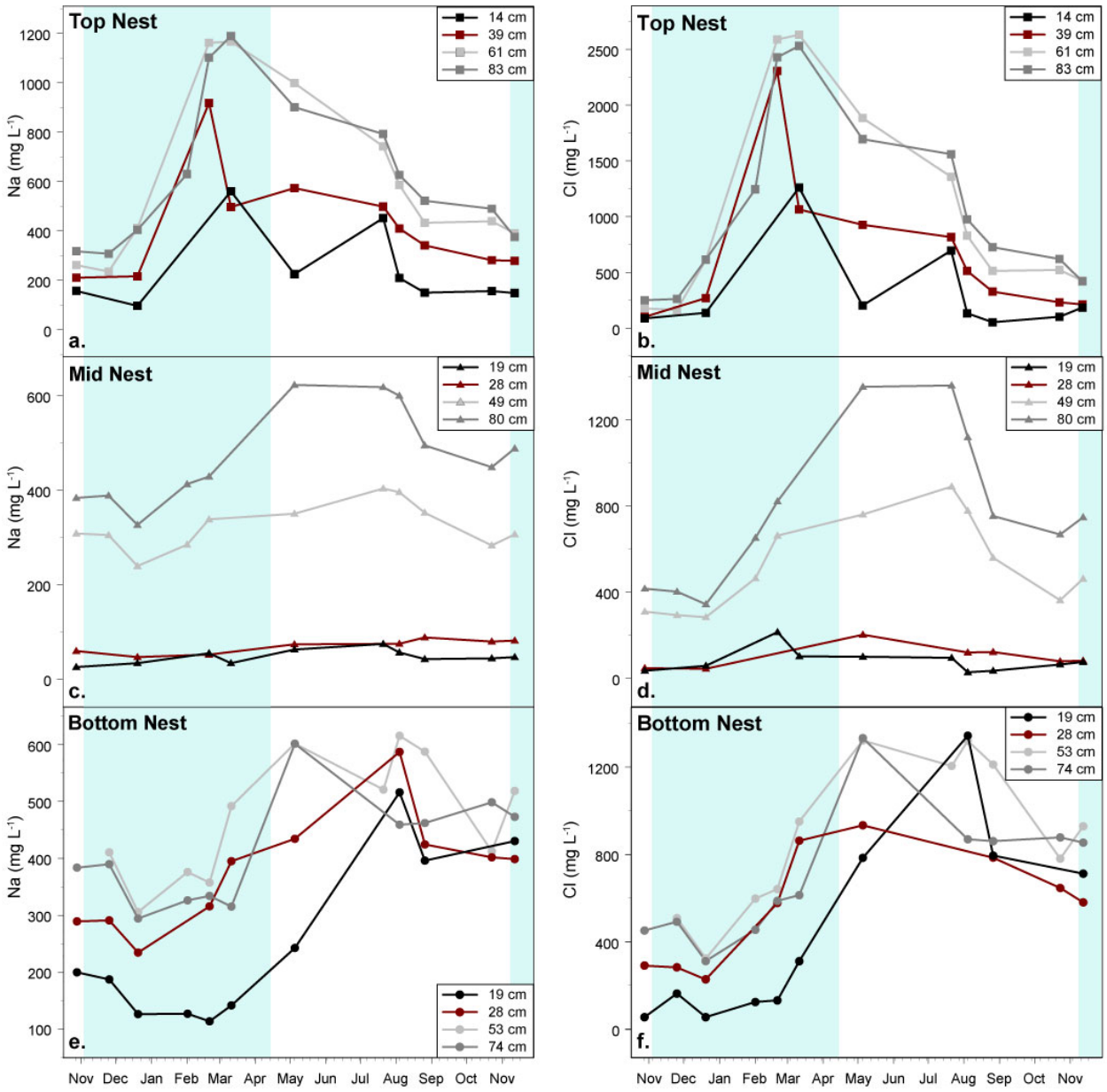

Figure 3-9. Measured soil water sodium and chloride concentrations in the top slope nest (a, b, respectively), mid slope nest (c, d, respectively), and bottom slope nest (e, f, respectively) over the one year sampling period. In all panels the *color* of the shape distinguishes the sampling depth. *Shaded boxes* designate the period when road salt is applied to roadways.

concentrations to be elevated by road deicing. In our samples, weakly extracted soil Na concentrations are highest in soils collected from the top slope station (Figure 3-8). Soil Na concentrations (weak extract) decrease with distance from the roadway (i.e., downslope),

approaching values observed in sampled parent materials (Figure 3-8 *dashed line*). Furthermore, at all sampling stations, weakly extracted Na concentrations peak at approximately 35 – 50 cm in depth, and decrease in deeper soils. While this pattern is apparent in the soil depth profile of each station, the maximum concentration decreases with increasing distance from the roadside (Figure 3-8).

Distance from the roadside also influences the timing of soil water Na^+ and Cl^- concentration maximums, as Na^+ and Cl^- concentrations in sampled soil waters peak at different times throughout the year relative to the location of the sampling nest. Soil water Na^+ and Cl^- concentration maximums are associated with relative soil water saturation (r^2 = 0.44 and 0.21, respectively), specifically, both soil water Na^+ and Cl^- concentrations increase with increasing relative soil water saturation. In particular, the earliest soil water Na^+ and Cl^- concentration maximums occur in the top nest soil waters in late February/early March in the intermediate depth (39 and 61 cm depth) lysimeters (Figure 3-9a & b).

The seasonal trend in soil water Na^+ and Cl^- concentrations at the top nest station is generally independent of sampling depth, however at the mid-slope nest shallow soil water Na^+ and Cl^- concentrations display seasonality whereas and deep soil water Na^+ and Cl^- concentrations do not. In particular, soil water Na^+ and Cl^- concentrations peak only in the deeper soil waters (49 and 80 cm depth) of the mid-slope nest. Additionally, Na^+ and Cl^- concentrations in the two deepest lysimeters are noticeably higher than the two shallowest lysimeters (Figure 3-9c & d). Furthermore, the peak in soil water Na^+ and Cl^- concentrations at the mid-slope nest (early May) lags the peak in soil water Na^+ and Cl^- concentrations at the top slope nest (early March) by roughly two months.

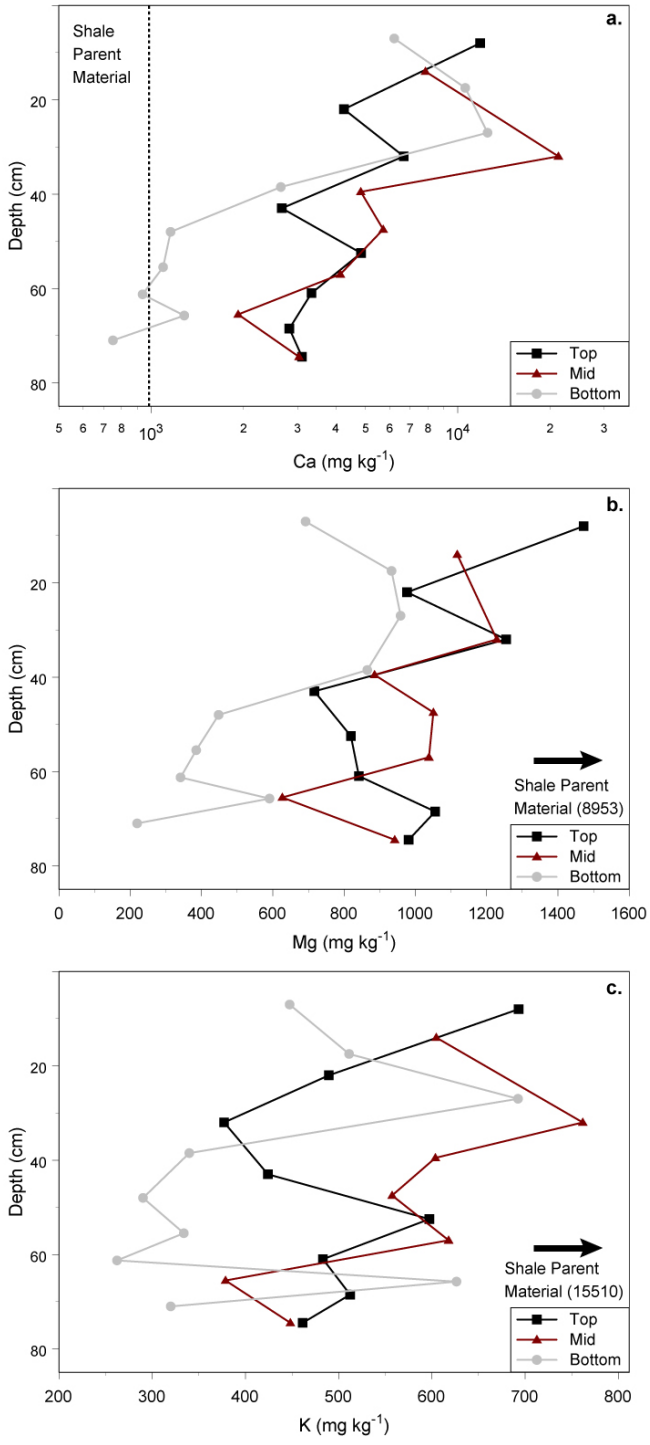

Figure 3-10. Soil calcium (a), magnesium (b), and potassium (c) concentrations versus depth for the top (*boxes*), mid (*triangles*), and bottom (*circles*) slope stations. The *dashed line* or *arrow* designates the average respective elemental concentration in parent material samples.

Similar to the lag in the timing of peak soil water Na^+ and Cl^- concentrations between the top and middle nests, the bottom nest lags the middle nest. However, there is also an additional lag between the timing of soil water Na^+ and Cl^- peaks in the shallow (19 and 28 cm) and deep (53 and 74 cm) soil waters (Figure 3-9e & f). Specifically, Na^+ and Cl^- concentrations in soil waters collected from the 53 and 74 cm depths both increase in early May (Figure 3-9e & f), whereas Na^+ and Cl^- concentrations in the shallow soil waters generally peak in early August (Figure 3-9e & f).

3.3.4 Soil Major Cation Concentration Patterns

Unlike weakly extracted soil Na concentrations, soil calcium (Ca), magnesium (Mg), and potassium (K) concentrations do not appear to be related to the distance from the roadway. In particular, soil samples from the mid-slope nest generally have the highest Ca, Mg, and K concentrations (Figure 3-10). However, deeper (i.e., > 35 cm depth) top slope soils are relatively enriched with Ca and Mg in comparison to deeper bottom slope soils (Figure 3-10a). Specifically, Ca concentrations decrease with sampling depth, and approach values typical of sampled parent material in the deeper bottom slope samples. However, soil magnesium (Mg) (Figure 3-10b), or potassium (K) (Figure 3-10c) concentrations are not enriched in comparison to parent material values. Instead, soil Mg and K concentrations appear to be roughly an order of magnitude lower than values observed in local parent materials.

While weakly extracted Ca, Mg, and K concentrations in soil samples are poorly, or not at all related to Na concentrations (r^2 = 0.002, 0.12, and 0.07, respectively), Ca^{2+} and Mg^{2+}

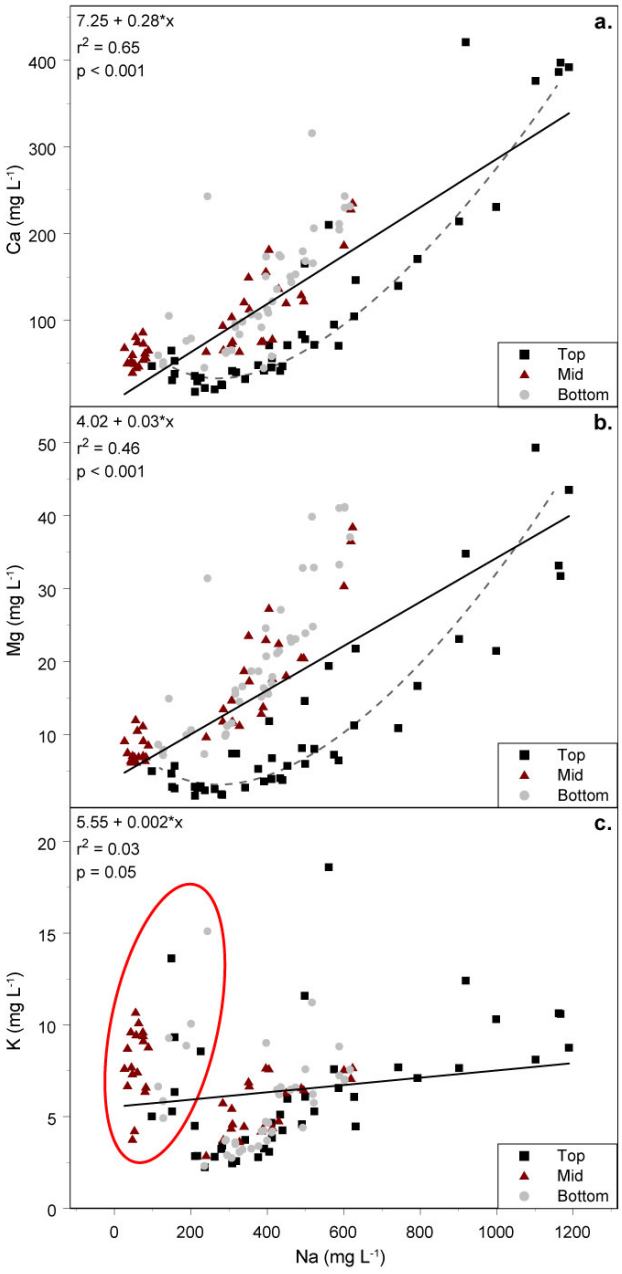

Figure 3-11. Soil water calcium (a), magnesium (b), and potassium (c) concentrations versus soil water sodium concentrations. Samples collected from the top slope nest are indicated by *black squares*, mid slope nest by *red triangles*, and bottom slope nest by *light grey circles*. The *dashed lines* (a,b) highlight the different trend lines which appear to be driven by distance from the roadside. Samples within the *red circle* in panel c are shallow samples from all nests in the transect (i.e., < 20 cm depth at the top and bottom slope stations and < 30 cm depth at the mid-slope station).

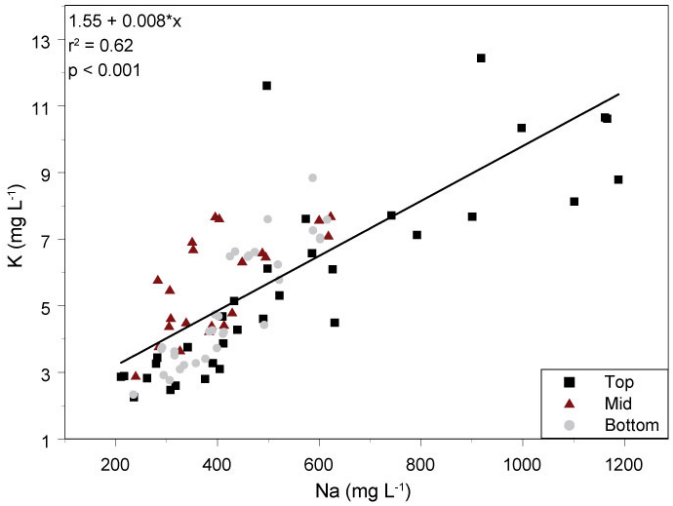

Figure 3-12. Soil water potassium concentrations versus soil water sodium concentrations in soil water samples collected from > 20 cm depth at the top and bottom slope stations, and > 30 cm depth at the mid slope station. Samples collected from the top slope nest are indicated by *squares*, mid slope nest by *triangles*, and bottom slope nest by *circles*.

concentrations are related to Na^+ concentrations in sampled soil water (r^2 = 0.65 and 0.46 respectively) (Figure 3-11a &b). Although both Ca^{2+} and Mg^{2+} concentrations increase with increasing Na^+ concentrations, the process driving this relationship seems to vary among the stations. In particular, the majority of top slope soil waters are relatively enriched with Na^+ in comparison to Ca^{2+} and Mg^{2+} (Figure 3-11a &b, *dashed lines*). However, at all lysimeter nests, only deeper (i.e., > 20 cm depth at the top and bottom slope stations and >30 cm depth at the mid-slope station) soil water K^+ concentrations appear to relate to soil water Na^+ concentrations (Figure 3-12, r^2 = 0.62). Conversely, shallow (i.e., < 20 cm depth at the top and bottom slope stations and < 30 cm depth at the mid-slope station) soil water K^+ concentrations are more weakly related (r^2 = 0.14) to soil water Na^+ concentrations (Figure 3-11c, *circled*).

Soil water Ca^{2+}, and Mg^{2+} concentrations follow seasonal patterns similar to Na^+ and Cl^-. Specifically, the timing of soil water Ca^{2+} and Mg^{2+} concentration maximums (Figure 3-13) occur

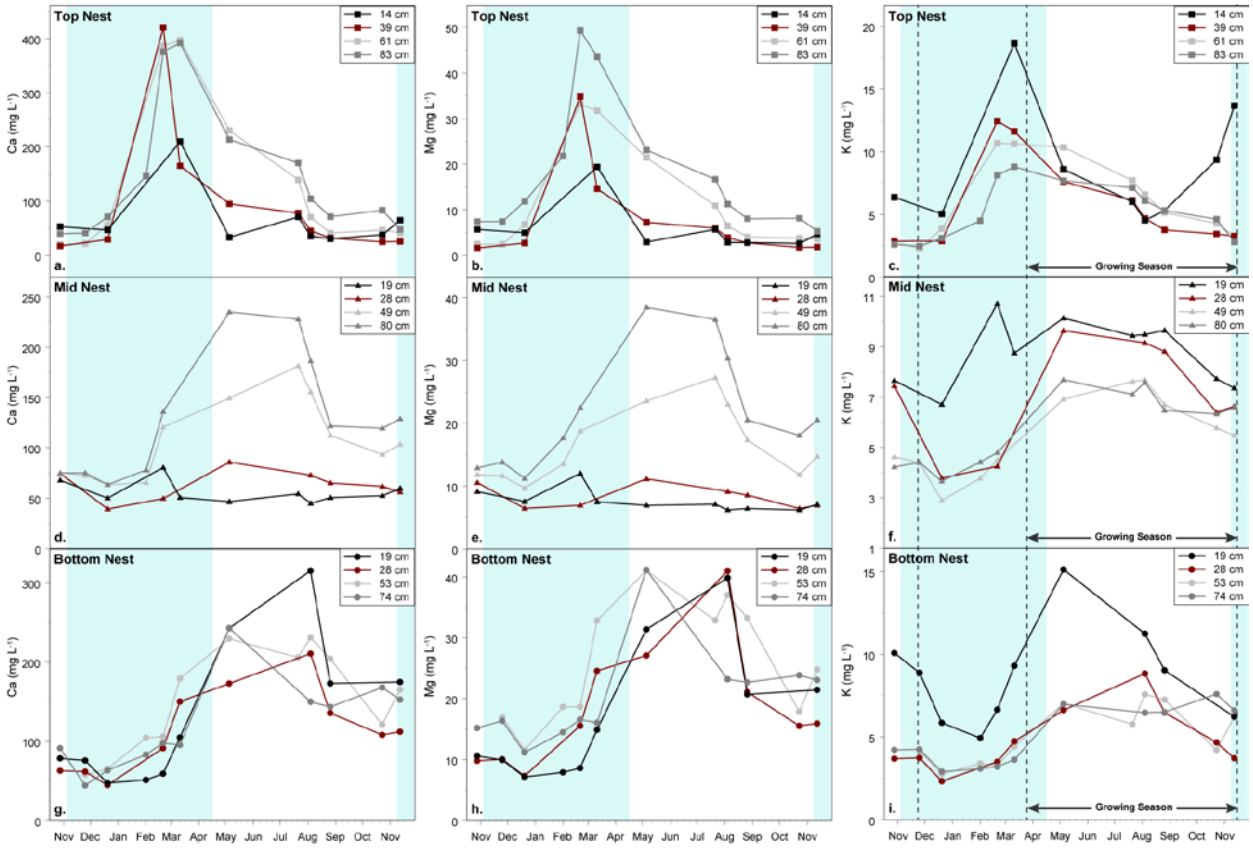

Figure 3-13. Measured soil water calcium, magnesium, and potassium concentrations in the top slope nest (a, b, c, respectively), mid slope nest (d, e, f, respectively), and bottom slope nest (g, h, i, respectively) over the one year sampling period. In all panels the *color* of the shape distinguishes the sampling depth. *Shaded boxes* designate the period when road salt is applied to roadways, and in panels c, f, and i dashed *vertical lines* indicate the end and beginning of the growing season.

at the same time as soil water Na and Cl^- (Figure 3-9) concentration maximums. Also, the highest Ca^{2+} and Mg^{2+} concentrations occur in top slope soil waters during late February and early March (Figure 3-13a & b). Furthermore, peaks in soil water Ca^{2+} and Mg^{2+} concentrations only occur in deeper mid-slope soil waters, and no seasonal trend is present in shallow mid-slope soil water Ca^{2+} and Mg^{2+} concentrations (Figure 3-13d & e). Similarly, peaks in shallow bottom slope soil water Ca^{2+} and Mg^{2+} concentrations lag peaks in deeper bottom slope soil water Ca^{2+} and Mg^{2+} concentrations (Figure 3-13g & h).

The timing of soil water K^+ concentration maximums also generally mimic the timing of soil water Na^+ and Cl^- concentration maximums. However, several discrepancies exist between seasonal patterns in soil water K^+ concentrations and seasonal patterns in soil water Na^+ and Cl^- concentrations. Firstly, there is a second increase in shallow (i.e., 14 cm depth) top slope soil water K^+ concentrations, that is not present in other elements (Figure 3-13a-c). Furthermore, while in general at the top slope nest, the lowest Na^+ (Figure 3-9a), Cl^- (Figure 3-9b), Ca^{2+} (Figure 3-13a), and Mg^{2+} (Figure 3-13b), concentrations occur in shallow soil waters, these same waters have the highest K^+ concentrations (Figure 3-13c). Additionally, although no seasonal trend exists in Na^+ (Figure 3-9c), Cl^- (Figure 3-9d), Ca^{2+} (Figure 3-13d), and Mg^{2+} (Figure 3-13e) concentrations in the shallowest (i.e., 19 and 20 cm depth) sampled mid-slope soil waters, K^+ concentrations exhibit a seasonal pattern in all sampled mid-slope soil waters (Figure 3-13f). Lastly, K^+ concentrations in shallow (i.e., 19 cm depth) bottom slope soil waters are noticeably higher that K^+ concentrations in soil water samples collected from other depths (Figure 3-13i), unlike Na^+ (Figure 3-9c), Cl^- (Figure 3-9d), Ca^{2+} (Figure 3-13d), and Mg^{2+} (Figure 3-13e) concentrations in these sampled soil waters.

3.4 DISCUSSION

3.4.1 Soil Moisture Response Suggests Multiple Flowpaths

The discrepancies in soil moisture response to storm events suggest that multiple soil flowpaths interact with mid hillslope soils. Specifically, and as expected, most (n = 59) soil

moisture events occur in the shallow (21 cm depth) mid-slope soils, suggesting these soils are most affected by infiltration from precipitation events. Moreover, precipitation inputs exceed the change in soil water storage (ΔSWS) in 64 % of the observed soil moisture events in these soils. However, while precipitation inputs also exceed ΔSWS in 64 % of the observed soil moisture events in intermediate depth mid-slope soils, four times during the period of our observations, soil moisture in intermediate (41 cm) mid-slope soils rises without an associated precipitation event, or an associated soil moisture event in shallow soils. Furthermore, the shortest average lag time between the beginning of a precipitation event and the beginning of a soil moisture event in intermediate depth (41 cm) mid-slope soils (417 min) is smaller than the average lag time (486 min) in shallow mid-slope soils (Table 3-2), suggesting intermediate depth mid-slope soils receive a relatively more rapid input of water than shallow mid-slope soils. These discrepancies in soil moisture wetting up sequence suggest multiple soil water flowpaths interact with mid-slope soils at different depths.

Shallow (20 cm) and intermediate (40 cm) bottom hillslope soils also appear to receive water inputs predominately from precipitation, illustrated by the shorter average lag times (236 and 421 min, respectively) at these depths relative to other depths, and the percentage of times that precipitation inputs exceed ΔSWS in observed soil moisture events (93 and 55 %, respectively) (Table 3-2). However, unlike shallow and intermediate depth mid-slope soils, shallow and intermediate depth bottom slope soils only react to medium and high volume precipitation events. This discrepancy could result from the relatively denser canopy cover at the bottom slope station, which would intercept low magnitude precipitation inputs (Helvey and Patric, 1965; Xiao *et al.*, 2000). This inconsistency could also be caused by nearby

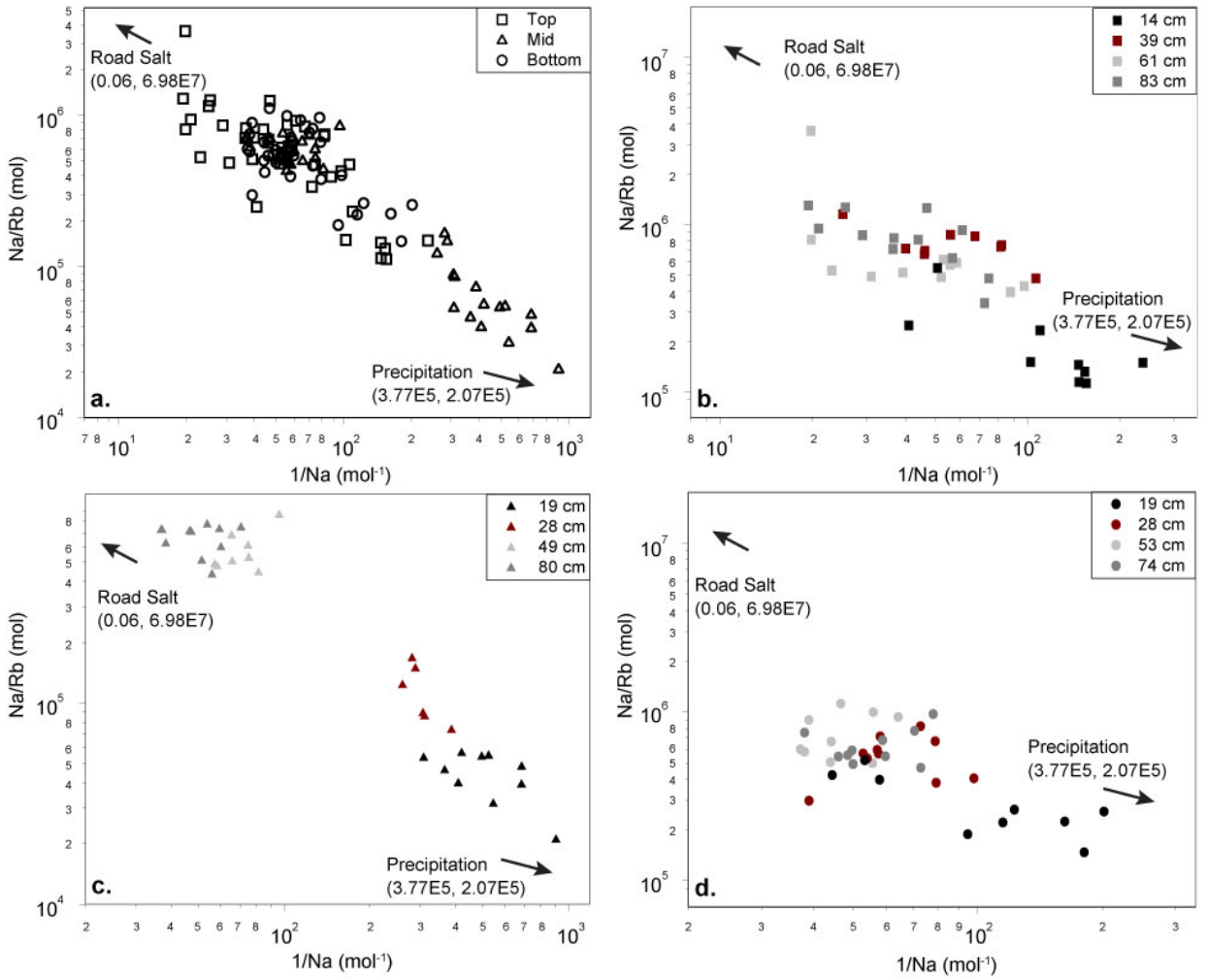

Figure 3-14. Soil water sodium concentrations normalized with soil water rubidium concentrations for all nests (a), top slope nest (b), mid slope nest (c), and bottom slope nest (d). In panel a top slope nest samples are represented by *boxes*, mid slope nest samples are represented by *triangles*, and bottom slope nest are represented by *circles*. In panels b-d the *color of the shape* distinguishes the sampling depth. Samples with relatively higher Na/Rb ratios plot towards values measured in PennDOT road salt samples, whereas samples with relatively lower Na/Rb ratios plot towards values measured in precipitation samples previously collected within the catchment.

impervious roadway surfaces discharging precipitation inputs to near-road soils (Dunne and Leopold, 1978), thereby augmenting low volume precipitation event inputs to mid-slope soils.

3.4.2 Sodium and Chloride Concentrations Provide Evidence for Multiple Flowpaths

The relatively elevated Na concentrations we observe in near-road soils is not surprising, as the application of road deicers (i.e., NaCl), should enrich near-road soils with Na (Blomqvist and Johansson, 1999; Buttle and Labadia, 1999). Mixing model analysis suggests that near-road soil solutions (i.e., top slope nest), and by extension, near-road soils, are more likely influenced from the dissolution of road-salt (Figure 3-14b). The spike in soil Na concentrations (Figure 3-8) appears to be somewhat associated (r^2 = 0.23) with an increase in sediment surface area, and thus exchange capacity (Essington, 2004), as soils at this depth (50-55 cm) have relatively higher CS (Figure 3-7b). However, this relationship may also result from Na^+ being transported to depth via subsurface flowpaths.

Temporal and depth patterns in soil water Na^+ and Cl^- concentrations suggest subsurface flowpaths to near-road soils influence Na^+ and Cl^- dynamics. In particular, at the top slope lysimeter nest, soil water Na^+ and Cl^- concentrations in the deeper lysimeters (i.e., 39, 61, and 83 cm) reach maximum values before the shallowest lysimeter (Figure 3-9a & b), indicating that high TDS waters interact with deeper soils first. Conceptually, high TDS runoff from the highway is expected to enter the soil column via infiltration (Labadia and Buttle, 1996), thus producing a peak in soil water Na^+ concentrations in the shallowest lysimeter first. Therefore, the infiltration of a solute front from the top of the soil is not the only, or even the primary process transporting Na^+ and Cl^- to deeper roadside soils. Instead, Na^+ and Cl^- may be transported to these depths via lateral flow originating from leaking highway stormwater infrastructure and the locally dominant horizontal bedrock layers. However, as Na^+

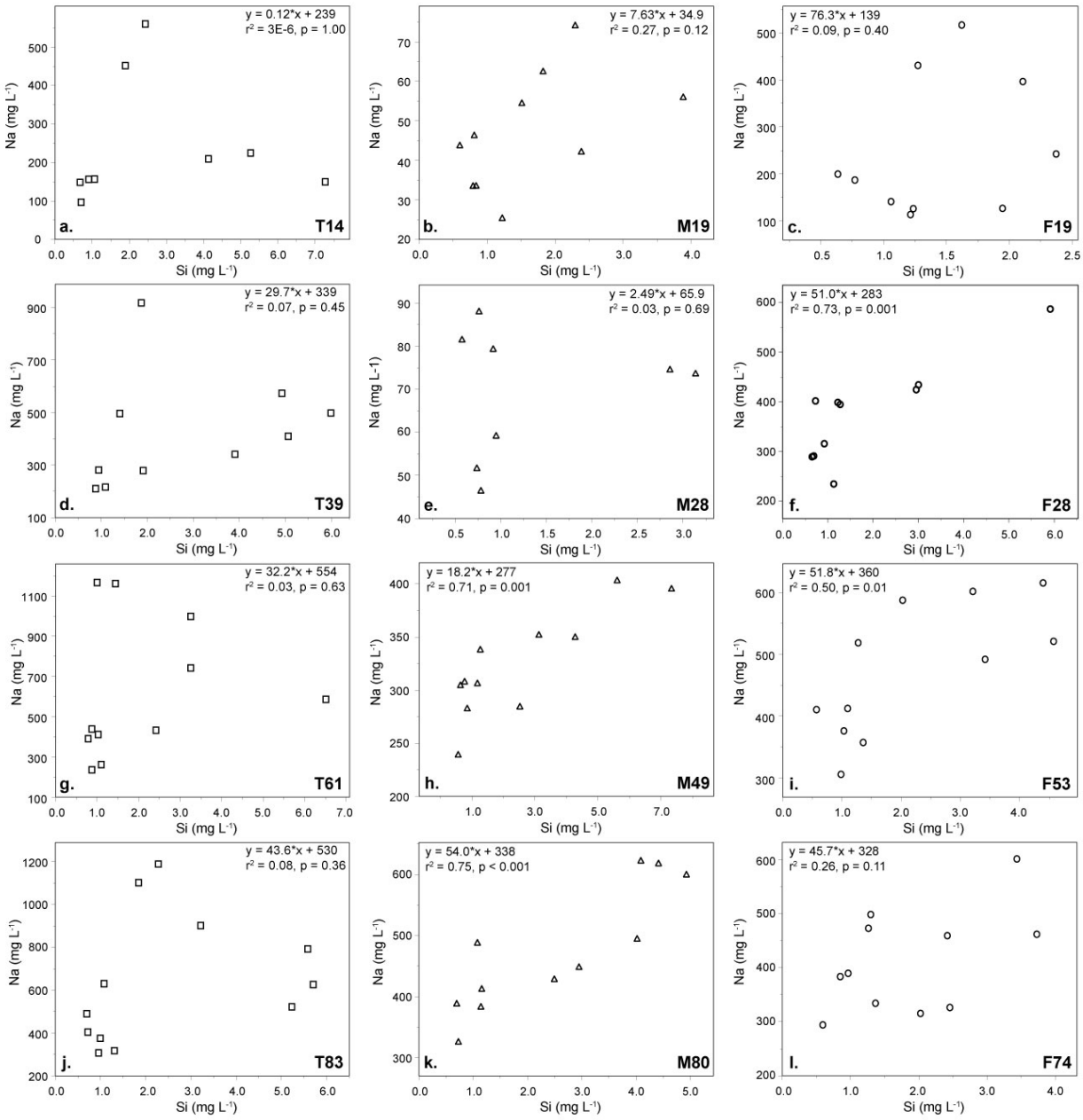

Figure 3-15. Soil water sodium concentrations versus soil water silicon concentrations. Samples collected from the top slope nest are indicated by *squares*, mid slope nest by *triangles*, and bottom slope nest by *circles*. The alpha numerical label in the bottom right of each panel designates the lysimeter nest and sampling depth (e.g., T14 is the top slope nest and the 14 cm soil water sampler).

concentrations are poorly related (r^2 < 0.09) to silicon (Si^{4+}) concentration in top slope soil water samples (Figure 3-15a, d, g, & j), it is unlikely that groundwater flow is the source of this

lateral flow (Uhlenbrook *et al.*, 2000; Uchida *et al.*, 2003; Rodgers *et al.*, 2004).

As deicers melt snow and ice on the roadway, high TDS meltwaters are typically routed to drainage infrastructure located along the shoulder of the roadway. Specifically, the road length adjacent to our study transect is outfitted with road drains (Figure 3-2a), and thus highway runoff does not appear to be discharged to near-road soils (Figure 3-2b). Given this portion of I-376 was opened in 1953 (Pennsylvania. Dept. of Highways United States. Bureau of Public Roads, 1953), it is probable that the aging road drains are leaking (Ellis *et al.*, 2004). Exfiltration from storm water infrastructure has been shown to recharge local groundwater, thus affecting groundwater chemistry (Lerner, 1986; Bhaskar and Welty, 2012). Likewise, leaking drainage infrastructure can impact Na^+ and Cl^- loadings in urban catchments (Cooper *et al.*, 2014). Therefore the relatively early peak of soil water Na^+ and Cl^- concentrations in the deeper top slope lysimeters could result from Na^+ and Cl^- inputs via leaking roadway drainage networks. Additionally, the increase of soil water Na^+ and Cl^- concentrations with depth in these lysimeters (Figure 3-9a & b) is consistent with Na^+ and Cl^- accumulation in groundwater (Ostendorf *et al.*, 2001; Godwin *et al.*, 2003; Cunningham *et al.*, 2008; Kelly *et al.*, 2008; Cooper *et al.*, 2014).

The accumulation of Na^+ and Cl^- in soil water can affect the duration and timing of relatively high Na^+ and Cl^- loadings to roadside soils. In particular, Na loadings to soils persist beyond the period when deicers are applied to roadways (Ostendorf *et al.*, 2001; Godwin *et al.*, 2003; Cunningham *et al.*, 2008; Kelly *et al.*, 2008; Cooper *et al.*, 2014). In our samples, the distance from the roadside affects when soil water Na^+ concentrations reach a maximum value , suggesting that Na moves relatively slowly through roadside soils throughout the non-salting

period. Specifically, while top slope soil water Na^+ and Cl^- concentration maximums occur within a month after the cessation of road deicing (Figure 3-9a & b), soil water Na^+ and Cl^- concentration maximums at the mid (Figure 3-9c & d) and bottom (Figure 3-9e & f) hillslope stations occur later in the year.

While the onset of elevated soil water Na^+ and Cl^- concentrations at the mid-slope nest generally lag peaks at the top slope nest by approximately two months (Figure 3-9a – d), elevated Na^+ and Cl^- concentrations are only observed in the deeper soil waters. This discrepancy could result as a consequence of the Na^+ and Cl^- delivery mechanism. Mixing model analysis suggests that Na^+ in deeper mid-slope soil waters is influenced by road deicers, whereas Na^+ in shallow mid-slope soil waters is influenced by precipitation inputs (Figure 3-14c). Furthermore, in 49 and 80 cm mid-slope soil water samples, Na^+ concentrations are strongly related to Si^{4+} concentrations (r^2 = 0.71 & 0.75, respectively) (Figure 3-15h & k). Thus, Na^+ and Cl^- in mid-slope soil solutions appear to be primarily input to soils via subsurface flow. This discrepancy could result from a relatively impermeable clay-rich layer indicated by the increased CS values measured at approximately 40 cm depth at the mid-slope station (Figure 3-7b). Such a layer would reduce hydrologic communication between shallow and deep soils and prevent the input of deeper, road salt impacted waters to shallow soils. Yet, this layer alone would not explain the relatively low soil water Na^+ concentrations observed in mid-slope soil waters, as relatively Na-rich highway runoff could still interact with shallow mid-slope soils via overland flow and infiltration. However, it is likely saturated overland flow from the road does not reach this position on the hill slope. Therefore, these shallow soil waters in the mid-slope nest would only be affected by precipitation.

Similar relationships between soil water Na^+ concentrations and sampling depth are not observed in bottom slope soil water Na^+ concentrations. Specifically, the magnitude of soil water Na^+ concentrations do not correspond simply with increasing or decreasing sampling depth (Figure 3c), instead, it appears that distinct sources of water interact with shallow (i.e., 19 cm) and deeper (i.e., 28, 53, and 74 cm) depth bottom slope soils. The flowpath that supplies Na^+ to 28, 53, and 74 cm depth bottom slope soils is likely longer, slower water flowpaths, given the relationship between soil water Na^+ and Si^{4+} concentrations (r^2 = 0.73, 0.50 & 0.26, respectively, Figure 7f, i, & l). Furthermore, the relatively enriched Na^+ concentrations observed in 28 cm depth soil solutions (Figure 3-9e), could result from Na^+ being transported from depth, and adsorbed by the relatively increased exchange capacity observed at approximately 30 cm depth (Figure 3-7b). Conversely, Na^+ concentrations in 19 cm depth bottom slope soil solutions appear to be influenced by local precipitation (Figure 3-14d), suggesting that these soils are primarily influenced by infiltration of precipitation waters, particularly given the weak relationship (r^2 = 0.08) between Na^+ and Si^{4+} concentrations (Figure 3-15c). Thus it is possible the delivery of Na^+ to shallow bottom slope soils is dependent upon precipitation physically transporting Na downslope, though somewhat unlikely given observations at the mid-slope.

3.4.3 Major Cation Dynamics

In general, the timing of soil water Ca^{2+} and Mg^{2+} concentration maximums (Figure 3-13) mirror the occurrence of soil water Na^+ concentration maximums (Figure 3-9). This relationship is unsurprising, as increased Na loadings are known to mobilize soil Ca and Mg via cation

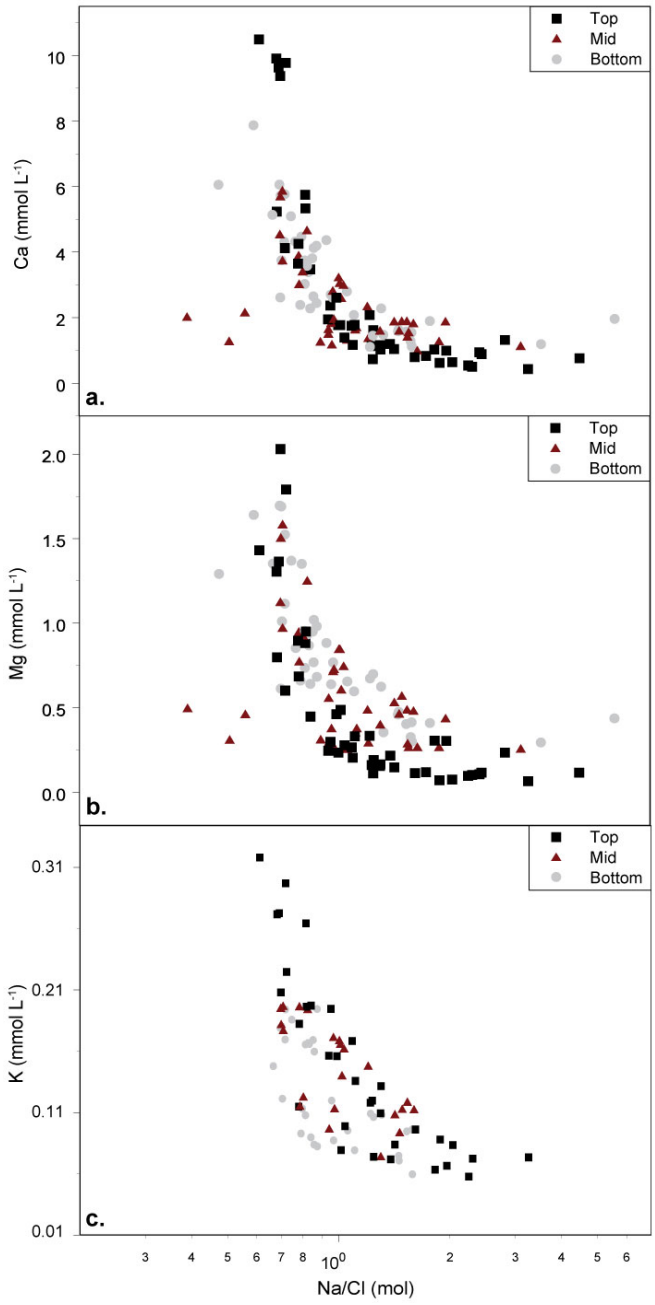

Figure 3-16. Soil water calcium (a), magnesium (b), and potassium (c) concentrations compared to soil water molar Na/Cl ratios. In all panels top slope nest samples are represented by *boxes*, mid slope nest samples are represented by *triangles*, and bottom slope nest are represented by *circles*. In panel c only soil water samples collected from > 20 cm depth at the top and bottom slope stations, and > 30 cm depth at the mid slope station are considered. The exponential relationship suggests that increased soil water calcium, magnesium, and potassium concentrations result from exchange reactions with sodium.

exchange reactions (Davidson, 1971; Shanley, 1994; Mason *et al.*, 1999; Norrström and Bergstedt, 2001). This mobilization via exchange reactions is further suggested by comparing soil water Ca^{2+} and Mg^{2+} molar concentrations to soil water Na/Cl molar ratios. As soil water Na/Cl molar ratios decrease towards a value of 1, the ratio of Na^{+} to Cl^{-} in halite, soil water Ca^{2+} and Mg^{2+} concentrations rise exponentially (Figure 3-16a & b), further suggesting that soil Ca and Mg pools are mobilized via interactions with Na-rich waters.

The higher Ca^{2+} and Mg^{2+} concentrations observed in the deeper (i.e., 53 and 74 cm depth) top slope (Figure 3-13a & b) and mid-slope (Figure 3-13d & e) soil waters suggests that both Ca^{2+} and Mg^{2+} are mobilized to depth. However, top and mid-slope soils appear to be relatively enriched with Ca, but not Mg (Figure 3-10a & b). Thus it is likely that Ca^{2+} inputs via weathering of concrete road materials (Bain *et al.*, 2012; Rossi *et al.*, 2015) offset Ca^{2+}

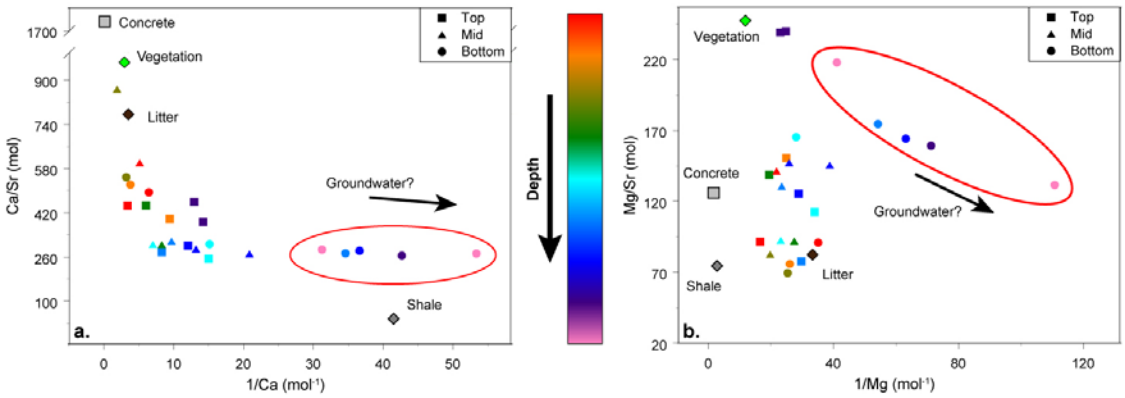

Figure 3-17. Soil calcium (a) and magnesium (b) concentrations normalized with soil strontium concentrations. In both panels top slope nest samples are represented by *boxes*, mid slope nest samples are represented by *triangles*, and bottom slope nest samples are represented by *circles*. The *square* represents values typical of cement (Idriss et al., 2009), and the *diamonds* represent average values of collected leaves and leaf litter. The color of each symbol represents sampling depth. Circled samples are influenced by an unknown endmember, possibly local ground water.

mobilization via high TDS waters.

Elemental mixing models demonstrate that concrete is a significant source endmember of shallow soil Ca (Figure 3-17a), but not a dominant source of soil Mg (Figure 3-17b), confirming the influence of concrete weathering inputs on soil Ca pools. Furthermore, mixing analysis suggests that deeper (> 44 cm) bottom slope soils are influenced by an additional source, possibly local groundwater (Figure 3-17, *circled*). As this study did not collect groundwater samples from the small perched aquifers characteristic of the area (Kozar *et al.*, 2012), this influence cannot currently be confirmed.

Unlike top and mid-slope soil waters, Ca^{2+} and Mg^{2+} do not have a clear relationship with sampling depth in bottom slope soil solutions (Figure 3-13g & h). The wetting profile of these soils (i.e., top down) is expected to transport Ca^{2+} and Mg^{2+} to depth. The absence of increasing concentrations with depth may reflect the influence of other flowpaths interacting

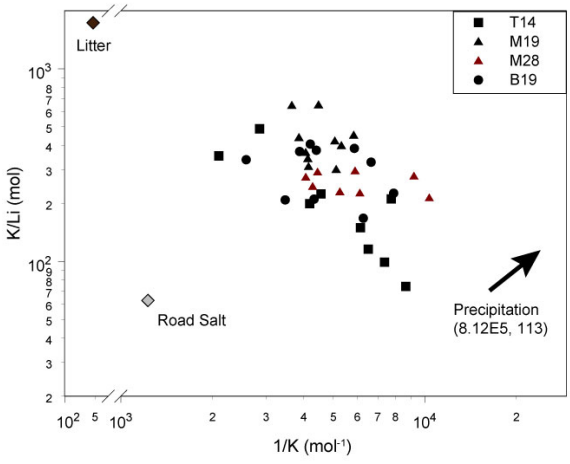

Figure 3-18. Soil water potassium concentrations normalized with soil water lithium concentrations for shallow soil waters. The color of the shape distinguishes the sampling depth. The *grey diamond* represents the average value measured in PennDOT road salt samples, the *brown diamond* represents the average value of collected leaf litter samples, and the *arrow* designates the average value of collected precipitation samples.

with bottom slope soils. As deeper (>19 cm depth) bottom slope soil waters appear to interact with ground waters (Figure 3-15f, i, & l), it is possible localized ground water discharges transport Ca^{2+} and Mg^{2+} upwards, obscuring concentration patterns with depth. Likewise, 19 cm deep bottom slope soil waters appear to be more affected by precipitation inputs (Figure 3-15c, Table 3-2).

The decomposition of vegetation appears to influence patterns in soil water K^+ concentrations. Specifically, mixing model analysis suggests shallow soil water K^+ concentrations are primarily influenced by vegetative litter and precipitation (Figure 3-18). Additionally, shallow bottom slope soil water K^+ concentrations begin to increase approximately 60 days after the end of the growing season (Figure 3-13i), which coincides with when other studies have observed major K losses from leaf litter (Blair, 1988). Moreover, the seasonal trend observed in shallow mid-slope soil water K^+ concentrations possibly results from K release from litter decomposition (Blair, 1988), or K leaching via the forest canopy (Swank, 1986). While K inputs via vegetation appear to affect shallow soil water K^+ dynamics, interactions with high TDS waters seem to drive K^+ dynamics in deeper waters. In particular, as soil water Na/Cl molar ratios approach a value of 1:1, soil water K^+ concentrations rise exponentially (Figure 3-16c), suggesting that deeper soil K^+ pools are mobilized via cation exchange reactions.

3.5 CONCLUSIONS

In our study, we observe multiple peaks in soil water sodium (Na) and chloride (Cl^-) concentrations. The timing of these concentration maximums appears to be a function of 1)

distance from the nearby interstate and 2) sampling depth. Additionally, while deeper (i.e., > 30 cm depth) mid-slope soils and all bottom slope soils are affected by road salt application, shallow (i.e., < 30 cm depth) mid-slope soils show no influence from road dicer inputs. These Na^+ and Cl^- concentration maximums in deeper mid-slope soil waters do not occur until early May (Figure 3-9c & d). Similarly, deeper bottom slope soil water Na^+ and Cl^- concentration maximums also occur in early May, but Na^+ and Cl^- concentration maximums in shallow bottom slope soil waters do not occur until early August (Figure 3-9e & f). These relationships suggest that multiple soil water flowpaths (e.g., highway runoff, lateral flow at the soil-bedrock interface), interact with soils, governing Na transport along our study transect.

This study is consistent with previous work that observed persistence of Na loadings to soils beyond the period of road salt application. In general, relatively elevated soil water Na^+ and Cl^- concentrations appear to persist throughout the year. For example, relatively elevated soil water Na and Cl^- concentrations at the top slope nest continue until early fall (Figure 3-9a & b), and demonstrate that excess Na^+ and Cl^- content persists in soils waters long after road deicing ends in late March. Retained Na in soils is known to continue to export Na^+ to nearby areas after road salting season (Kelly *et al.*, 2008). Thus, Na^+ and Cl^- appears to move as a slow wave and the distance from the roadside affects the timing of peak soil water Na^+ and Cl^- concentrations (Figure 3-9), suggesting that sodium is released from roadside soils throughout the spring and summer.

Sodium inputs appear to drive seasonal patterns in major soil water cation concentrations along our study transect. Specifically, we observe the mobilization of soil Ca, Mg, and K via interactions with road salt-rich waters (Figure 3-16). This mobilization depends

upon soil water sampling depth, distance from the roadway, and the element. In particular, the relative slow release of Na throughout the year affects the timing in soil water Ca^{2+}, Mg^{2+}, and K^{+} concentration maximums (Figure 3-13). Additionally, although roadside soil Ca and Mg pools appear to be mobilized, Ca inputs attributed to concrete road materials offset potential Ca depletion in near-road soils (Figure 3-10, Figure 3-17). While soil Ca and Mg are mobilized in all soils that are in communication with high TDS solutions, shallow soil water K^{+} dynamics seem to be affected by inputs of K from vegetative material (e.g., leaf litter). Therefore soil cation dynamics in urban areas receiving road deicer inputs depend on the variation in sodium delivery influenced by both topographically and infrascturally driven hydrological flowpaths.

Most of the road salt literature focuses nearly exclusively on in-stream and groundwater chemistry as an indicator of road salt impacts. This work demonstrates that at least for roadside soil environments, the timing and magnitude of salt pulses is not that simple. Moreover, the potential role of leaking drainage infrastructure can further complicate this transport. Previous literature characterizes acute high TDS pulses, however this work suggests that chronic high TDS impairments will grow increasingly common due to storage and release from near-road soils. Chronic elevated Na concentrations can impair aquatic ecosystems (Isabelle *et al.*, 1987; Bridgeman *et al.*, 2000; Blasius and Merritt, 2002; Karraker *et al.*, 2008). Furthermore, these Na dynamics likely will mobilize trace metals (e.g., Pb, Cd, Zn) bound to soil exchange sites (Amrhein *et al.*, 1992; Bäckström *et al.*, 2004a). Thus, a further clarification of processes occurring during exchange of roadside soils with high TDS solutions is necessary to effectively restore and manage hydrologic systems affected by transportation networks.

4.0 RECONSTRUCTING EARLY INDUSTRIAL CONTRIBUTIONS TO LEGACY TRACE METAL CONTAMINATION IN SOUTHWESTERN PENNSYLVANIA

4.1 INTRODUCTION

Human activities have increased trace metal inputs to the environment, primarily via modern vehicular and industrial emissions (Nriagu and Pacyna, 1988; Pacyna and Pacyna, 2001). In particular, trace metal loadings from metallurgical facilities (Van Alphen, 1999; Vermillion *et al.*, 2005; Mattielli *et al.*, 2009) are relatively well characterized. However, trace metal loadings from early and pre-industrial activities, though also potential sources of trace metal inputs, are poorly characterized. Specifically, while the use of trace metals in early human activities is noted (e.g., As use in historical leather tanning) (Nriagu, 2001), the magnitude and distribution of contamination associated with these activities is often unknown. Furthermore, the sequential input of trace metal contamination from multiple industries (e.g., leather tanneries, metallurgical facilities) accumulates. Consequently, elevated trace metal loadings often stretch beyond the lifespan of a single pollution source and can result in a significant amount of trace metal contamination that is challenging to detect.

Alluvial and lacustrine sediments can accumulate trace metals (Mielke *et al.*, 2000; Bain and Brush, 2005; Rhoades *et al.*, 2009), and by extension, record periods of significant trace

metal contamination (Graney *et al.*, 1995; Spliethoff and Hemond, 1996; Mahler *et al.*, 2006; Hillman *et al.*, 2015). However, the accumulation of trace metals in alluvial systems results in a reservoir of contamination with a strong potential to remobilize (Axtmann and Luoma, 1991; Spliethoff and Hemond, 1996; Steding *et al.*, 2000; Tao *et al.*, 2005; Pizzuto, 2014). Moreover, as potential changes in global precipitation patterns will increase the probability of extreme precipitation events (Palmer and Räisänen, 2002) and flooding is likely to also increase (Jongman *et al.*, 2012). Thus, changing climate can increase mobilization of contaminated alluvial sediments and effective risk assessment requires characterization of legacy trace metal contamination.

This study reconstructs substantial trace metal contamination from early industrial activities using a lake sediment record from an oxbow lake in Southwestern Pennsylvania, USA. Specifically, we characterize trace metal loadings from changes in land use and industry in the 19^{th} and 20^{th} centuries by examining major and trace metal chemistry, bulk density, and magnetic susceptibility in an approximately 210 year lake sediment record (169 cm). Additionally, we combine historical documentation and elemental molar ratios to identify principal sources of trace metal loadings. This reconstruction documents modern trace metal contamination from the Donora Zinc Works, a notorious environmental polluter (Snyder, 1994). More importantly, this study highlights the potential for accumulation of complicated mixes of trace metal contaminants in alluvial sediments. As industry and industrial hygiene have evolved, waste materials have also evolved. While the examination of single contaminants are common (Van Alphen, 1999; Vermillion *et al.*, 2005; Mattielli *et al.*, 2009; Romero *et al.*, 2010), the relative impacts of these mixtures is less clear.

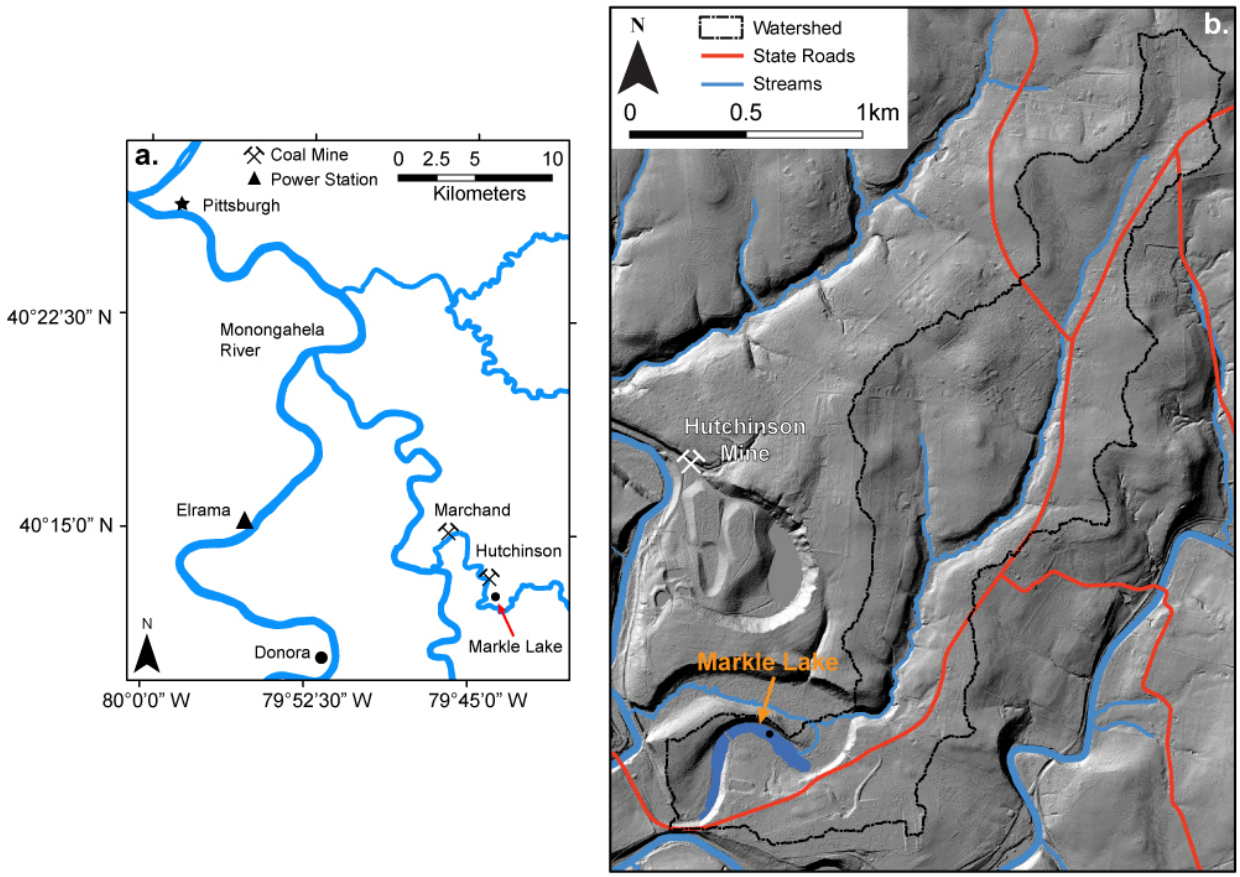

Figure 4-1. Location of the Markle Lake (*circle*), local coal mines (Marchand and Hutchinson), coal-fired power station (*triangle*), and the nearby town of Donora, PA (a). Panel b details the Markle Lake watershed (2.48 km^2), nearby state roads (Pennsylvania Department of Transportation, Bureau of Planning and Research, 2015) **and streams, hillshaded LiDAR terrain (1 m resolution)** (PAMAP Program PA Department of Conservation and Natural Resources Bureau of Topographic and Geologic Survey, 2006), **the nearby Hutchinson coal mine** (United States Geologic Survey, 1954), **and the sediment core collection location (40°12'48" N, 79°43'47" W, *circle*). Markle Lake has a surface area of 0.04 km^2 and drains a 2.48 km^2 watershed** (PAMAP Program PA Department of Conservation and Natural Resources Bureau of Topographic and Geologic Survey, 2006)**.**

4.2 STUDY LOCATION AND METHODS

In September 2014, three sediment cores (C14, D14, E14) were collected from an unnamed oxbow lake hereafter referred to as Markle Lake (Figure 4-1). Water depth at the coring site was 1.06 m (Figure 4-1b, *circle*), and the composite record totals 169 cm. At C14,an 80 cm long core (C14 surf) with an intact sediment−water interface was collected using a lightweight percussion coring system. The upper 50 cm of core C14 was extruded in the field at 1 cm intervals and used for geochemical analysis and ^{210}Pb dating. Deeper sediments (D14 D1 & D2, E14 D1) were collected with a steel barrel Livingston corer. Sediment cores were wrapped, transported to the University of Pittsburgh, split lengthwise, and immediately described. Sedimentary structures, grain size, and Munsell color were characterized for each core. Overlapping sections at D14 and E14 were identified via field measurements and confirmed with stratigraphic correlation of visible sedimentology, magnetic susceptibility, and geochemical data. Because sites C14, D14, and E14 are separated by <1 m and have a similar water depth, the sediment cores from these three sites were combined into one composite record using field notes and stratigraphic correlation of geochemical data.

The prevailing direction of winds in the region is from the southwest (The Office of the Pennsylvania State Climatologist, 2007). In the late 19th century and until the mid-20th century widespread coal mining occurred nearby (Wilson, 1962), however no substantial strip mining or acid mine drainage treatment is recorded within the Markle Lake catchment (Pennsylvania Department of Environmental Protection, 2016). The upper Markle Lake catchment is underlain by the Permian and Pennsylvanian age Waynesburg Formation, whereas the lower catchment

and Markle Lake are underlain by the Pennsylvanian age Monongahela Group (Berg *et al.*, 1980). Both the Waynesburg Formation and the Monongahela Group consist of cyclic sequences of sandstone, shale, limestone, and contain commercial coals (Waynesburg and Pittsburgh coals, respectively) (Berg *et al.*, 1980).

4.2.1 Bulk Density, and Loss-On-Ignition Analysis

Bulk density, and loss on ignition (LOI) were measured at 1 cm intervals using 1 cm^3 samples. Bulk density was inferred by mass difference after oven drying samples at 60 °C for 48 h. Likewise, percent organic matter was inferred by mass difference after combusting oven-dried samples in a muffle furnace at 550 °C for 4 h. Magnetic susceptibility was measured on all sediment cores at 2 mm intervals with a Magnetic Susceptibility Meter (Bartington MS2) at the University of Pittsburgh. Magnetic susceptibility values were not measured on samples from the upper 50 cm of the core that was extruded in the field. Select 1 cm samples spanning the composite sediment core were analyzed and described via smear-slide mineralogy (Schnurrenberger *et al.*, 2003).

4.2.2 Geochronology

Sediment samples were collected from the upper 40 cm of C14, lyophilized, homogenized, sealed, allowed to reach secular equilibrium, and analyzed for radioisotope (^{210}Pb, ^{137}Cs, and ^{214}Pb) activities by direct γ counting on a high-purity, broad-energy germanium detector (Canberra BE-3825) at the University of Pittsburgh. Sediment ages were

subsequently determined using a constant rate of supply (CRS) ^{210}Pb age model (Appleby and Oldfield, 1983). To date the deeper sediments, two radiocarbon ages of terrestrial macrofossils (e.g., wood) were measured on the D14 sediment core (137.5 and 151.5 cm composite depth). Samples were pretreated using the standard acid, alkali, acid procedure (Abbott and Stafford Jr, 1996), measured at the Keck Center for Accelerator Mass Spectrometry at the University of California Irvine, and calibrated using Calib 7.0 (Reimer *et al.*, 2013).

4.2.3 Chemical Analysis

Sediment samples, taken at 1 cm increments from both extruded and non-extruded cores, were lyophilized and homogenized in a mortar and pestle (agate). Sorbed and exchangeable metal concentrations in sediment samples were measured using a weak acid extraction (10% nitric acid) (Graney *et al.*, 1995). Sediment extracts were diluted with 2% nitric acid (vol/vol, sub boil distilled), spiked with an internal standard of Be, Ge, and Tl, and analyzed for trace metal concentrations on an inductively coupled plasma mass spectrometer (Perkin-Elmer Nexion ICP-MS) at the University of Pittsburgh. Sample As concentrations were measured using the kinetic energy discrimination (KED) method. Duplicates were run every seven samples and were generally within 10% of each other. Blanks were run every ten samples to check for memory effects and were below the calibration blank intensities. Instrument drift was assessed by running a drift check after every ten samples, which were generally within 10% of previous sample measurements.

4.3 RESULTS

4.3.1 Sediment Properties

The earliest portion of the Markle Lake sediment record (169 - 166 cm) consists of relatively dense sand/silt sized grey (10 YR 6/2) sediment (Figure 4-2b). At 166 cm depth, bulk density (BD) abruptly drops across a sharp, uneven contact, transitioning to brown (10 YR 3/2) silt (Figure 4-2b). Another sharp, uneven contact occurs at 159 cm depth (Figure 4-2), where sediments sharply transition to black (10 YR 2/1) organic rich material, containing several small (<1 cm) pieces of brick. The final sharp, uneven contact marked by an increase in BD and an increase in organic matter occurs at 131 cm depth (Figure 4-2, *red dashed line*), visibly transitioning to grey fine-grained clay (10 YR 5/1). A gradual transition from fine-grained clay to silt with no pronounced color change takes place at 79 cm. This unit continues up core until 34 cm when sediments gradually transition into fine-grained light grey (10 YR 5/1) clay.

The several sharp changes in sedimentology, BD and organic matter content in the sediment record coincide with erosional, uneven stratigraphic contacts (Figure 4-2, *red dashed lines*). While radiometric dating could confirm the discontinuous nature of these transitions, given the weight of sedimentological evidence and the uncertainties in radio dating materials from the 1800's, we interpret these contacts to be unconformities. After the last abrupt and

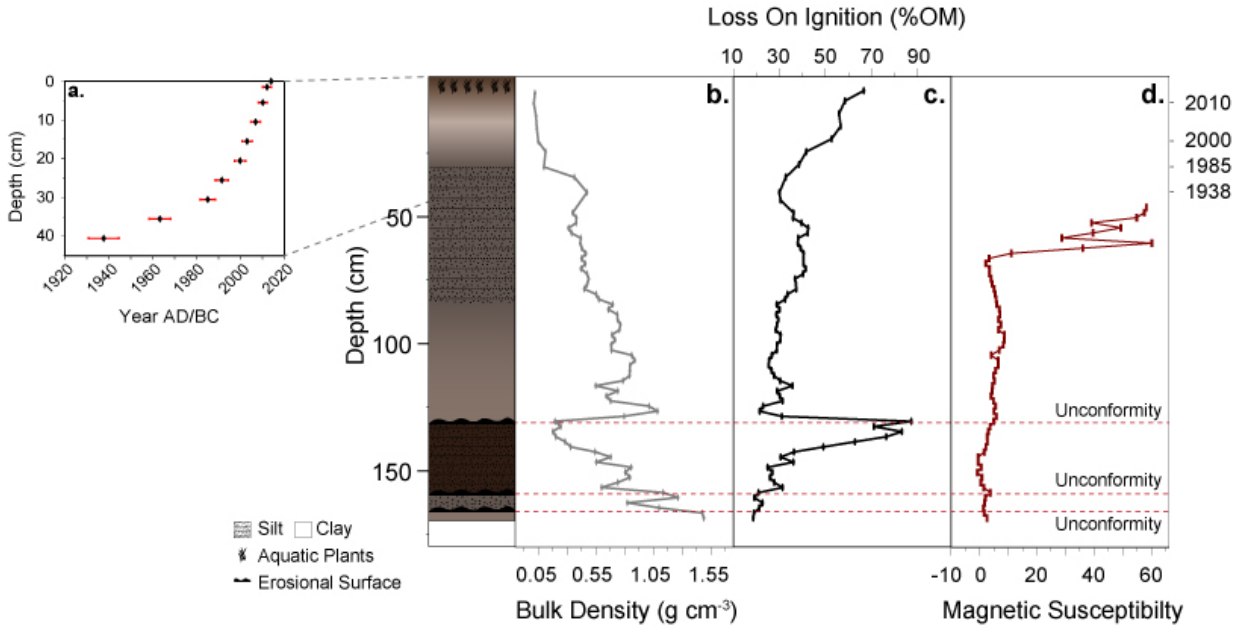

Figure 4-2. Polynomial Markle Lake age-depth model (a), with 210Pb dates (*black*) and 2-sigma error bars (*red*). The color ramp provides a simplified core stratigraphy. Sediment core bulk density, loss on ignition, and magnetic susceptibility are displayed in panels b – d, respectively. The *red dashed lines* indicate the three inferred unconformities observed in the Markle Lake sediment record, which correspond to sharp changes in sediment bulk density and organic matter content. Sediment ages generated by the ^{210}Pb age model (< 40 cm) are provided on the secondary y-axis.

uneven sedimentological transition (131 cm) the sediment record appears uninterrupted until present day, as we observe no sedimentological features through these intervals to suggest an erosional surface nor sharp changes in sediment BD or LOI (Figure 4-2b & c). Although sediment BD or LOI do not sharply change during this period, sediment magnetic susceptibility (MS) sharply increases at 68.5 cm depth (Figure 4-2d).

4.3.2 Sediment Smear Slide Analysis

The earliest portion of the Markle Lake sediments between 169 and 166 cm depth consist of sand/silt sized sediment characterized by angular, poorly sorted clasts. Smear-slide analysis shows a large proportion (nearly 100%) of silicate minerals and the absence of diatoms. Smear-slides show that sediments across this uneven contact at 166 cm depth are characterized by ~80-90% angular, poorly sorted silicate minerals with ~10-20% amorphous organic material and the absence of diatoms.

Smear slides taken above the next uneven contact at 159 cm depth show ~80% amorphous organic material with occasional discrete aquatic macrofossils, ~20% sub-angular silicate minerals, and the absence of diatoms. Smear slides collected from 131 cm depth show ~30-40% centric and pennate diatoms of relatively uniform size and ~60-70% very fine-grained rounded silicate minerals. This unit continues up-core with an increasing proportion of diatoms, reaching as high as 50% around 90 cm. After the gradual transition from fine-grained clay to silt at 79 cm, smear slides show a higher proportion (70%) of rounded and sub-angular silicate minerals and a decreased proportion (30%) of diatoms.

Above 34 cm depth smear slide analysis shows a similar sediment character to the below unit with 30-40% centric and pennate diatoms of varying sizes, 10% sub-angular silicate minerals, and 50-60% amorphous organic material. The uppermost 10 cm of the sediment core have an increased proportion (60-70%) of organic material with several discrete aquatic plants identified as Myriophyllum.

Table 4-1. Radionuclide data and age model for Markle Lake core.

Depth Interval (cm)	Dry sample mass (g)	^{137}Cs Activity (Bq g^{-1})	±1σ	^{210}Pb Activity (Bq g^{-1})	±1σ	Supported ^{210}Pb or ^{214}Pb Activity (Bq g^{-1})	±1σ	Excess ^{210}Pb Activity (Bq g^{-1})	±1σ	Date AD	Sed Rate (cm yr^{-1})
0										2014	
1-2	0.62	0.000	0.000	0.39	0.08	0.00	0.00	0.39	0.08	2012	0.79
5-6	0.30	0.000	0.000	0.54	0.11	0.00	0.00	0.54	0.11	2010	2.07
10-11	0.89	0.000	0.000	0.36	0.05	0.04	0.01	0.32	0.04	2007	1.53
15-16	1.11	0.000	0.000	0.39	0.05	0.11	0.01	0.28	0.04	2003	1.29
20-21	1.36	0.000	0.000	0.19	0.03	0.03	0.01	0.15	0.02	2000	1.56
25-26	1.72	0.015	0.004	0.19	0.03	0.05	0.01	0.15	0.02	1992	0.60
30-31	2.72	0.023	0.003	0.16	0.02	0.06	0.01	0.10	0.02	1985	0.78
35-36	4.25	0.030	0.003	0.11	0.02	0.04	0.00	0.06	0.01	1963	0.23
40-41	6.56	0.040	0.003	0.08	0.01	0.05	0.00	0.03	0.01	1938	0.20
44-46	6.13	0.027	0.002	0.07	0.01	0.04	0.00	0.03	0.01		
48-50	1.22	0.000	0.000	0.00	0.00	0.08	0.01	0.00	0.00		
50-52	1.16	0.000	0.000	0.00	0.00	0.10	0.01	0.00	0.00		

4.3.3 Geochronology

We attempted to establish a geochronology for the sediment core using a combination of a ^{210}Pb radioactive decay series (Table 4-1) and AMS radiocarbon dates (Table 4-2) on presumably discrete terrestrial macrofossils. However, the radiocarbon ages of these materials were far older than expected (~8500 yr BP) (Table 4-2). In particular, several pieces of brick were found at a depth (154 cm) below both radiocarbon samples (151.5 and 137.5 cm), suggesting these radiocarbon ages do not accurately reflect the timing of sediment deposition. The exact cause for this inaccuracy is not immediately apparent, though multiple possibilities exist. For example, macrofossils derived from aquatic vegetation could have been misidentified as terrestrial material. Given that Pennsylvanian age carbonates directly underlie Markle Lake

Table 4-2. AMS radiocarbon dates for samples collected from Markle Lake core D14 D2.

UCI Number	Composite Core Depth Interval (cm)	Material	^{14}C age (BP)	Error ±	Median age (BP)	2-σ range (year BP)
151981	137-138	Wood	7790	30	8571	8479-8633
151982	151-152	Wood	7915	25	8716	8609-8972

(Berg *et al.*, 1980), ages of aquatic vegetation would likely be influenced by a hard water effect due to the dissolution of carbonate (Deevey *et al.*, 1954; Macdonald *et al.*, 1987; Törnqvist *et al.*, 1992), and thus return older radiocarbon ages. Alternatively, it is possible that that terrestrial macrofossils were reworked from catchment soils or previously deposited lacustrine sediments and re-deposited into younger sediments, thus obscuring the radiocarbon ages (Törnqvist *et al.*, 1992). Given the presence of reworked anthropogenic building materials (brick) and sedimentological evidence of erosional hiatuses in the section (irregular contacts, abrupt changes in sediment composition and grain size), we exclude the radiocarbon ages from the development of our age model, and instead use a combination of the ^{210}Pb age model (Figure 4-2a)and historical documentation matched with chemo stratigraphy to create the age model for the composited sediment core. Uncertainty within the ^{210}Pb chronology, which spans the upper 40.5 cm, is generally ±4 years.

4.3.4 Patterns in Early Sediment Metal Concentrations

Spikes in sediment As, Cd, and Zn, concentrations occur during the early portion (~163 - 127 cm) of the Markle Lake sediment record (Figure 4-3a, e, & f). However, the most remarkable feature of this period is the extended period of elevated As concentrations

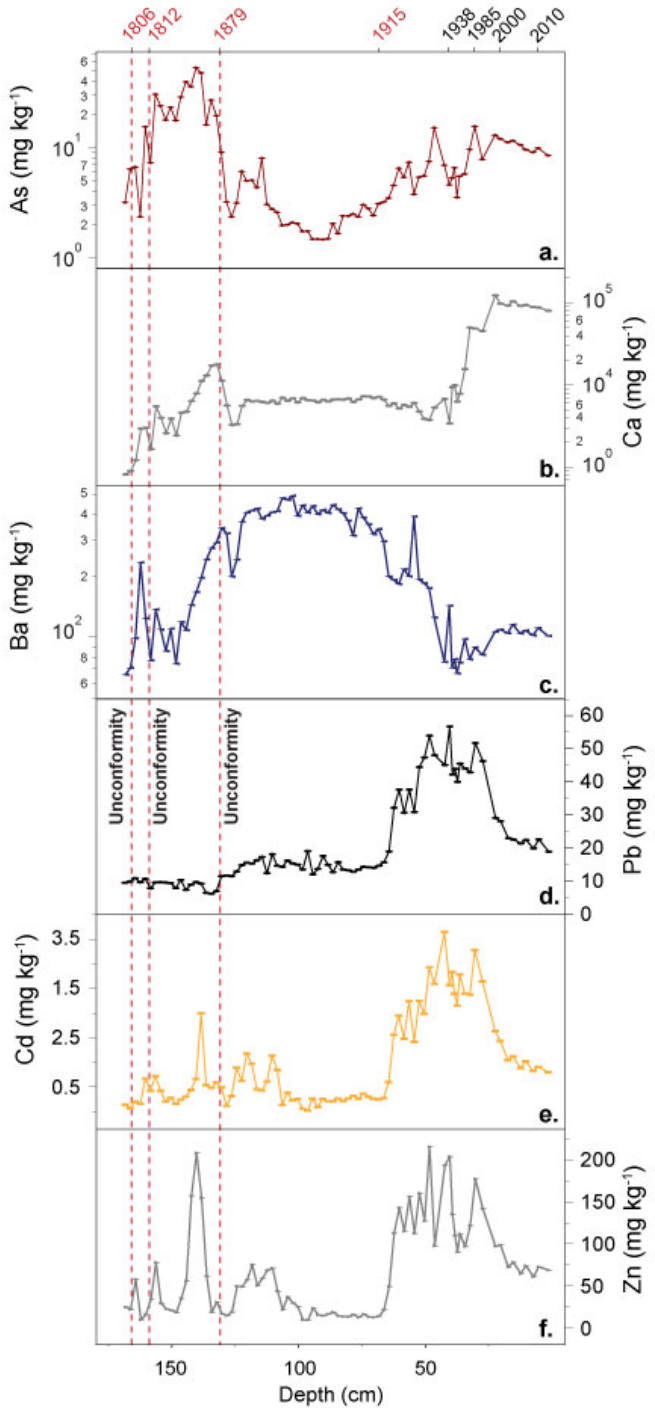

Figure 4-3. Sediment core arsenic (a), calcium (b), barium (c), lead (d), zinc (e), and cadmium (f) concentrations. The *red dashed lines* indicate the three unconformities observed in the Markle Lake sediment record. Sediment ages determined by the ^{210}Pb age model (*black*) and by historical documents (*red*) are provided on the secondary y-axis.

(Figure 4-3a). Specifically, sediment As concentrations are elevated for approximately 30 cm of the Markle Lake sediment record (Figure 4-3a), in contrast to sediment Cd and Zn concentrations, whose peaks are relatively shortly lived (137 – 143 and 135 – 149 cm, respectively). Additionally during this period (1812 – 1879), there is a relative increase in sediment Ca concentrations (Figure 4-3b). Lastly, unlike the patterns in other sediment trace metal concentrations during this period, sediment Pb concentrations are relatively constant ($\bar{x}$ = 8.46 mg kg^{-1}) and generally close to average crustal abundance (11.1 mg kg^{-1}) (Figure 4-3d) (Turekian and Wedepohl, 1961).

Shortly after (~120 cm) the final observed erosional contact (131 cm), there are additional peaks in As, Cd, and Zn concentrations (Figure 4-3a, e, & f), which coincide with a rise in sediment Ba and Pb concentrations (Figure 4-3d & c). However, while the elevated sediment Ba and Pb concentrations appear relatively persistent during this period of the sediment record (131 – 68.5 cm), sediment Zn and Cd concentrations return to lower concentrations above ~120 cm. Additionally, sediment As concentrations also decrease after 113 cm, however the decrease is short-lived, as sediment As concentrations begin to increase, albeit slowly, near the end of this period (~80 cm).

4.3.5 Patterns in 20th Century Sediment Metal Concentrations

Sediment As, Cd, Pb, and Zn concentrations all increase at 68.5 cm depth (Figure 4-3a, d – f). Specifically, this increase is more pronounced in sediment Cd, Pb, and Zn concentrations (Figure 4-3d – f), and occurs in conjunction with the sharp increase in sediment MS (Figure

4-2d). Furthermore, during this period (68.5 – 40.5 cm), which corresponds to 1915 – 1938, the highest observed sediment Cd, Pb, and Zn concentrations occur (Figure 4-3d – f). These increased trace metal loadings persist until the mid-20th century (40.5 cm), when sediment As, Cd, Pb, and Zn concentrations decrease (Figure 4-3a, d – f). However, this decrease is short lived, as sediment As, Cd, Pb, and Zn concentrations once again increase until the late-20th century (Figure 4-3a, d – f). At this point (i.e., the late 20th century), sediment As, Cd, Pb, and Zn concentrations all begin to decrease until present day (Figure 4-3a, d – f), however sediment Cd, Pb, and Zn concentrations decrease faster than sediment As concentrations.

4.4 DISCUSSION

4.4.1 Abrupt Changes in Sedimentology Provide Age Control for Pre and Early-20th Century Sediments

Given the inaccuracies in radiocarbon dating, we instead rely on the observed abrupt changes in sedimentology within the Markle Lake sediment record to provide age control for sediments deeper than 40 cm. Specifically, given the uneven and abrupt nature of the sediment contacts observed at 166, 159, and 131 cm depth, we interpret these transitions as unconformities wherein changes in catchment land use or flood events caused erosion of previously deposited sediments. For example, we interpret the lowermost unit as an alluvial stream deposit, likely representing a high-energy environment, or the abandoned meander of Big Sewickley Creek. The abrupt change in BD and uneven contact at 166 cm depth suggests a

change in the depositional environment, but the sedimentology still suggests a relatively high-energy environment given the large, poorly sorted clasts. This transition likely represents the construction of a nearby grist mill in 1806, when a mill race and tunnel extending to the nearby Big Sewickley Creek were constructed at this time to power the mill (Figure 4-4) (Albert, 1882). Water was likely routed from Big Sewickley Creek to augment Markle Lake's level during dry periods so the lake could serve as a constant head reservoir to power the mill (Reynolds, 2002). Lake levels likely fluctuated during this period, as water also appears to have been diverted from the unnamed tributary of Big Sewickley Creek, creating the inflow of Markle Lake (Figure 4-1b). Periods of low lake levels would allow lakebed sediments to be eroded, and produce the observed uneven contact. Thus we infer an unconformity at 166 cm in the sediment record that we assign an age of ~1806.

We interpret the two other observed erosional surfaces at 159 and 131 cm as unconformities resulting from significant 19th century floods. In particular, in 1812 a flood destroyed the mill dam servicing the grist mill (Albert, 1882), providing a high enough energy environment to disturb lakebed sediments and produce an erosional unconformity. The sedimentological unit following this event suggests a great deal of organic matter deposition occurred during this period, which would be consistent with discharges of organic-rich tannery waste into Markle Lake (Clark, 1897).

Likewise, the sharp, uneven contact at 131 cm depth likely reflects an 1879 flood (Albert, 1882), again, an event that would have disturbed lake sediments to cause an erosional unconformity (Figure 4-2, *color ramp*). Because there are no extended changes in BD in the time following both of these unconformities, it is likely that both of these were relatively short

Figure 4-4. Digitized locations of historical structures (*black squares*), paper mill (*green triangle*), grist mill (*red circle*), and the tannery (*brick red square*) (Lake and Ames, 1857; Beers and Beers, 1867, 1876)**.The location of the historical mill dam (*pink*) was determined via 0.5 meter aerial imagery** (PAMAP Program PA Department of Conservation and Natural Resources Bureau of Topographic and Geologic Survey, 2006)**, and the mill race (*orange*) was digitized from historical county atlases** (Lake and Ames, 1857; Beers and Beers, 1867, 1876) **and the 1954 United States Geologic Survey topographic map** (United States Geologic Survey, 1954)**. The *orange dashed line* designates the general location of tunnel which connected Big Sewickley Creek and the mill race.**

lived flood events, and thus do not reflect an extended period of altered of catchment hydrologic regimes.

Between 131 cm and the start of our ^{210}Pb chronology (40.5 cm) we observe no changes in BD or organic matter that suggest an abrupt change in depositional environment. This is supported by the sedimentology, which suggests a relatively lower energy lacustrine environment with moderately high and stable lake levels, conducive to the growth of diatoms. The uninterrupted deposition of similar sediment characterized by gradual transitions and the lack of abrupt, uneven contacts leads us to conclude that sediment deposition has been continuous from 131 cm to the top of the core.

Since we infer no erosional events and by extension, no possible sediment age controls, instead, we use the sharp increase in sediment MS (Figure 4-2d), and sediment Cd, Pb, and Zn concentrations (Figure 4-3d – f) at 68.5 cm as the final inferred sediment age in the Markle Lake record. Specifically, the increased MS values observed in this portion (<68.5 cm) of the sediment record suggests that these sediments are relatively enriched with ferromagnetic materials (Hatfield and Stoner, 2013). As ferromagnetic materials are contained within dust and fly ash emitted from metallurgical facilities (Strzyszcz *et al.*, 1996), this rise in magnetic susceptibility could indicate the opening of the nearby Union Steel Company rod mill, the American Steel and Wire Works, and/or the Donora Zinc Works.

These facilities opened in 1901, 1908, and 1915 respectively (Schrenk *et al.*, 1949), and utilized coal as a fuel (Schrenk *et al.*, 1949). When combusted, coal emits dust with relatively high magnetic susceptibility (Strzyszcz *et al.*, 1996; Kapička *et al.*, 1999). In particular, the Donora Zinc Works is probably the dominant source of coal fly ash, as in 1916 it was the largest

coal-fired smelter in the United States (Ingalls, 1916), and furthermore, the largest zinc smelter in the world (Bleiwas and DiFrancesco, 2010). As only sediment Cd, Pb, and Zn concentrations sharply increase at 68.5 cm, the rise in sediment MS most likely represents the opening of the Donora Zinc Works, and thus 1915.

4.4.2 Sediment Arsenic Contamination Results from Historical Leather Tanning

Arsenic, Cd, and Zn, concentrations all spike during the early portion (~163 - 127 cm) of the Markle Lake sediment record (Figure 4-3a, e, & f). However, the duration of elevated Cd and Zn concentrations are much shorter (~14 cm) than the duration of elevated As concentrations (36 cm), suggesting the variability in concentrations result from distinct processes. In particular, pieces of coal and brick were found within these sediments, though not widespread, suggesting that refuse was sometimes dumped directly into the lake and could provide relatively short, but intense loadings of Cd and Zn-rich materials (e.g., coal). This pattern is consistent with observed brief spikes in sediment Cd and Zn concentrations (137 – 143 and 135 – 149 cm, respectively). However, refuse dumping in the lake is not consistent with extended periods of elevated As concentrations. In particular, these As concentrations, exceed average crustal abundance of As (2.85 mg kg^{-1}) (Turekian and Wedepohl, 1961) by a factor of ten for several core increments.

The high As concentrations are the most notable feature of the 19th century portion (~163 - 127 cm) of the Markle Lake sediment record (Figure 4-3a). Specifically, these historical As loadings are nearly five times the As loadings during the portion of the sediment record

when the Donora metallurgical facilities, namely the Donora Zinc Works, were online (~68.5 – 37.5 cm). It is possible that the increases in As result from a natural source of As, such as the weathering of As-rich parent materials (e.g., coal) (Kabata-Pendias, 2011). However, if weathering of coal was the source of the increased As loadings, this signal should be present through the entire sediment record, as changes in catchment hydrology are minor during this period compared to more recent activities (e.g., underground mining, etc.). Therefore this As contamination likely occurs due to human activity, especially given the historical documentation of a leather tannery on the shore of Markle Lake (Figure 4-4).

Humans have used As pesticides since antiquity (Nriagu, 2001), and subsequently As has been employed as a pesticide during leather tanning (Davis *et al.*, 1994; Sadler *et al.*, 1994; Nriagu, 2001). For example, effluents from 19th century leather tanneries in Massachusetts, USA were noted to contain relatively elevated As concentrations (Clark, 1897). The exact date of the tannery opening at Markle Lake cannot be established with absolute certainty. However, the tannery, and other buildings constructed in the early 19th century are all portrayed on the 1857 county atlas (Figure 4-4) (Lake and Ames, 1857). Other buildings in the immediate vicinity of Markle lake were constructed between 1806 and 1811, therefore the tannery was likely constructed in a similar timeframe (Albert, 1882). The tannery operated until at least 1876 (Beers and Beers, 1876), and appears to have released As-rich effluent to the lake, resulting in the increased sediment As concentrations during this period. The elevated Ca concentrations in core sediments during the same period (Figure 4-3b), further suggest the influence of the nearby tannery, as lime was used to dehair hides during the leather tanning process (Clark, 1897).

4.4.3 Markle Lake Sediments Record Legacy Contamination Remobilization

The additional peak in sediment As, Cd, and Zn concentrations that occurs shortly after (~120 cm) the final unconformity (131 cm) suggests prior trace metal contamination was remobilized (Figure 4-3a, e & f). While the exact mechanism of this remobilization is likely impossible to identify, this spike does occur immediately following the unconformity generated by the 1879 flood. During this flood, it is possible catchment sediments, and by extension, legacy As contamination were physically remobilized. Mobilization via this mechanism would be consistent with Spliethoff and Hemond's observations of remobilized legacy As contamination in Mystic Lake sediments, which they attribute to the disturbance of catchment sediments (Spliethoff and Hemond, 1996). Remobilization from fluvial sediments is consistent with the relatively slow decline of sediment As concentrations after ~120 cm depth. A flood event could also physically transport Cd and Zn-rich materials (e.g., coal) to lake waters, resulting in the relatively brief period (127 – 107 cm) of elevated sediment Cd and Zn concentrations, after which sediment Cd concentrations return to values near average crustal abundance (0.16 mg kg^{-1}) and sediment Zn concentrations return to values measured in carbonates (which directly underlie Markle Lake) (20.0 mg kg^{-1}) (Turekian and Wedepohl, 1961).

4.4.4 Coal Extraction Alters Sediment Trace Metal Loadings

The rise in sediment Ba concentrations (~120 cm) following the final observed erosional contact (Figure 4-3c), appears to signify the onset of the consequences of acidic mine drainage from coal extraction in the region. Specifically, coal mining alters local water quality regimes,

and ultimately results in increased sulfate loadings to stream waters (Johnson and Hallberg, 2005). Dissolved Ba in turn, rapidly precipitates in the presence of sulfates, forming relatively insoluble barite ($BaSO_4$) (Kabata-Pendias, 2011). In the Markle Lake record, sediment Ba concentrations are relatively elevated between 1879 and 1915 (121 – 68 cm depth), the beginning of which corresponds to the onset of nearby coal industries. In particular, the nearby Marchand coal mine first appears on the 1876 county atlas (Beers and Beers, 1876; Wilson, 1962), along with numerous coke works (Beers and Beers, 1876; Wilson, 1962). Furthermore, an increase in sulfate loadings during the late 19^{th} century is confirmed in the written record, which note an increase of stream water sulfate concentrations (Boucher, 1906). While studies have observed mine drainage waters relatively saturated in respect to barite (Banks *et al.*, 1997a, 1997b), or the formation of secondary barite via the dissociation of sulfide minerals (Romero *et al.*, 2010), our study suggests downstream lake environments also seem to be relatively sensitive to acid mine drainage.

Coal mining operations appear to have significantly altered regional surface water chemistry for an extended period of time. Much like the rise in sediment Ba concentrations reflects the onset of significant coal mining operations, and the resulting increase of sulfate loadings to surface waters, the decline in sediment Ba concentrations in 1915 (68.5 cm) (Figure 4-3c), likely reflects a decrease of sulfate loadings to surface waters. Specifically, decreased sulfate loadings seem to result from a lowered groundwater table. In particular, the written record notes low groundwater levels in the nearby mining town of Hutchinson in 1927 (Wilson, 1962), which presumably resulted from local coal mining operations. Thus, we attribute the rise and fall in sediment Ba concentrations to significant nearby coal mining operations, which

appear to have significantly altered regional surface water chemistry for approximately thirty-six years.

4.4.5 Increased Cd, Pb, and Zn Loadings via Donora Industry

The onset of metallurgical facilities in Donora, namely the Donora Zinc Works (DZW), dramatically affected regional trace metal loadings. Specifically, sediment Cd, Pb, and Zn concentrations (Figure 4-6c – e), and sediment MS (Figure 4-2d), all sharply increase upon the opening of the DZW in 1915. This relationship is expected, as notable amounts of Cd, Pb, and Zn were measured by the United States Public Health Service (USPHS) in DZW

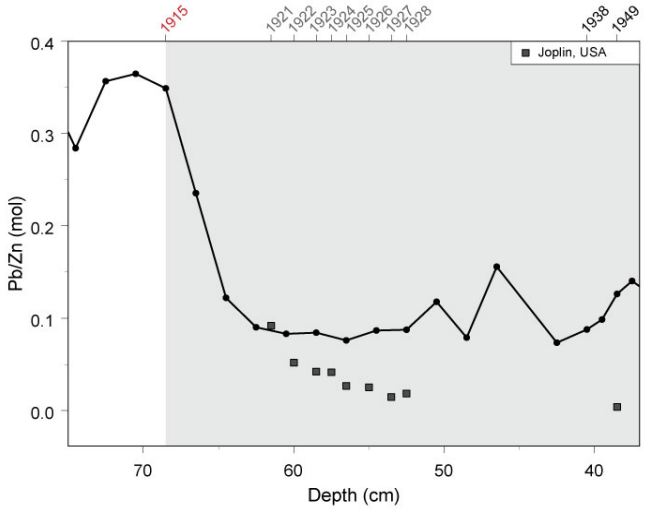

Figure 4-5. Lead zinc molar ratios during the early to mid-20th century portion of the Markle Lake sediment record. The *grey shaded area* indicates the approximate lifespan of the Donora Zinc Works. The boxes designate yearly average values of lead zinc ratios in zinc ores produced from Joplin, Missouri, USA (American Bureau of Metal Statistics, 1928; Smith and Moyer, 1949)**. Sediment ages determined by the ^{210}Pb age model (*black*), historical documents (*red*) and estimation via the extrapolation of calculated sedimentation rates (*grey*) are provided on the secondary x-axis.**

emissions, with the USPHS concluding roughly 5% of the DZW Zn production capacity escaped into the atmosphere (Schrenk *et al.*, 1949). In addition to historical documentation, the influence of the zinc works is also suggested by sediment molar Pb/Zn ratios.

Patterns in sediment molar Pb/Zn ratios both confirm the influence of the DZW, and appear to respond to changes in feedstock materials processed at the DZW. Because Zn ores contain varying Pb and Cd contents (Kabata-Pendias, 2011), ratios of these elements can characterize the locality of different Zn ores (Siebenthal, 1915). Here we utilize sediment molar Pb/Zn ratios for source identification, due to the scarcity of assayed Cd content in Zn concentrates processed at the DZW. Specifically, sediment Pb/Zn ratios decrease in 1915 (68.5 cm), approaching a relatively consistent value typical of Joplin, Missouri Zn concentrates (Figure 4-5). This relationship is unsurprising, as during the 1920s the DZW processed Zn concentrates from the Joplin district of Missouri, USA (Bleiwas and DiFrancesco, 2010). The decrease in sediment Pb/Zn values from 68.5 to approximately 60 cm depth likely reflects an increase in the purity of Joplin Zn concentrates processed at the DZW, as a similar decrease is observed in Pb/Zn values of Joplin Zn concentrates (Figure 4-5, *boxes*) (American Bureau of Metal Statistics, 1928; Smith and Moyer, 1949). Likewise, the increased variability of sediment Pb/Zn values during the early 1930s likely reflects Zn concentrates processed from a wide variety of localities in the 1930's including, among others, Ducktown, Tennessee and Blamat-Edwards, New York (Bleiwas and DiFrancesco, 2010). Thus, the elevated sediment Cd, Pb, and Zn concentrations between ~67 and 41 cm depth reflect increased Cd, Pb, and Zn loadings via DZW emissions.

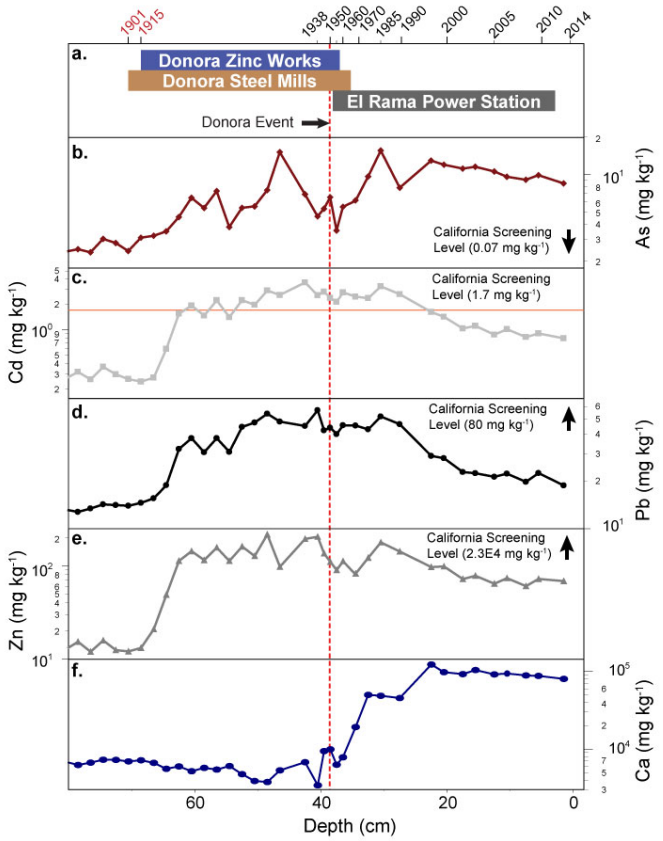

Figure 4-6. The *navy*, *gold*, and *grey* bars in panel *(a)* indicate the period when the Donora Zinc Works (Schrenk et al., 1949), Donora Steel Mills (Schrenk et al., 1949), and Elrama Power Plant (United States Energy Information Administration, 2014), respectively were online. Panels b –f provide sediment core arsenic, cadmium, lead, zinc, and calcium concentrations, respectively and the appropriate California soil screening levels (the most stringent levels in the United States) (OEHHA, 2010). Sediment ages determined by the ^{210}Pb age model (*black*) and by historical documents (*red*) are provided on the secondary x-axis.

While the opening of the DZW relatively rapidly resulted in a sustained period of increased sediment Cd, Pb, and Zn loadings, sediment As concentrations do not appear as sensitive to this event. For example, the opening of these facilities is only marked by a gradual increase in sediment As concentrations (Figure 4-6b). Instead, the most dramatic rise in sediment As concentrations during the lifespan of the DZW occurs during the late

1920s or early 1930s (54.5 cm). This timing appears to coincide with the addition of a Dwight Lloyd sintering plant at the DZW (1927) (Bleiwas and DiFrancesco, 2010), noted by the USPHS to emit both gaseous and particulate forms of As (Schrenk *et al.*, 1949). After this period (46.5 cm) sediment As concentrations decrease, possibly reflecting an increased usage of natural gas in the Donora metallurgical facilities, or the installation of a precipitator to recover fugitive emissions from the sintering plant (Schrenk *et al.*, 1949). However, without further documentation, the exact cause of the decrease in sediment As concentrations at this time cannot be confirmed.

Beginning in the late-1940s sediment Cd, Pb, and Zn concentrations all decrease, though the decrease at this time is most pronounced in sediment Zn concentrations (Figure 4-6c – e). This decline could possibly relate to a decrease in production, or improved Zn recovery methods implemented at the DZW. However, due to the lack of documentation during this period (e.g., DZW production reports are only available for 1932 – 1938) (United States Steel Corporation, 1933, 1935, 1937, 1939), the exact cause of the decline during this period cannot be ascertained. This decrease continues into the mid-1950s presumably reflecting the closure of the DZW in 1957 (Bleiwas and DiFrancesco, 2010). However the trend of decreased trace metal loadings is short-lived, ending with the construction of a coal-fired power plant nearby.

4.4.6 Coal-Fired Power Plant Emissions Sustain Elevated Trace Metal Loadings

During the mid to late-20th century (~37 cm) sediment As, Zn, and Ca concentrations increase, apparently in response to the opening of the nearby Elrama coal-fired power station in 1952 (Figure 4-1a) (United States Energy Information Administration, 2014). The sharp increase in sediment As and Ca concentrations, in contrast to the relatively smaller increase in sediment Zn concentrations, suggests that the opening of the Elrama power station affected As and Ca loadings more strongly than Zn loadings (Figure 4-6b, e, & f)**.** The increase in As loadings via coal combustion is expected, as coal combustion products in the Appalachian region, in particular fly ash, contain relatively high As concentrations (Swanson *et al.*, 2013). Furthermore, the dramatic increase in sediment Ca concentrations at this time likely reflects the use of lime (CaO) during coal combustion, which increases the heat output of the coal during combustion (Dallas, 1903). The continual rise of sediment As concentrations during the 1950s to 80s likely reflects the extra generators, and thereby capacity, added until the Elrama power station reached its full capacity in 1960 (United States Energy Information Administration, 2014). Likewise, the installation of a high Ca lime flue gas scrubber at the Elrama power station likely is responsible for the continual rise of sediment Ca concentrations during this period (Biondo and Marten, 1977). Furthermore, emissions from this type of scrubber have been noted to contain relatively higher loadings of both Zn and As than electrostatic precipitators (Ondov *et al.*, 1979). Although sediment As and Zn concentrations increase in response to the opening of the Elrama power station, sediment Cd and Pb concentrations appear largely unaffected by this event (Figure 4-6c & d)**.** This discrepancy could result from these elements being associated with

relatively different particle sizes of coal combustion products. However, fly ash from a coal-fired power station burning Appalachian coals was noted to contain 48 and 54 percent by mass of As and Pb respectively (Swanson *et al.*, 2013). Thus, an association of As and Zn with different particle sizes does not appear to drive the contrast between patterns in sediment As and Zn concentrations and patterns in sediment Cd and Pb concentrations. Instead, this discrepancy could result from Southwestern Pennsylvania coals containing relatively higher average concentrations of As and Zn than Cd and Pb ($2.42x10^{-3}$, $1.46x10^{-3}$, $8.17x10^{-6}$, and $6.50x10^{-4}$, percent by mass, respectively) (Palmer *et al.*, 2015).

Loadings of As, Cd, Pb, and Zn decrease beginning in the late 1980s, presumably in response to changes in electricity generation and environmental air quality legislation. While the decline in sediment Pb concentrations does appear to coincide with the 91% phase out of leaded gasoline mandated in 1986 (Schwartz *et al.*, 1985), the relatively similar patterns of sediment As, Cd, Pb, and Zn concentrations suggests that leaded gasoline is not the source

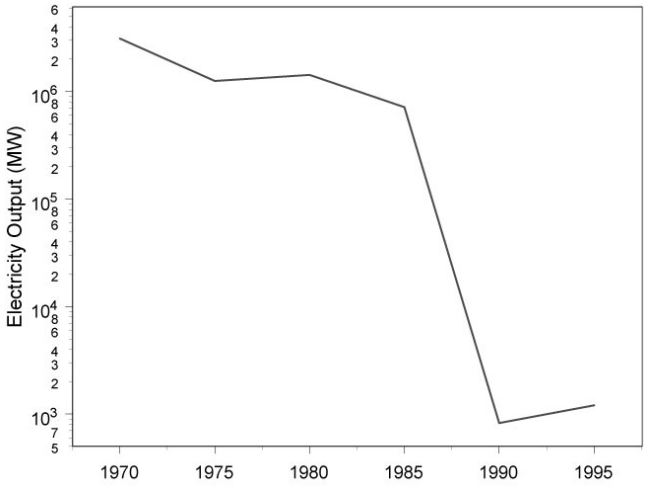

Figure 4-7. Electricity output of the Elrama coal-fired power station for the years 1970-1995 (United States Energy Information Administration)**.**

of these loadings. Instead, this decline appears to be linked to decreases in coal combustion, and therefore particulate matter emissions from the nearby Elrama power station. For example, the decline in sediment As, Cd, Pb, and Zn concentrations after 1985 coincides with a drop off in electricity output from the Elrama plant (Figure 4-7).(United States Energy Information Administration) Furthermore, this decline also coincides with enactment of the 1990 amendments to the United States Clean Air Act, which defined several trace metals, including As, Cd, and Pb, as a toxic air pollutants,(United States Environmental Protection Agency, 1990) and limited emissions of these trace metals by stationary sources (e.g., coal-fired power stations).

The relatively slow decline of sediment As, Cd, Pb, and Zn concentrations is likely driven by continued particulate matter loadings via Elrama power station. For example, the Elrama station is listed as emitting 504 tonnes yr^{-1} of $PM_{2.5}$ in the 2002 USEPA emission inventory (United States Environmental Protection Agency, 2002). Furthermore, the closure of the Elrama power station was determined to significantly decrease regional $PM_{2.5}$ concentrations (Russell, 2015). Thus, particulate emissions from Elrama likely continued to augment regional trace metal loadings, despite environmental legislation, until the closure of the Elrama plant in 2012. Although trace metal loadings have decreased during the late-20^{th} century until present day, sediment As, Cd, Pb, and Zn concentrations are still elevated above background concentrations. In particular, sediment As concentrations exceed recommended screening levels established by the state of California (Figure 4-6b) (OEHHA, 2010).

4.5 IMPLICATIONS

Reconstruction of the Markle Lake sediment record demonstrates that while modern trace metal (e.g., As, Cd, Pb, Zn) loadings are substantial, historical trace metal loadings can potentially be as large or larger. Specifically, legacy sediment As contamination exceeds ten times the average crustal abundance of As (Turekian and Wedepohl, 1961), and is nearly five times the amount of As contamination caused by the infamous Donora Zinc Works (Figure 4-3a) (Snyder, 1994). Furthermore, during this period, sediment As concentrations are at or exceed five hundred times soil screening levels established by the state of California (OEHHA, 2010). Subsequently, this significant As contamination has interacted with extreme hydrologic events (i.e., floods of 1812, 1879), confirming legacy contamination has the potential to impair ecosystems during modern periods. Four thousand four hundred and fifteen leather tanneries existed in the United States in 1810 (Coxe, 1814). If the legacy As contamination observed at Markle Lake occurs at even a fraction of these tanneries, this risk is distributed across the eastern United States.

This study also demonstrates that progress in decreasing trace metal emissions from one industry can be quickly lost due to establishment of other industries. Together, this history sequence results in extended periods of trace metal contamination, despite apparent incremental improvements in industrial hygiene. For example, while sediment Cd and Pb concentrations relatively rapidly increase in response to the opening of the Donora Zinc Works, sediment Cd and Pb concentrations do not rapidly decline in response to the closing of this facility. Instead, sediment Cd and Pb concentrations remain elevated for nearly forty

years beyond the lifetime of the smelter (Figure 4-6c – d). Subsequently, sediment Cd concentrations exceed recommended screening levels for approximately eighty years (Figure 4-6c) (OEHHA, 2010). Moreover, although sediment As, Cd, Pb, and Zn concentrations decrease after the enactment of environmental legislation (e.g., Clean Air Act), the rate of this decrease appears to be retarded by particulate emissions from a coal-fired power station. As a consequence, present day sediment concentrations remain elevated above average crustal abundance (Turekian and Wedepohl, 1961), despite a relative lack of metallurgical activity for the past forty years.

Characterizing legacy trace metal contamination is essential to effective ecosystem management, as the remobilization of legacy contamination poses a threat to both ecosystem and human health. Remobilization of legacy contamination can occur through anthropogenic or natural processes, including alterations to surface water geochemistry via the extraction of energy reserves. This is particularly important in regions like Southwestern Pennsylvania, where rapid increases in unconventional gas extraction have created substantial challenges in the disposal of flowback waters (Wilson and VanBriesen, 2012). Furthermore, changing global climate alters global hydrologic regimes, thereby increasing the probability of extreme precipitation events (Palmer and Räisänen, 2002) and flooding events (Jongman *et al.*, 2012). Interactions between changing water chemistry and hydrologic regimes are even more of a challenge to predict. For example, flood events can remobilize alluvial sediments and during such a flood, increased salinity could promote partitioning to the dissolved phase in unexpected ways, creating potentially more dangerous conditions. Thus, documentation of significant legacy trace metal storage is essential for a realistic assessment of ecosystem impacts,

particularly in regions with multiple historical industrial impacts and ongoing, rapid changes in industrial activity.

5.0 PHOSPHORUS DEPOSITION AND ACCUMULATION IN ROADSIDE SOILS: THE ROLE OF VEHICULAR SOURCES IN PHOSPHORUS BUDGETS

5.1 INTRODUCTION

The role of Phosphorus (P) in global biogeochemical cycles is well established, however the variety of sources to global budgets have not been well characterized. Phosphorus is a major component of fertilizers (Jasinski, 2013), and with the beginning of industrial agricultural fertilization in the mid-20th century, application rates of P to agricultural soils have greatly increased (Crop Reporting Board, 1966). While the role of agricultural P sources in global budgets are relatively well characterized (e.g., Smil, 2000), the influence of atmospheric sources of P on global P budgets is generally less understood (Stoddard *et al.*, 2016). Regardless, increases in P inputs have transformed the global P cycle (Filippelli, 2008). Phosphorus is frequently a limiting nutrient in aquatic ecosystems (Elser *et al.*, 2007), and larger inputs of P increase the incidence of eutrophication events (Anderson *et al.*, 2002). Eutrophication events can lead to undesirable consequences, including the production of toxins by photosynthetic algae (Anderson *et al.*, 2002), depletion of dissolved oxygen in the water column, shifts in species composition, and fish kills (Smith, 1998). The role of P mobilization from agricultural soils in increasing P loadings to surface waters is well established (Wilcock, 1986; Vighi and

Chiaudani, 1987; Ward *et al.*, 1990; Uunk, 1991). This chapter documents the currently under characterized loadings of P to near-road areas from vehicular exhaust, which appear to be a potentially substantial component of global P budgets.

Diesel fuel (Pierson and Brachaczek, 1982; Spencer *et al.*, 2006) and both leaded (Pierson and Brachaczek, 1982), and unleaded (Pierson and Brachaczek, 1982; Spencer *et al.*, 2006) gasolines contain varying P contents. Additionally, lubricating oils contain P-based additives (Pierson and Brachaczek, 1982; Nicholls *et al.*, 2005; Spencer *et al.*, 2006; McDonald, 2009), namely Zinc dialkyl dithiophosphate (ZDDP) (McDonald, 2009), which was patented in 1944 (Freuler, 1944). As a result, vehicle emissions contain particulate matter with P content ranging from 0.0006 – 0.48 % by mass (non-diesel: Pierson and Brachaczek, 1982; Hildemann, 1991; Que Hee, 1994; Watson *et al.*, 1994), and 0.006 – 0.15 % by mass (diesel: Pierson and Brachaczek, 1982; Hildemann, 1991; Lowenthal *et al.*, 1994; Watson *et al.*, 1994). Because P-based additives have been used in lubricating oils for over 70 years (Freuler, 1944), and the P content of additives was unregulated for 45 years (Spikes, 2004), it is likely roadside soils have received substantial P inputs due to the deposition of vehicular exhaust.

This study synthesizes P and arsenic (As) concentration data in roadside soils across multiple cities, including a metropolitan-scale analysis of Southern California, USA and a roadside transect scale study of Pittsburgh, Pennsylvania, USA. At both scales and locations, total soil P increases closer to the roadside. Furthermore, in Southern California, soil molar P/As ratios become increasingly similar to literature P/As values for vehicular exhaust near the road edge. These patterns in soil chemistry suggest that roadside soils receive substantial loadings of P from the roadway. Specifically, soils less than 40 m from the road edge in the Los Angeles

Metropolitan Area have accumulated hundreds of kilograms of P per hectare, a substantial mass comparable to estimated accumulations of P in global agricultural soils. These results, coupled with the expansion of global road networks, necessitates managers to account for this legacy P pool in global P budgets.

5.2 METHODS

5.2.1 Site Descriptions

The soil samples analyzed in this study are archived samples collected from roadside areas in Southern California, USA and Pittsburgh, Pennsylvania, USA. Twenty-one samples were collected from surficial (< 5 cm sampling depth) park (i.e., city, state, or wildland reserves) soils in regions of Los Angeles and Riverside County Figure 5-1a). Mean annual temperature ranges from 9.5 to 19 °C and mean annual precipitation ranges from 223 to 706 mm (PRISM Climate Group Oregon State University, 2004) (Table 5-1). Parent material of southern California sample localities varies greatly, but primarily consists of Quaternary alluvial deposits and Mesozoic granitic intrusives (California Geological Survey, 2012). Likewise, a wide variety of soil types were sampled. Detailed descriptions of the soil types and bedrock geology of sampled areas are provided in Rossi *et al.* (2015).

In Pittsburgh, Pennsylvania, USA twenty-four soil samples were collected from a transect located perpendicular to a sixty-three year old (Pennsylvania. Dept. of Highways United States. Bureau of Public Roads, 1953) portion of I-376 (Figure 5-1b). The mean annual

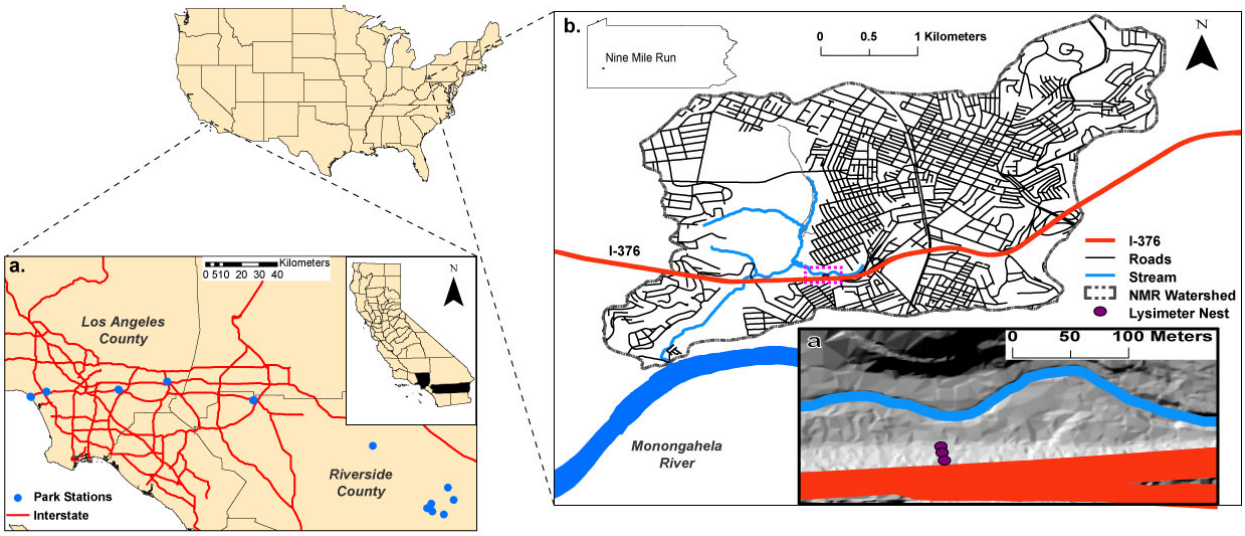

Figure 5-1. Map of sampling locations in Southern California, USA (a) and Pittsburgh, Pennsylvania, USA (b). Figures adapted from Rossi *et al.*, (2015b, 2016).

temperature and precipitation of the sampling transect are 11 °C (Arguez *et al.*, 2010) and 959 mm (PRISM Climate Group Oregon State University, 2004), respectively (Table 5-1). Geology underlying the sampling transect comprises cyclic sequences of Pennsylvanian age limestone, siltstone, shale, and sandstone (Leighton, 1927). Soils of the transect are Ultic Hapludalfs (Urban land-Culleoka complex), consisting of silt loams, channery silt loams, and flaggy clay loams (Newbury *et al.*, 1981; Soil Survey Staff *et al.*, 2013).

5.2.2 Sample Collection

Southern California soil samples were collected in July 2008, originally to examine soil respiration, and later, to examine soil acidification processes in roadside soils (Rossi *et al.*, 2015). Likewise, roadside soil samples were collected from Pittsburgh, Pennsylvania in July and August 2013 for a previous study examining major cation mobilization in roadside soils via

Table 5-1. Sampling distance from the roadside (Allegheny County Division of Computer Services Geographic Information Systems Group, 2006; Los Angeles County GIS Data Portal, 2012; Riverside County Transportation & Land Management Agency, 2012), average annual daily traffic (AADT), average annual daily truck traffic (ADTT) counts (California Department of Transportation, 2009; Pennsylvania Department of Transportation Bureau of Planning and Research Geographic Information Division, 2016), mean annual temperature (MAT) (PRISM Climate Group Oregon State University, 2004b; Arguez *et al.*, 2010)**, and mean annual precipitation** (PRISM Climate Group Oregon State University, 2004b) **for the Southern California sampling stations and the Pittsburgh, Pennsylvania roadside transect.**

Station	Distance from Road (m)	AADT	ADTT	MAT (°C)	MAP (mm)
		Southern California			
AGH	301	6,100	427	18.7	235
BDC	5031	*NA*	*NA*	13.6	379
JR	543	5,900	236	11.8	676
PF	957	*NA*	*NA*	13.9	420
FG1	63.9	329,000	22,579	18.4	464
FG2	17.6	329,000	22,579	18.4	464
FP1*	27.1	252,000	27,720	18.5	283
FP2*	8.34	252,000	27,720	18.5	283
PP1*	3.50	102,000	3,122	16.7	351
PP2*	32.3	102,000	3,122	16.9	355
PRP1ǂ	18.7	514,500	16,378	17.5	380
PRP2ǂ	2.08	514,500	16,378	17.5	380
SR5	2295	*NA*	*NA*	12.8	482
SR6	2921	*NA*	*NA*	11.1	582
SR7	4482	*NA*	*NA*	10.6	612
SR8	6975	*NA*	*NA*	9.47	666
WN1	29.1	460,000	36,291	19.2	394
WN2	24.7	460,000	36,291	19.2	394
		Pittsburgh, Pennsylvania			
Top-Slope	8.24	40,187	3,283	11.0	959
Mid-Slope	15.3	40,187	3,283	11.0	959
Bottom-Slope	24.4	40,187	3,283	11.0	959

*Traffic counts for only one lane were available.
ǂTraffic counts reflect the average between traffic counts collected at two post miles.

inputs of high total dissolved solid solutions (Rossi *et al.*, 2016). Detailed information pertaining to sample collection in Southern California, and Pittsburgh, Pennsylvania, are provided in chapter 2 (Rossi *et al.*, 2015) and chapter 3 (Rossi *et al.*, 2016), respectively.

5.2.3 Chemical and Laboratory Analysis

Samples collected from Pittsburgh, Pennsylvania were dried at 50 °C for 48 h and a portion powdered in a ball mill (tungsten carbide bomb). Powdered soil samples were nearly totally digested (i.e., magnetites and silicates were likely not dissolved) in aqua regia (3:1, vol/vol, concentrated, sub-boil distilled hydrochloric and nitric acid) with a dropwise addition of 30% hydrogen peroxide (vol/vol). Sediment extracts were diluted with 2% nitric acid (vol/vol, sub boil distilled), spiked with an internal standard of Be, Ge, and Tl, and analyzed for near-total As and P concentrations on an inductively coupled mass spectrometer (Perkin-Elmer Nexion 300x ICP-MS) at the University of Pittsburgh. Sample As concentrations were measured using the kinetic energy discrimination (KED) method. Duplicates were run every seven samples and were generally within 10% of each other. Blanks were run every ten samples to check for memory effects and were below the calibration blank intensities. Instrument drift was assessed by running a drift check after every ten samples, which were generally within 10% of previous sample measurements. Soil organic matter was measured via LOI, determined by combusting the dried sample in a muffle furnace at 550 °C for 4 h at the University of Pittsburgh.

Phosphorus source provenance was determined via mixing model analysis (Faure and Mensing, 2005). In mixing model analysis, elemental ratios are compared amongst collected

samples and endmembers to evaluate the influence of endmembers on observed soil chemistry. For our analysis, we normalize soil P concentrations with soil As concentrations. Arsenic was selected because it exhibits similar chemical behavior as P (Wenzel, 2013), and is found in vehicular components (e.g., brakes and tires) (McKenzie *et al.*, 2009).

5.2.4 Spatial and Statistical Analysis

Spatial analysis was conducted in ArcGIS 10.2. Road coverage data for Allegheny (Allegheny County Division of Computer Services Geographic Information Systems Group, 2006), Los Angeles (Los Angeles County GIS Data Portal, 2012), and Riverside (Riverside County Transportation & Land Management Agency, 2012) counties were obtained from county governments, and used to determine the distance of the sampling site from the roadway. Traffic volumes for Southern California and Pittsburgh, Pennsylvania were collected from state agencies (California Department of Transportation, 2009; Pennsylvania Department of Transportation Bureau of Planning and Research Geographic Information Division, 2016). For two sampling areas in Southern California (FP and PP), traffic counts were only available for one side of the roadway. Consequently these counts were doubled to consider traffic volumes in both directions (i.e., east and west bound). Similarly, because traffic volumes were not counted at the post mile near one sampling area (PRP), the average of traffic counts collected at the two nearest post miles was taken to represent the traffic volume near the sample collection area. To account for site variability within each sampling area, the average soil As and P concentrations for each area (e.g., concentrations for FP1 and FP2 were averaged to comprise

FP) were compared to traffic volumes. Data and statistical analysis were performed in Tibco Spotfire S+ 8.2.0. and the R software (R Core Team, 2016).

5.2.5 Phosphorous Accumulation Calculations

Phosphorus accumulation in Southern California roadside soils was determined first by selecting a breakpoint in soil P concentrations versus distance from the roadside. Specifically, 40 m was chosen as previous studies (e.g., Daines *et al.*, 1970; Wylie and Bell, 1973; Clift *et al.*, 1983; Kingston *et al.*, 1988) have determined that majority of gasoline associated lead is deposited between 30 and 50 m from the roadside. Next, soil P concentrations were averaged for each group (i.e., samples less than 40 m from the roadside, and samples greater than 40 m from the roadside). We assume the distant group to be representative of background soil P concentrations, and therefore the difference between the two averages represents the amount of P (in mg kg^{-1}) that has accumulated in near-road soils. Subsequently we determine the amount of P accumulated (P_{accum}, in kg ha^{-1}):

$$P_{accum} = \{[\overline{P}] \times (V_{soil} \times \rho_{sed} \times (1 - \phi_{soil}))\} \times (1 \times 10^{2}) \quad (\mathbf{1})$$

where, $[\overline{P}]$ is the amount of P (in mg kg^{-1}) that has accumulated in near-road soils, V_{soil} is the volume of soil sampled (5 cm^3), ρ_{sed} is the density of sediments (2.65×10^{-3}, kg cm^{-3}), and ϕ_{soil} is the porosity of soil (assumed to be 0.40). Finally, we assume a sample surface area of 1 cm^2 and multiply by 1×10^2, to determine the amount of P accumulated in kg ha^{-1}.

Because soil depth profiles were sampled along the Pittsburgh roadside transect we instead assess the degree of P accumulation by considering thickness weighted averages (P_{avg},

in mg kg^{-1}):

$$P_{avg} = 1/H \times \sum(h_i \times [P]) \quad (2)$$

where h_i is the thickness (i.e., depth range) of each sampled soil horizon (in cm), [P] is the P concentration (in mg kg^{-1}) of the sampled depth range, and H is the total thickness of the soil column (in cm).

To quantify P loadings from the weathering of asphalt paving materials, first the mass of P present in a 1 meter unit length of asphalt roadway at a sampling area was determined ($P_{Asphalt}$, in kg):

$$P_{Asphalt} = [\%B \times (w_{road} \times h_{Asphalt} \times \rho_{Asphalt})] \times \% P_{Asphalt} \quad \textbf{(3)}$$

where %B is the percent of asphalt binder (11.7 % by mass) (California Department of Transportation, 2012a), w_{road} is the width of the roadway near the sampling area (in m), $h_{Asphalt}$ is the thickness of the asphalt base course (assumed to be 0.15 m for the sampled regions) (California Department of Transportation, 2005, 2012b), $\rho_{Asphalt}$ is the density of asphalt (assumed to be 2390 kg m^{-3}) (California Department of Transportation, 2012a), and $\%P_{Asphalt}$ is the P content in asphalt (assumed to be 1.2 % by mass) (Reinke and Glidden, 2010).

Next, P loadings ($\overline{P}_{Asphalt}$, in kg ha^{-1} yr^{-1}) to near-road areas (i.e., within 40 meters from the roadside) via the weathering of asphalt were estimated:

$$\overline{P}_{Asphalt} = [P_{Asphalt} \times \tau) \div A] \div t_{PPA} \quad \textbf{(4)}$$

where $P_{Asphalt}$ is mass of P in a 1 meter length of roadway as determined by (3), τ is the assumed yearly road surface attrition rate (0.05 % by mass), A is the near-road area (80 m^2 or 0.008 ha),

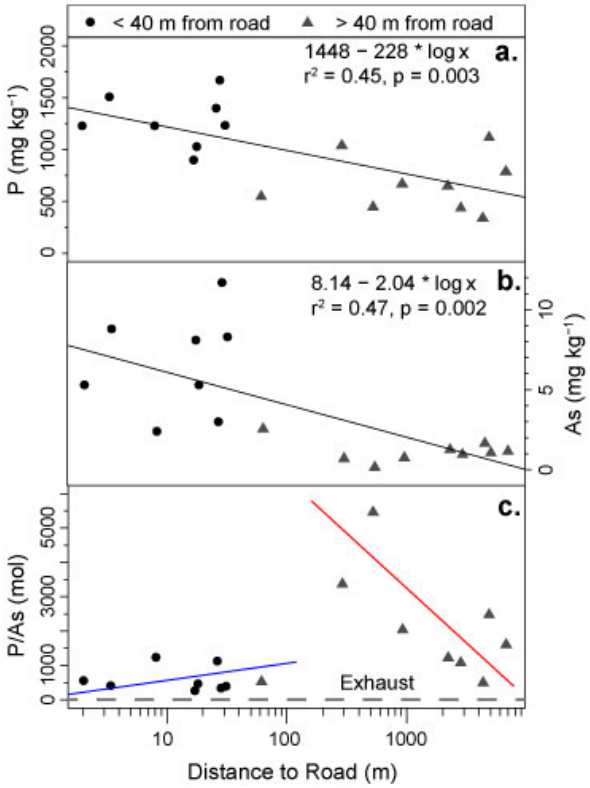

Figure 5-2. Southern California soil phosphorus (a), arsenic (b), and molar phosphorus arsenic ratios (c) versus the log transformed distance from roadside. The *dashed line* in panel c indicates the average of values (39.0) measured in vehicle exhaust (Hildemann, 1991; Lowenthal *et al.*, 1994; Gillies *et al.*, 2001). The *circles* represent samples collected within 40 m from the roadside, whereas the *triangles* indicate samples collected greater than 40 meters from the roadside. One outlying phosphorus and arsenic concentration (2480 mg kg^{-1}, not shown, 24.7 m from the road) likely reflects fertilizer inputs.

and t_{PPA} is the accumulation period (i.e., that P based asphalt additives have been used, or 35 yr) (Cao *et al.*, 2011).

Similarly, P loadings from vehicular exhaust ($\overline{P}_{Exhaust}$, in kg ha^{-1} yr^{-1}) were calculated:

$$\overline{P}_{Exhaust} = \{[(P_{Exhaust} \times m_{PM}) \times T] \div A\} \times t_{ZDDP} \quad \textbf{(5)}$$

where $P_{Exhaust}$ is the average mass of P in vehicular emissions (assumed to be 0.21 % by mass) (Pierson and Brachaczek, 1982; Hildemann, 1991; Lowenthal *et al.*, 1994; Watson *et al.*, 1994;

Cadle *et al.*, 1999, 2001; Gillies *et al.*, 2001), m_{PM} is the vehicular emission factor of particulate matter (3.3E-7 kg PM m^{-1}) (United States Environmental Protection Agency Office of Transportation and Air Quality, 2008a, 2008b), T is the sum of AADT and ADTT, A is the near-road area (80 m^2 or 0.008 ha), and t is the accumulation period (i.e., the length of time ZDDP has been used, or 64 yr) (Freuler, 1944).

5.3 RESULTS

5.3.1 Trends in Southern California Roadside Soil As and P Concentrations

In surficial southern California soil samples, P and As concentrations are related to the log transformed sampling distance from the roadway (r^2= 0.45 and 0.47, respectively). Specifically, near-road soils contain relatively higher soil P and As concentrations (Figure 5-2a & b). Furthermore, soil P concentrations are also related to average annual daily traffic (r^2 = 0.33), and soil As concentrations are also related to average annual daily traffic (r^2 = 0.50) (Table 5-2).

Table 5-2. R^2 and *p* values for linear regression analysis of Southern California samples.

	P		As	
	r^2	*p* value	r^2	*p* value
Average annual daily traffic (AADT)	0.31	0.20	0.50	0.08
Annual average daily truck traffic (ADTT)	0.33	0.17	0.42	0.12
Total Traffic (AADT + ADTT)	0.31	0.19	0.49	0.08

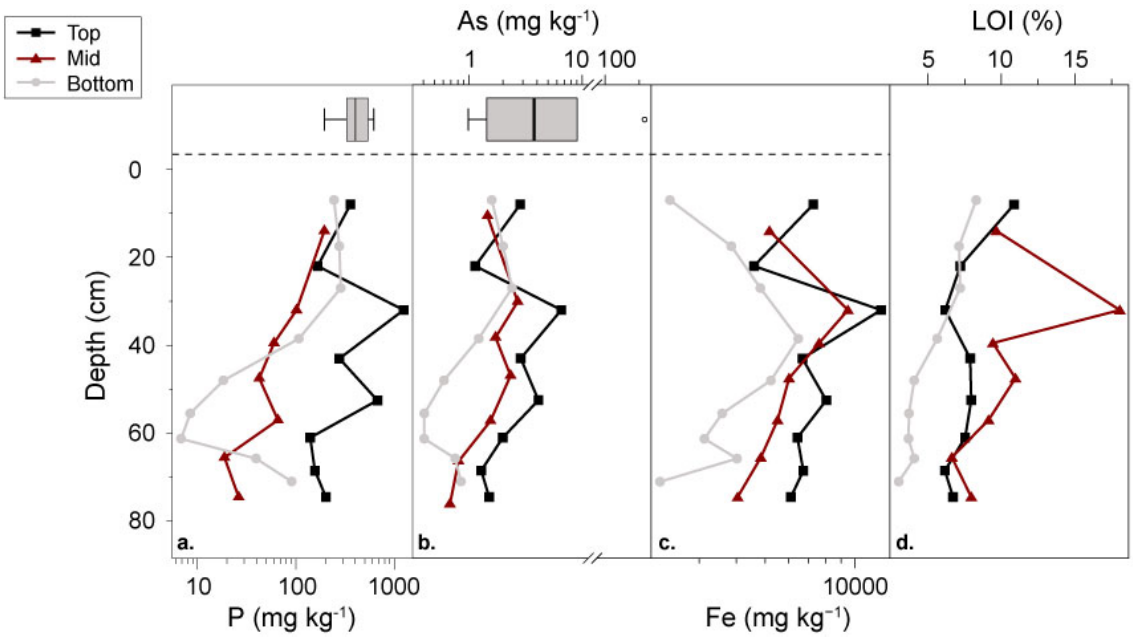

Figure 5-3. Depth profiles of phosphorus (a), arsenic (b), and iron (c) concentrations, and organic matter content (d) in soils sampled from a roadside transect in Pittsburgh, Pennsylvania, USA. The *color* and *shape* of the symbols indicate the position of the sample along the hillslope. The box plots in the *dashed box* in panels a & b display phosphorus and arsenic concentrations in sampled parent material. The outlying parent material arsenic concentration occurs in a shale sample with observable iron nodules, suggesting arsenic was concentrated during sediment deposition.

Soil P/As molar ratios also appear to be influenced by road proximity, decreasing towards values (39.0 ± 23.9) typical of vehicular exhaust (Figure 5-2c, *dashed line*) (Hildemann, 1991; Lowenthal *et al.*, 1994; Gillies *et al.*, 2001). Additionally, there is a break in soil P/As ratios that appears to occur at approximately 100 meters from the roadway (Figure 5-2c).

5.3.2 Patterns in Roadside Soil P and As Concentrations in Pittsburgh, Pennsylvania

In the soils collected from the roadside transect in Pittsburgh, Pennsylvania, P and As concentrations are also related to distance from the roadway. Specifically, soil P and As

concentrations are generally higher in near road soils (Figure 5-3a & b), with the highest concentrations occurring at 32 and 53 cm depth. Furthermore, intermediate depth (~43 & 53 cm depth) top slope soil P concentrations are relatively enriched in comparison to local bedrock (Figure 5-3a, box plot). At all depths, mid-slope soil P concentrations are relatively depleted in comparison to local parent material (Figure 5-3a, *box plot*). Additionally, bottom slope soils deeper than approximately 40 cm are relatively depleted in comparison to local bedrock (Figure 5-3a, *box plot*). In general, soil As concentrations are within the range of As concentrations measured in sampled bedrock (Figure 5-3b). However As concentrations in mid-slope and bottom slope soils deeper than approximately 40 cm are relatively depleted in comparison to

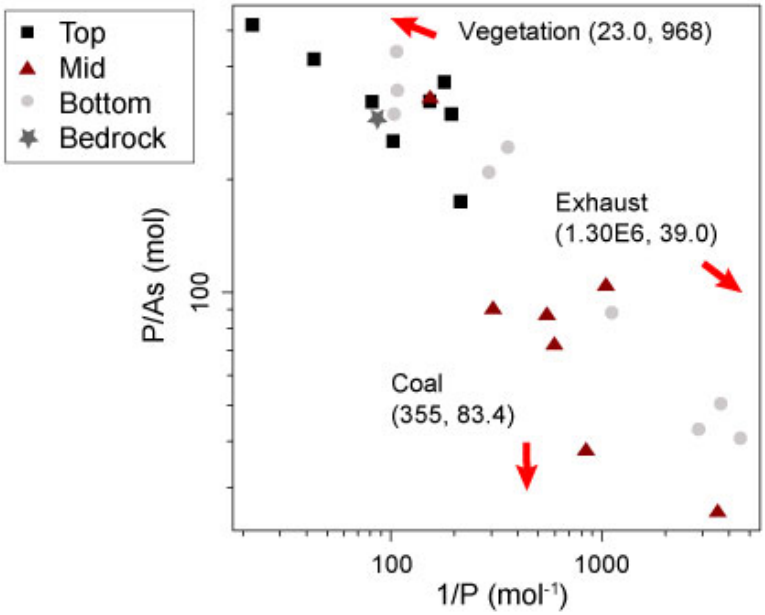

Figure 5-4. Pittsburgh soil phosphorus concentrations normalized with soil arsenic concentrations. Top slope nest samples are represented by *boxes*, mid slope nest samples are represented by *triangles*, and bottom slope nest samples are represented by *circles*. The *star* represents values measured in sampled bedrock. The *arrows* designate values of sampled leaves and leaf litter, average values of exhaust (Hildemann, 1991; Lowenthal *et al.*, 1994; Gillies *et al.*, 2001), and coal (Palmer *et al.*, 2015).

local bedrock (Figure 5-3b). Lastly, in general, soil organic matter content is highest in the mid-slope soils, and lowest in the bottom slope soils (Figure 5-3d).

Unlike Southern California, Pittsburgh transect soil P/As molar ratios do not display a clear influence from the roadway. However, soil P/As molar ratios do appear to be influenced by two source end members (Figure 5-4). Furthermore, at all sampling stations, soil P/As molar ratios are weakly related (r^2 = 0.25) to sampling depth. In particular, soil P/As values generally increase in shallow portions of the soil. In particular, top-slope soils appear to be influenced by an end member with relatively higher P/As values, and mid-slope soils appear to be influenced by an end member with relatively lower P/As values. However, bottom slope soils appear to be influenced by both of these end members.

5.3.3 Phosphorus Accumulation Calculations

In general, soils within 40 meters of the roadside in Southern Californian contain more P than soils greater than 40 meters from the roadway. Specifically, soils sampled within 40 meters from the roadside have an average P concentration of 1276 mg kg^{-1}, whereas soils sampled greater than 40 meters from have an average P concentration of 672 mg kg^{-1} (*t* test $p < 0.001$) (Table 5-3). Thus, it appears that 604 mg kg^{-1} of P has accumulated in roadside soils. Using this value (604 mg kg^{-1}) as the $[\overline{P}]$ term in (1) suggests roadside soils in Southern California receive P loadings of 480 kg P ha^{-1} over roughly the last 64 years.

Similarly, the results of solving (2) for each soil profile sampled along the roadside transect in Pittsburgh, Pennsylvania also suggests that near-road soils have accumulated P.

Specifically, top slope (8.24 meters from roadside) soils have the highest (362 mg kg^{-1}) thickness weighted average soil P concentrations (P_{avg}) (Table 5-4). The second highest P_{avg} (147 mg kg^{-1}), which is less than half of the P_{avg} of the top slope soils, occurs at the bottom slope station (24.4 meters from roadside) (Table 5-4). Finally, mid-slope soils (15.3 meters from roadside) have the lowest P_{avg} (100 mg kg^{-1}) (Table 5-4).

5.3.4 Loadings of Phosphorus from Asphalt and Exhaust Deposition

Solving (3) with average California highway design characteristics suggests that, in general, a 1 meter length of roadway (i.e., road width) could contain between ~ 17 – 21 kg of P (Table 5-5). While these results suggest asphalt pavement is a possible source of P, solving (4) suggests that $\overline{P}_{Asphalt}$ ranges from approximately 0.03 – 0.05 kg ha^{-1} yr^{-1} (Table 5-5). Conversely,

Table 5-3. Average phosphorus concentrations in sampled Southern California soils separated into soils collected from within 40 meters from the roadside, and soils collected from greater than 40 meters from the roadside. The high phosphorus concentrations observed in sample WN2 with was deemed to result from fertilizer application. Consequently this sample was not considered during analysis.

Station	Distance from Road (m)	P (mg kg^{-1})	Station	Distance from Road (m)	P (mg kg^{-1})
PRP2	2.08	1230	FG1	63.9	550
PP1	3.50	1510	AGH	301	1040
FP2	8.34	1230	JR	543	450
FG2	17.6	900	PF	957	670
PRP1	18.7	1030	SR5	2295	650
WN2*	24.7	2840	SR6	2921	440
FP1	27.1	1400	SR7	4482	340
WN1	29.1	1670	BDC	5031	1120
PP2	32.3	1240	SR8	6975	790
< 40 meters average		*1276*	*> 40 meters average*		*672*

*Fertilizer influence

Table 5-4. Phosphorus thickness weighted averages for soils sampled from a roadside transect in Pittsburgh, Pennsylvania, USA.

Depth Range	h (cm)	[P] (mg kg^{-1})	h* [P]	Σ h* [P]	P_{avg} (mg kg^{-1})
Top Slope (8.24 meters from roadside)					
0-16	16	360	5760		
16-28	12	170	2040		
28-36	8	1200	9600		
36-50	14	280	3920	28,629	***362***
50-55	5	670	3350		
55-67	12	140	1679		
67-70	3	160	480		
70-79	9	200	1800		
Mid-Slope (15.3 meters from roadside)					
0-28	28	190	5320		
28-36	8	100	800		
36-43	7	60.1	421		
43-52	9	42.6	383	8,003	***100***
52-62	10	65.7	657		
62-69	7	18.9	132		
69-80	11	26.3	289		
Bottom Slope (24.4 meters from roadside)					
0-14	14	240	3360		
14-21	7	280	1933		
21-33	12	290	3430		
33-44	11	110	1181		
44-52	8	20	147	10,865	***147***
52-59	7	8.49	59.4		
59-63.5	4.5	6.85	30.8		
63.5-68	4.5	39.5	178		
68-74	6	90	545		

loadings of P loadings from the weathering of asphalt ($\overline{P}_{Asphalt}$) are relatively minimal. Specifically from vehicular emissions ($\overline{P}_{Exhaust}$) appear to be much larger, ranging from 0.28 – 1.39 kg ha^{-1} yr^{-1} (Table 5-5).

Table 5-5. Calculated phosphorus content of asphalt ($P_{Asphalt}$), phosphorus loadings from asphalt weathering ($\vec{P}_{Asphalt}$), and phosphorus loadings from exhaust deposition ($\vec{P}_{Exhaust}$) for five sampled near-road areas in Southern California, and the entire Pittsburgh transect.

Station	AADT	ADTT	Traffic	Road Width (m)	$P_{Asphalt}$ (kg)	$\vec{P}_{Asphalt}$ (kg ha^{-1} yr^{-1})	$\vec{P}_{Exhaust}$ (kg ha^{-1} yr^{-1})
				Southern California			
PRP	514,500	16,378	530,878	42.0	21.1	0.04	2.98
FP	252,000	27,720	279,720	34.0	17.1	0.03	1.57
PP	102,000	3,122	105,122	40.0	20.1	0.04	0.59
WN	460,000	36,291	496,291	52.0	26	0.05	2.78
FG	329,000	22,579	351,579	34.0	17.1	0.03	1.97
				Pittsburgh			
Transect	40,187	3,283	43,470	30	15.1	0.03	0.23

5.4 DISCUSSION

5.4.1 Vehicular Emissions Input P and As to Los Angeles Roadside Soils

In Southern California, surficial soils within 40 meters from the roadway are relatively enriched with P and As (Figure 5-2a & b). The relatively higher soil As concentrations in these roadside soils is hardly surprising, as the enrichment of As, and other trace metals in roadside environments is widely reported (Lagerwerff and Specht, 1970; Page and Ganje, 1970; Jaradat and Momani, 1999; Al-Chalabi and Hawker, 2000; Yun *et al.*, 2000; Pagotto *et al.*, 2001; Fakayode and Olu-Owolabi, 2003; Akbar *et al.*, 2006; Christoforidis and Stamatis, 2009; Ezer, 2009) However, fewer studies have reported noticeably higher P concentrations in near-road soils (Lagerwerff and Specht, 1970). While the relatively higher P concentrations in roadside

soils could possibly result from other human activities (e.g., fertilizer application), this is unlikely, as the same soils are relatively depleted in K (Rossi *et al.*, 2015), a common component of commercial fertilizers (Jasinski, 2013). Similarly, the relatively elevated soil P concentrations in near-road (i.e., within 40 meters of the road edge) soils likely do arise from P accumulation during cycles of vegetative uptake and decomposition. For example, P concentrations are not related ($r^2 < 0.01$) to soil organic matter. Instead, because the relatively higher concentrations within 40 meters from the roadway (Figure 5-2a & b, *circles*), are consistent with the depositional patterns of vehicular emissions reported in previous studies (Lagerwerff and Specht, 1970; Jaradat and Momani, 1999; Fakayode and Olu-Owolabi, 2003; Cape *et al.*, 2004), P and As appear to be sourced from the roadway.

Soil molar ratios also suggest that vehicular emissions are the source of the relatively elevated soil P concentrations in near-road soils. Specifically, as they approach the roadway, soil P/As molar ratios decrease towards values typical of vehicular exhaust (Figure 5-2d, *dashed line*). T The exact cause of the break in soil P/As molar ratios at 100 m from the roadside is not entirely clear, but may indicate mixing of multiple source end members. Soils distant from the roadway appear influenced by a source end member with low P/As values, possibly local granitic parent material (California Geological Survey, 2012). Likewise, samples at approximately 100 meters from the roadway could be influenced by a source end member with relatively high P/As ratios. However, soil molar P/As ratios could also possibly reflect a difference in the biogeochemical cycling of P and As. Specifically, P is a relatively tightly cycled nutrient (Ryan, 2014), thus soil P is likely tightly cycled by the vegetation. Conversely, As is generally toxic to vegetation (Kabata-Pendias, 2011), and therefore uptake by vegetation

should be minimal. These differences would allow soil P pools to remain relatively constant, whereas soil As pools would eventually be depleted over time by leaching, thus resulting in higher soil P/As ratios. As trace element chemistry, namely As, of local parent materials and local vegetation is not available in the literature, these end members cannot be confirmed at the present time.

5.4.2 Vehicular Emissions Also Input P and As to Pittsburgh Roadside Soils

Phosphorus concentrations in the Pittsburgh roadside transect soils also appear to be influenced by exhaust deposition, though not as strongly as in Southern California soils. In particular, the relatively elevated P concentrations in the top slope (i.e., near-road) soils (Figure 5-3a), suggest a roadway influence. However, unlike Southern California, P concentrations do not vary strongly with distance from the roadway, but instead depend on sampling depth (Figure 5-3a). For example, soil P concentrations peak in top slope soils at approximately 32 cm below the land surface, and again at 53 cm depth (Figure 5-3a). Additionally, top slope soil Fe concentrations also peak at these same depths (Figure 5-3c).

This relationship could reflect P leaching to depth (Miller *et al.*, 2001) and sorbing to Fe oxyhydroxides (Parfitt, 1989; Miller *et al.*, 2001). Soil P also appears to be leached in mid and bottom slope soils, as in general, P concentrations decrease with increasing depth in these soils (Figure 5-3a). The rise in soil P concentrations in deeper bottom slope soils (> 60 cm depth) could result from leached P accumulating at depth, or P being transported upward by fluctuations of the local groundwater. While the exact cause for this rise in P concentrations is

not clear from the current data, the upwards transport of P would be in line with previously theorized Ca and Mg transport patterns in these same soils (Rossi *et al.*, 2016).

5.4.3 Implications for Roadside Geochemistry

The combination of the Southern California and Pittsburgh studies suggests that, nationally, if not globally, roadside soils are a potentially significant pool of P. Specifically, when considering the data from either study alone, one could argue that the observed influence of vehicular emissions on near-road soil P concentrations represents a localized phenomenon. However, the presence of this relationship across a regional gradient (i.e., Southern California) and at multiple locations seems to indicate our observations do not reflect small scale patterns. Additionally, our findings appear to be relatively independent of local geology and soil type, suggesting that our observations are minimally influenced by the local geochemical setting. Thus, it appears that in general, vehicular emissions are a significant source of near-road P.

5.4.4 Loadings of P via Asphalt Weathering are Minimal

While previous studies have suggested the possibility of P enrichment via exhaust deposition (Lagerwerff and Specht, 1970), this work appears to be the first clear documentation of P accumulation in roadside areas. Previous work examining P in urban environments have claimed the importance of roadways as a source of P loadings (Bannerman *et al.*, 1993; Gilbert and Clausen, 2006; Metson *et al.*, 2012), albeit through a less probable mechanism. In particular, these studies have attributed asphalt pavement as the source of the relatively higher

P concentrations observed in stormwater runoff. Moreover, P additives have been used in asphalt in in various amounts since 1973 (Cao *et al.*, 2011), although not widespread until the 1990's (Reinke and Glidden, 2010). While construction materials do influence urban soil chemistry (e.g., Bain *et al.*, 2012; Rossi *et al.*, 2015, 2016), loadings of P from asphalt weathering are too minimal to drive the observations reported here (Table 5-5). Thus, it appears that previous studies (e.g., Gilbert and Clausen, 2006; Metson *et al.*, 2012) have incorrectly identified asphalt as the source of the relatively higher P concentrations in stormwater runoff.

In particular, asphalt pavement likely does not contain a large enough P content to significantly influence near-road geochemistry. Specifically, asphalt binders contain relatively minimal amounts of P, typically < 1.2% by mass (Reinke and Glidden, 2010). Additionally, asphalt binders comprise a minimal amount of roadways. For example, the California Department of Transportation highway design manual specifies that asphalt pavement should contain ~ 12% by mass of asphalt binder (California Department of Transportation, 2012a). This specification is not unique to our study region, as European asphalts also contain similar amounts (5 – 10 %) of binder (Ntziachristos and Boulter, 2003). Taking these percentages into account, the P content of asphalt is more on the order of 0.001 % by mass.

Similarly our calculations are relatively conservative and likely grossly overestimate the wear of asphalt surfaces, and by extension, P loadings via asphalt weathering. Specifically, we assume a yearly road surface attrition rate of 0.05 %. Other studies have determined yearly rates of road surface wear anywhere between 0.0001 – 0.01 % (Muschack, 1990; Kennedy *et al.*, 2002; Klimont *et al.*, 2002), thus this assumed rate reflects a very high weathering rate and

is suitably conservative. While it is possible that we under estimate rates of road wear in areas where studded tires are used, studded tire use is minimal in the Los Angeles Metropolitan area. Moreover, the depositional patterns we observe would necessitate a relatively small particle size of road surface wear particles. While fine particles could conceivably be generated via interactions of vehicle tires and the road surface, roadway surfaces of Southern Californian state highways are generally Portland Cement Concrete, and "very erosion resistant" hot mix asphalt is used as the roadway base course (California Department of Transportation, 2012a). Thus, leaching would be the primary mechanism which would input P to near-road soils. However the arid Southern California climate, likely minimizes leaching rates, making this an unlikely P delivery mechanism. Therefore, it is unsurprising that our calculated P loadings via exhaust deposition dwarf P loadings via asphalt inputs (Table 5-5).

5.4.5 Implications for Global Phosphorus Budgets

The accumulation of P in roadside soils has important implications for surrounding natural systems, and by extension, global P budgets. In particular, loadings of P from vehicular emissions appear to have resulted in the accumulation of 480 kg P ha^{-1} in Southern California roadside areas, which when divided by the lifespan of ZDDP equates to 7.50 kg P ha^{-1} yr^{-1}, a value slightly less than measured annual accumulations (12.8 kg P $ha^{-1}yr^{-1}$) of P in European agricultural soils (Runge-Metzger, 1995), and larger than global estimates of annual (5.57 kg P $ha^{-1}yr^{-1}$) P accumulation in agricultural soils (Bennett *et al.*, 2001).

Currently, in global P budgets, agricultural activities (e.g., fertilizer and manure application) are generally considered to be the dominant anthropogenic source of P loadings to soils, and ultimately surface waters, via erosional losses (e.g., Smil, 2000; Peñuelas *et al.*, 2013). However, our results suggest that atmospheric deposition can be a significant contributor of P to terrestrial environments. This conclusion has also been reached in the current literature, as other studies have suggested the growing importance of the atmospheric deposition of P (Mahowald *et al.*, 2008; Brahney *et al.*, 2015; Wang *et al.*, 2015; Stoddard *et al.*, 2016). However, our study demonstrates the potential significance of vehicular emissions to the atmospheric P budget, whereas previous attempts to close the atmospheric P budget (e.g., Wang *et al.*, 2015) have ignored this seemingly significant source of atmospheric P.

Our findings suggest that vehicular sourced P must be incorporated into global P budgets, especially in the context of the global expansion of road networks. In particular, in 2014 there were 35.8 million km of roadways on the planet (United States Central Intellegence Agency, 2014). Assuming a depositional area of 80 m per one meter length of roadway, this constitutes an affected area of roughly 286 million ha, or 2.2 percent of the terrestrial surface of Earth, excluding Antarctica. Forecasts by the International Energy Agency predict that by 2050 the total length of roadways will expand by 25.3 million km (Dulac, 2013), thereby expanding the amount of land that receiving loadings of vehicular sourced P to roughly 489 million ha or 3.8 percent of the terrestrial surface of Earth.

In contrast, the amount of arable land is predicted to expand at much slower rates than the expansion of global road networks. Specifically, in 2013 there were 1,408 million ha of arable land on the planet (Food and Agriculture Organization, 2015), or approximately 11

percent of the terrestrial surface of Earth. Forecasts by the United Nations Food and Agriculture Organization predict that by 2050 this amount will increase to 1,661 million ha (Alexandratos and Bruinsma, 2012), or roughly 13 percent of the terrestrial surface of Earth. This expansion only represents an 18 percent increase, a value much smaller than the expansion of global roadways, which are projected to increase by 71 percent.

Ultimately, the relatively rapid expansion of global road networks poses a significant concern for managers seeking to minimize P inputs. Specifically, recent literature has recognized the need to consider the role of legacy P pools in modern P cycles (e.g., Sharpley *et al.*, 2014; Powers *et al.*, 2016). Because road networks are known to increase both rates of soil erosion (Forman and Alexander, 1998; Jones *et al.*, 2000), and runoff (Dunne and Leopold, 1978), and soil P losses occur primarily during erosional and runoff events (Sharpley *et al.*, 1992), the accumulation of P in roadside soils creates a P pool with a high propensity to be mobilized, and therefore should be carefully accounted for in future P budgets.

5.5 CONCLUSIONS

The increased soil P and As concentrations observed in Southern California roadside soils appear to result from the deposition of vehicular exhaust (Figure 5-2a & b). Specifically, the use of P-based additives in fuels and lubricating oils (Pierson and Brachaczek, 1982; Nicholls *et al.*, 2005; Spencer *et al.*, 2006; McDonald, 2009) appears to contribute significant amounts of P to near-road soils, as the relationships of soil P concentrations match previously reported depositional patterns of other roadway sourced contaminants (Lagerwerff and Specht, 1970;

Jaradat and Momani, 1999; Fakayode and Olu-Owolabi, 2003). Because these patterns persist across a regional gradients of bedrock lithologies, climate, and vegetation composition, it is unlikely the observed relationships result from a natural source of P. Moreover, soil molar P/As ratios highlight the influence vehicle emissions on roadside soil P and As concentrations (Figure 5-2c).

Likewise, soils along a roadside transect in Pittsburgh, Pennsylvania also appear to have accumulated P from the deposition of vehicular exhaust (Figure 5-3a). Specifically, thickness weighted averages of three sampled soil profiles located 8, 15, and 24 meters from a major interstate demonstrate that near-road soils contain, on average, more than twice as much P as other soils (Table 5-4). However, the accumulation of P in Pittsburgh soils is not as striking as the P accumulation in Southern California roadside areas. This discrepancy likely results from the relatively smaller traffic volumes in Pittsburgh (Table 5-5). Furthermore, the relatively humid climate promotes the leaching of roadway P and As, thereby obscuring a clear vehicle exhaust source signature.

This work clearly documents the accumulation of P in roadside areas, building on previous literature suggesting the possibility of P enrichment via exhaust deposition (e.g., Lagerwerff and Specht, 1970). Additionally, although previous studies have identified roadways, specifically asphalt, as a source of P loadings (Bannerman *et al.*, 1993; Gilbert and Clausen, 2006; Metson *et al.*, 2012). It is doubtful that the weathering of asphalt would provide enough P to drive our observations, as the average calculated P loading from asphalt weathering (0.04 kg ha^{-1} yr^{-1}) are over ten times smaller than the average calculated P loading via vehicular exhaust (0.92 kg ha^{-1} yr^{-1}) (Table 5-5). Consequently, these traffic borne P loadings appear to

have resulted in annual accumulation of 7.50 kg P ha^{-1} yr^{-1} in Southern California roadside areas, which is larger than previously estimated rates (5.57 kg P $ha^{-1}yr^{-1}$) of P accumulation in global agricultural soils (Bennett *et al.*, 2001). Thus, inputs of P due to the deposition of vehicular exhaust appear to represent a relatively significant flux of the terrestrial P cycle, and therefore should be considered in future nutrient abatement efforts.

6.0 CLOSING REMARKS

This dissertation, like previous literature, has demonstrated that human activities have had a substantial impact on both loadings and dynamics of metals. However, while existing literature generally documents effects of isolated processes (e.g., considering only the impacts of soil acidification), fewer studies have examined urban soil metal dynamics that result from the interaction of multiple processes. This research documents some of these interactions, including the interactions between the weathering of road construction materials and soil acidification processes. This research also characterizes relatively poorly understood and undercharacterized sources of notorious environmental contaminants (e.g., the accumulation of phosphorus in near-road soils), that have resulted in significant legacy contamination. Furthermore, this dissertation demonstrates that while periods of metal contamination are commonly thought to reflect the lifespan of the polluter, the historical sequence of multiple industries likely results in extended periods of trace metal contamination. Moreover, rapid shifts in industry (e.g., unconventional gas extraction), or extreme hydrologic events can mobilize this legacy contamination, and pose a substantial risk to ecosystem and human health. Thus consideration of these interactions is essential for effective landscape management, particularly in areas where legacy contamination is poorly characterized.

Chapter 2 demonstrated that soil acidification processes observed in forested soils also occur in the roadside environment. However, these processes are relatively nuanced, as they are heavily influenced by local lithology and human activities. In particular, while multiple elements were depleted in roadside soils, calcium pools were largely unaffected, due to calcium inputs from the weathering of concrete road materials. The insensitivity of soil calcium pools to soil acidification is contrary to observations made in forested ecosystems, as calcium depletion is a well reported repercussion of soil acidification. Thus, building materials appear to exert strong control on urban soil chemistry.

Chapter 3 emphasized the importance of the local hydrologic setting on seasonal cation dynamics in urban ecosystems. Specifically, the influence of both topographically and infrastructurally driven hydrological flowpaths on sodium transport was documented. These multiple flowpaths resulted in an extended period of elevated soil water sodium and chloride concentrations, and subsequently chronic sodium loadings to coupled systems. However, once again, the built environment heavily influenced the observed soil metal dynamics, as the transport of sodium appeared to be driven by aging highway drainage infrastructure. Additionally, roadside soils were enriched with calcium via the weathering of concrete road materials.

Chapter 4 underlined the lasting influence of legacy industries on regional metal chemistry. In the approximately 210 year sediment record, trace metal loadings via multiple industries (e.g., leather tanning, coal extraction, metallurgy) were reconstructed. Notably, modern arsenic loadings were overshadowed by historic trace metal loadings. Furthermore, Chapter 4 also demonstrated that progress in decreasing trace metal emissions from one

industry can be quickly lost due to establishment of other industries. Together, this history sequence can result in extended periods of trace metal contamination, that can be remobilized through anthropogenic or natural (e.g., extreme hydrologic events) processes. This is especially relevant to areas experiencing rapid changes in industrial activity (e.g., Southwestern Pennsylvania), that can alter surface water chemistry via the extraction of energy reserves and perturb the local geochemical setting.

Chapter 5 illustrated the significant accumulation of phosphorus in Southern California roadside soils. While other studies have identified roadways, specifically asphalt, as a source of P loadings, calculated P loadings via asphalt weathering (0.04 kg ha^{-1} yr^{-1}) are over ten times smaller than calculated P loadings via vehicular exhaust (0.92 kg ha^{-1} yr^{-1}). We estimate the accumulation of 800 kg P ha^{-1} in Southern California roadside areas, which when divided by the lifespan of ZDDP equates to 12.5 kg P ha^{-1} yr^{-1}, a value comparable to measured annual accumulations (12.8 kg P $ha^{-1}yr^{-1}$) of P in European agricultural soils (Runge-Metzger, 1995), and larger than global estimates of annual (4.85 kg P $ha^{-1}yr^{-1}$) P accumulation in agricultural soils (Bennett *et al.*, 2001).

BIBLIOGRAPHY

Abbott MB, Stafford Jr TW. 1996. Radiocarbon geochemistry of modern and ancient Arctic lake systems, Baffin Island, Canada. *Quaternary Research* **45** (3): 300–311

Aber J, Nadelhoffer K, Steudler P, Melillo JM. 1989. Nitrogen saturation in northern forest ecosystems. *BioScience* **39** (6): 378–386

Akbar K, Hale W, Headley A, Athar M. 2006. Heavy metal contamination of roadside soils of Northern England. *Soil & Water Research* **1** (4): 158–163

Albert GD. 1882. *History of the County of Westmoreland, PA.* L.H. Everts & co.: Philadelphia, PA.

Al-Chalabi A, Hawker D. 2000. Distribution of vehicular lead in roadside soils of major roads of Brisbane, Australia. *Water, Air, and Soil Pollution* **118** (1988): 299–310

Alexander FW, Delves HT. 1981. Blood lead levels during pregnancy. *International Archives of Occupational and Environmental Health* **48** (1): 35–9

Alexandratos N, Bruinsma J. 2012. World agriculture towards 2015/2030: the 2012 revision. In *ESA Working Paper No. 12-03*Food and Agriculture Organization: Rome; 1–147. DOI: 10.1016/S0264-8377(03)00047-4

Allegheny County Division of Computer Services Geographic Information Systems Group. 2006. Allegheny County - Street Centerlines Available at: http://www.pasda.psu.edu/uci/MetadataDisplay.aspx?entry=PASDA&file=AlleghenyCounty_Streetcl2006.xml&dataset=1224

Van Alphen M. 1999. Atmospheric heavy metal deposition plumes adjacent to a primary lead-zinc smelter. *Science of the Total Environment* **236** (1–3): 119–134 DOI: 10.1016/S0048-9697(99)00272-7

American Bureau of Metal Statistics. 1928. Ninth Annual Issue - 1928. *Yearbook of the American Bureau of Metal Statistics* **9**

Amrhein C, Strong JE, Mosher PA. 1992. Effect of deicing salts on metal and organic matter mobilization in roadside soils. *Environmental Science & Technology* **26** (4): 703–709

Anderson DM, Glibert PM, Burkholder JM. 2002. Harmful algal blooms and eutrophication: nutrient sources, compositions, and consequences. *Estuaries* **25** (4): 704–726 DOI: 10.1016/j.hal.2008.08.017

Andrews FT, Croke BFW, Jakeman AJ. 2011. Hydrological Model Assessment and Development. *Environmental Modelling & Software* **26** (10): 1171–1185

Appelo CA., Postma D. 2005. Geochemistry, Groundwater and Pollution. In *Geochemistry, Groundwater and Pollution*CRC Press: Leiden; 241.

Appleby P, Oldfield F. 1983. The assessment of 210Pb data from sites with varying sediment accumulation rates. *Hydrobiologia* **103**: 29–35

Arguez A, Durre I, Applequist S, Squires M, Vose R, Yin X, Bilotta R. 2010. PITTSBURGH ALLEGHENY CO AIRPORT PA US. In *NOAA's U.S. Climate Normals (1981-2010)*NOAA National Centers for Environmental Information. DOI: 10.7289/V5PN93JP

Ashley K, Cordell D, Mavinic D. 2011. A brief history of phosphorus: From the philosopher's stone to nutrient recovery and reuse. *Chemosphere* **84** (6): 737–746 DOI: 10.1016/j.chemosphere.2011.03.001

Axtmann E V, Luoma SN. 1991. Large-scale distribution of metal contamination in the fine-grained sediments of the Clark Fork River, Montana, U.S.A. *Applied Geochemistry* **6** (1): 75–88 DOI: 10.1016/0883-2927(91)90064-V

Bäckström M, Karlsson S, Allard B. 2004a. Metal leachability and anthropogenic signal in roadside soils estimated from sequential extraction and stable lead isotopes. *Environmental Monitoring and Assessment* **90** (1–3): 135–160

Bäckström M, Karlsson S, Bäckman L, Folkeson L, Lind B. 2004b. Mobilisation of heavy metals by deicing salts in a roadside environment. *Water Research* **38** (3): 720–32 DOI: 10.1016/j.watres.2003.11.006

Bain DJ, Brush GS. 2005. Early chromite mining and agricultural clearance: Opportunities for the investigation of agricultural sediment dynamics in the Eastern Piedmont (USA). *American Journal of Science* **305** (9): 957–981 DOI: 10.2475/ajs.305.9.957

Bain DJ, Yesilonis ID, Pouyat R V. 2012. Metal concentrations in urban riparian sediments along an urbanization gradient. *Biogeochemistry* **107** (1–3): 67–79 DOI: 10.1007/s10533-010-9532-4

Baird A, Miesch A. 1984. Batholithic rocks of southern California: A model for the petrochemical nature of their source materials. *United States Geological Survey Professional Paper* **1284**: 1–42

Banks D, Burke SP, Gray CG. 1997a. Hydrogeochemistry of coal mine drainage and other

ferruginous waters in north Derbyshire and south Yorkshire, UK. *Quarterly Journal of Engineering Geology and Hydrogeology* **30** (3): 257–280 DOI: 10.1144/gsl.qjeg.1997.030.p3.07

Banks D, Younger PL, Arnesen R-T, Iversen ER, Banks SB. 1997b. Mine-water chemistry: The good, the bad and the ugly. *Environmental Geology* **32** (3): 157–174 DOI: 10.1007/s002540050204

Bannerman RT, Owens DW, Dodds RB, Hornewer NJ. 1993. Sources of pollutants in wisconson stormwater. *Water Science and Technology* **28** (3–5): 241–259

Bauske B, Goetz D. 1993. Effects of Deicing-Salts on Heavy Metal Mobility. *Acta Hydrochimica et Hydrobiologica* **21** (1): 38–42

Beers SN, Beers DG. 1867. *Atlas of Westmoreland County, Pennsylvania: From Actual Surveys*. A. Pomeroy: Philadelphia, PA.

Beers SN, Beers DG. 1876. *Atlas of Westmoreland County, Pennsylvania: From Actual Surveys*. A. Pomeroy: Philadelphia, PA.

Bennett EM, Carpenter SR, Caraco NF. 2001. Human Impact on Erodable Phosphorus and Eutrophication: A Global Perspective. *BioScience* **51** (3): 227–234 DOI: 10.1641/0006-3568(2001)051[0227:HIOEPA]2.0.CO;2

Berg T, Edmunds W, Geyer A. 1980. Geologic map of Pennsylvania: Pennsylvania Geological Survey, 4th Series

Bettez ND, Marino R, Howarth RW, Davidson E a. 2013. Roads as nitrogen deposition hot spots. *Biogeochemistry* **114** (1–3): 149–163 DOI: 10.1007/s10533-013-9847-z

Bhaskar AS, Welty C. 2012. Water balances along an urban-to-rural gradient of metropolitan baltimore, 2001-2009. *Environmental and Engineering Geoscience* **18** (1): 37–50 DOI: 10.2113/gseegeosci.18.1.37

Bintliff JL, Davies B, Gaffney C. 1990. *Trace metal accumulation in soils on and around ancient settlements in Greece*.

Biondo S, Marten J. 1977. A History Of Flue Gas Desulfurization Systems Since 1850. Research Development and Demonstration. *Journal of the Air Pollution Control Association* **27** (10): 948–960 DOI: 10.1080/00022470.1977.10470518

Blair JM. 1988. Nutrient release from decomposing foliar litter of three tree species with spicial reference to calcium, magnesium and potassium dynamics. *Plant and Soil* **110** (1): 49–55 DOI: 10.1007/BF02143538

Blanton P, Marcus WA. 2009. Railroads, roads and lateral disconnection in the river landscapes

of the continental United States. *Geomorphology* **112** (3–4): 212–227 DOI: 10.1016/j.geomorph.2009.06.008

Blasius BJ, Merritt RW. 2002. Field and laboratory investigations on the effects of road salt (NaCl) on stream macroinvertebrate communities. *Environmental Pollution* **120** (2): 219–31

Bleiwas DI, DiFrancesco C. 2010. Historical Zinc Smelting in New Jersey, Pennsylvania, Virginia, West Virginia, and Washington, D.C., with Estimates of Atmospheric Zinc Emissions and Other Materials. *United States Geological Survey Open-File Report* **2010** (1131): 1–189

Blomqvist G, Johansson E-LL. 1999. Airborne spreading and deposition of de-icing salt — a case study. *Science of The Total Environment* **235** (1–3): 161–168 DOI: 10.1016/S0048-9697(99)00209-0

Bobbink R, Hornung M, Roelofs JG. 1998. The effects of air-borne nitrogen pollutants on species diversity in natural and semi-natural European vegetation. *Journal of Ecology* **86** (5): 717–738

Borkow G, Gabbay J. 2009. Copper, an ancient remedy returning to fight microbial, fungal and viral infections. *Current Chemical Biology* **3** (3): 272–278

Boucher JN. 1906. *History of Westmoreland County, Pennsylvania* (JW Jordan, ed.). Lewis Publishing Company: New York.

Bouzoubaa N, Zhang M. 1997. The effect of grinding on the physical properties of fly ashes and a Portland cement clinker. *Cement and Concrete Research* **27** (12): 1861–1874

Brahney J, Mahowald N, Ward DS, Ballantyne AP, Neff JC. 2015. Is atmospheric phosphorus pollution altering global alpine lake stoichiometry? *Global Biogeochemical Cycles* **29** (9): 1199–1214 DOI: 10.1002/2014GB004832.Received

Bridgeman TB, Wallace CD, Carter GS, Carvajal R, Schiesari LC, Aslam S, Cloyd E, Elder D, Field A, Schulz KL, et al. 2000. A limnological survey of Third Sister Lake, Michigan with historical comparisons. *Lake and Reservoir Management* **16** (4): 253–267

Buttle J, Labadia C. 1999. Deicing salt accumulation and loss in highway snowbanks. *Journal of Environmental Quality* **28** (1): 155–164

Bytnerowicz A, Fenn ME. 1996. Nitrogen deposition in California forests: a review. *Environmental pollution* **92** (2): 127–46

Cadle SH, Mulawa P, Groblicki P, Laroo C, Ragazzi RA, Nelson K, Gallagher G, Zielinska B. 2001. In-use light-duty gasoline vehicle particulate matter emissions on three driving cycles. *Environmental Science and Technology* **35** (1): 26–32 DOI: 10.1021/es0010554

Cadle SH, Mulawa PA, Hunsanger EC, Nelson K, Ragazzi RA, Barrett R, Gallagher GL, Lawson DR, Knapp KT, Snow R. 1999. Composition of light-duty motor vehicle exhaust particulate matter in the Denver, Colorado area. *Environmental Science and Technology* **33** (14): 2328–2339 DOI: 10.1021/es9810843

California Department of Transportation. 2005. Caltrans Pavement Climate Regions Available at: http://www.dot.ca.gov/hq/maint/Pavement/Offices/Pavement_Engineering/Climate.html [Accessed 13 June 2016]

California Department of Transportation. 2009. 2008 Annual Average Daily Truck Traffic on the California State Highway System Available at: http://www.dot.ca.gov/trafficops/census/ [Accessed 13 June 2016]

California Department of Transportation. 2012a. Chapter 660 Base and Subbase. In *California Highway Design Manual*1–4.

California Department of Transportation. 2012b. Chapter 620 Rigid Pavement. In *California Highway Design Manual*1–31.

California Geological Survey. 2012. Geologic Compilation of Quaternary Surficial Deposits in Southern California

Cao W, Liu S, Mao H. 2011. Experimental study on polyphosphoric acid (PPA) modified asphalt binders. *Advanced Materials Research* **152**: 288–294

Cape JN, Tang YS, van Dijk N, Love L, Sutton M a, Palmer SCF. 2004. Concentrations of ammonia and nitrogen dioxide at roadside verges, and their contribution to nitrogen deposition. *Environmental Pollution* **132** (3): 469–78 DOI: 10.1016/j.envpol.2004.05.009

Center for Conservation Biology at the University of California - Riverside. 2006. Total Annual Deposition of Reduced and Oxidized Nitrogen During 2002 Available at: http://ccb.ucr.edu/biocomplexityfiles/data/California 2002.zip

Chaney RL. 2010. Cadmium and Zinc. In *Trace Elements in Soils*, Hooda P (ed.).Wiley: Chichester; 409–439.

Chillrud SN, Bopp RF, Simpson HJ, Ross JM, Shuster EL, Chaky D a, Walsh DC, Choy CC, Tolley L-R, Yarme A. 1999. Twentieth Century Atmospheric Metal Fluxes into Central Park Lake, New York City. *Environmental Science & Technology* **33** (5): 657–662 DOI: 10.1021/es9807892

Christoforidis A, Stamatis N. 2009. Heavy metal contamination in street dust and roadside soil along the major national road in Kavala's region, Greece. *Geoderma* **151** (3): 257–263

Cione NK, Padgett PE, Allen EB. 2002. Restoration of a native shrubland impacted by exotic

grasses, frequent fire, and nitrogen deposition in southern California. *Restoration Ecology* **10** (2): 376–384 DOI: 10.1046/j.1526-100X.2002.02038.x

Clark HW. 1897. Volume IV: Experiments upon the purification of sewage and water at the Lawrence Experiment Station. In *Public Documents of Massachusetts: Annual Reports of Various Public Officers and Institutions for the Year 1896*Secretary of the Commonwealth: Boston, MA; 427–578.

Clarke L, Jenerette G, Bain D. 2015a. Urban legacies and soil management affect the concentration and speciation of trace metals in Los Angeles community garden soils. *Environmental Pollution*: 1–12

Clarke LW, Jenerette GD, Bain DJ. 2015b. Urban legacies and soil management affect the concentration and speciation of trace metals in Los Angeles community garden soils. *Environmental Pollution* **197**: 1–12 DOI: 10.1016/j.envpol.2014.11.015

Cooper CA, Mayer PM, Faulkner BR. 2014. Effects of road salts on groundwater and surface water dynamics of sodium and chloride in an urban restored stream. *Biogeochemistry* **121** (1): 149–166 DOI: 10.1007/s10533-014-9968-z

Correll DL. 1999. Phosphorus: a rate limiting nutrient in surface waters. *Poultry science* **78** (5): 674–682 DOI: 10.1093/ps/78.5.674

Coxe T. 1814. *A Statement of the Arts and Manufactures of the United States of America, for the Year 1810*. A. Cornman: Philadelphia, PA.

Cozzarelli IM, Herman JS, Parnell RA. 1987. The mobilization of aluminum in a natural soil system: Effects of hydrologic pathways. *Water Resources Research* **23** (5): 859–874 DOI: 10.1029/WR023i005p00859

Crabtree CG, Seaman TM. 2006. Suction Lysimeter Modifications to Improve Sampling Efficiency and Prevent Wildlife Damage. *Vadose Zone Journal* **5** (1): 77 DOI: 10.2136/vzj2005.0049

Cronan C, Schofield C. 1979. Aluminum Leaching Response to Acid Precipitation: Effects on High-Elevation Watersheds in the Northeast. *Science* **204** (4390): 304–306

Crop Reporting Board. 1966. Consumption of commercial fertilizers and primary plant nutrients in the United States, 1850 - 1964, and by states, 1945 - 64. *United States Department of Agriculture Statistical Bulletin No.* **375**: 1–84

Cunningham MA, Snyder E, Yonkin D, Ross M, Elsen T. 2008. Accumulation of deicing salts in soils in an urban environment. *Urban Ecosystems* **11**: 17–31 DOI: 10.1007/s11252-007-0031-x

Dallas GM. 1903. Compound for promoting combustion in coal: 1

Davidson A. 1971. The effects of de-icing salt on roadside verges. *J. Appl. Ecol* **8** (2): 555–561

Davies JP, Clarke BA, Whiter JT, Cunningham RJ. 2001. Factors influencing the structural deterioration and collapse of rigid sewer pipes. *Urban Water* **3** (1): 73–89 DOI: 10.1016/S1462-0758(01)00017-6

Davies P, Wright I, Jonasson O, Findlay S. 2010. Impact of concrete and PVC pipes on urban water chemistry. *Urban Water Journal* **7** (4): 233–241

Davis A, Kempton JH, Nicholson A, Yare B. 1994. Groundwater transport of arsenic and chromium at a historical tannery, Woburn, Massachusetts, U.S.A. *Applied Geochemistry* **9** (5): 569–582 DOI: 10.1016/0883-2927(94)90019-1

Davis III JA, Jacknow J. 1975. Heavy metals in waste water in three urban areas. *Journal (Water Pollution Control Federation)* **47** (9): 2292–2297

Deevey ES, Gross MS, Hutchinson GE, Kraybill HL. 1954. The natural C14 contents of materials from hard-water lakes. *Proceedings of the National Academy of Sciences* **40** (5): 285–288

Diamond J. 1955. Flame photometric determination of strontium in Portland cement. *Analytical Chemistry* **27** (6): 4–6

Dodge F. 1972. Trace-element contents of some plutonic rocks of the Sierra Nevada batholith. *United States Geological Survey Bulletin* **1113–F**: 1–13

Dodge F, Ross D. 1971. Coexisting hornblendes and biotites from granitic rocks near the San Andreas Fault, California. *The Journal of Geology* **79** (2): 158–172

Driscoll CT. 1985. Aluminum in acidic surface waters: chemistry, transport, and effects. *Environmental Health Perspectives* **63** (13): 93–104

Driscoll CT, Schecher W. 1990. The chemistry of aluminum in the environment. *Environmental Geochemistry and Health* **12** (1–2): 28–49

Driscoll CT, Driscoll KM, Mitchell MJ, Raynal DJ. 2003. Effects of acidic deposition on forest and aquatic ecosystems in New York State. *Environmental Pollution* **123** (3): 327–336 DOI: 10.1016/S0269-7491(03)00019-8

Dulac J. 2013. *Global Land Transport Infrastructure Requirements: Estimating Road and Railway Infrastructure Capacity and Costs to 2050*. Internation Energy Agency: Paris, France.

Dunne T, Leopold LB. 1978. *Water in Environmental Planning*. Macmillan: New York.

Eatough DJ, Mangelson NF, Anderson RR, Martello D V, Pekney NJ, Davidson CI, Modey WK. 2007. Apportionment of ambient primary and secondary fine particulate matter during a 2001 summer intensive study at the CMU Supersite and NETL Pittsburgh site. *Journal of*

the Air & Waste Management Association **57** (10): 1251–1267 DOI: 10.3155/1047-3289.57.10.1251

Edwards PJ, Kochenderfer J, Coble D, Adams MB. 2002. Soil leachate responses during 10 years of induced whole-watershed acidification. *Water, Air, and Soil Pollution* **140** (1–4): 99–118

Ellis JB, Revitt DM, Blackwood DJ, Gilmour DJ. 2004. Leaky sewers: assessing the hydrology and impact of exfiltration in urban sewers. In *Hydrology: Science and Practices for the 21st Century*, Webb B, , Acreman M, , Maksimovic C, , Smithers H, , Kirby C (eds).British Hydrological Society: Imperial College, London; 266–271.

Environmental Resources Reseach Institute. 2014. ERRI Small Watersheds 2014 Available at: http://www.pasda.psu.edu/uci/MetadataDisplay.aspx?entry=PASDA&file=ERRISmallWatersheds2014.xml&dataset=3047 [Accessed 5 June 2015]

Essington ME. 2004. Soil and Water Chemistry: An Integrative Approach.CRC Press: Boca Raton, FL; 109.

Ezer M. 2009. Heavy metal content of roadside soil in Kahramanmaraş, Turkey. *Fresenius Environmental Bulletin* **18** (5a): 704–708

Fakayode S, Olu-Owolabi B. 2003. Heavy metal contamination of roadside topsoil in Osogbo, Nigeria: Its relationship to traffic density and proximity to highways. *Environmental Geology* **44** (2): 150–157 DOI: 10.1007/s00254-002-0739-0

Faure G, Mensing T. 2005. *Isotopes: Principles and Applications*. Wiley: Hoboken, NJ.

Fay L, Shi X. 2012. Environmental impacts of chemicals for snow and ice control: State of the knowledge. *Water, Air, & Soil Pollution* **223** (5): 2751–2770 DOI: 10.1007/s11270-011-1064-6

Federer CA, Hornbeck J. 1989. Long-term depletion of calcium and other nutrients in eastern US forests. *Environmental Management* **13** (5): 593–601

Feliu S, Morcillo M, Chico B. 1999. Effect of Distance from Sea on Atmospheric Corrosion Rate. *Corrosion* **55** (9): 883–891 DOI: 10.5006/1.3284045

Fenn ME, Bytnerowicz A. 1997. Summer throughfall and winter deposition in the San Bernardino Mountains in Southern California. *Atmospheric Environment* **31** (5): 673–683 DOI: 10.1016/S1352-2310(96)00238-5

Fenn ME, Poth MA, Johnson DW. 1996. Evidence for nitrogen saturation in the San Bernardino Mountains in southern California. *Forest Ecology and Management* **82** (1–3): 211–230 DOI: 10.1016/0378-1127(95)03668-7

Fenn ME, Poth MA, Schilling SL, Grainger DB. 2000. Throughfall and fog deposition of nitrogen

and sulfur at an N-limited and N-saturated site in the San Bernardino Mountains, southern California. *Canadian Journal of Forest Research* **30** (9): 1476–1488 DOI: 10.1139/x00-076

Fernandez IJ, Rustad LE, Norton SA, Kahl JS, Cosby BJ. 2003. Experimental acidification causes soil base-cation depletion at the Bear Brook Watershed in Maine. *Soil Science Society of America Journal* **67** (6): 1909–1919

Filippelli GM. 2008. The Global Phosphorus Cycle: Past, Present, and Future. *Elements* **4** (2): 89–95

Food and Agriculture Organization. 2015. FAOSTAT Available at: http://faostat3.fao.org/browse/R/RL/E [Accessed 13 September 2016]

Forman RTT, Alexander LE. 1998. Roads and Their Major Ecological Effects. *Annual Review of Ecology and Systematics* **29** (1): 207–231 DOI: 10.1146/annurev.ecolsys.29.1.207

Foy C, Chaney RL, White M. 1978. The physiology of metal toxicity in plants. *Annual Review of Plant Physiology* **29**: 511–566

Freuler HC. 1944. Modified lubricating oil

Garcia-Miragaya J, Castro S, Paolini J. 1981. Lead and zinc levels and chemical fractionation in road-side soils of Caracas, Venezuela. *Water, Air, and Soil Pollution* **15**: 285–297

Gilbert JK, Clausen JC. 2006. Stormwater runoff quality and quantity from asphalt, paver, and crushed stone driveways in Connecticut. *Water Research* **40** (4): 826–832 DOI: 10.1016/j.watres.2005.12.006

Gillies JA, Gertler AW, Sagebiel JC, Dippel WA. 2001. On-Road Particulate Matter (PM2.5 and PM10) Emissions in the Sepulveda Tunnel, Los Angeles, California. *Environmental Science & Technology* **35** (6): 1054–1063 DOI: 10.1017/CBO9781107415324.004

Godwin K, Hafner S, Buff M. 2003. Long-term trends in sodium and chloride in the Mohawk River, New York: the effect of fifty years of road-salt application. *Environmental Pollution* **124** (2): 273–281 DOI: 10.1016/S0269-7491(02)00481-5

Göransson H, Edwards PJ, Perreijn K, Smittenberg RH, Olde Venterink H. 2014. Rocks create nitrogen hotspots and N:P heterogeneity by funnelling rain. *Biogeochemistry* **121** (2): 329–338 DOI: 10.1007/s10533-014-0031-x

Granato G, Church P, Stone V. 1995. Mobilization of major and trace constituents of highway runoff in groundwater potentially caused by deicing chemical migration. *Transportation Research Record* **1483**: 92–104

Graney JR, Halliday AN, Keeler GJ, Nriagu JO, Robbins JA, Norton SA. 1995. Isotopic record of lead pollution in lake sediments from the northeastern United States. *Geochimica et*

Cosmochimica Acta **59** (9): 1715–1728 DOI: 10.1016/0016-7037(95)00077-D

Gray JT. 1982. Comparative nutrient relations in adjacent stands of chaparral and coastal sage scrub. In *Symposium on Dynamics and Management of Mediterranean-Type Ecosystems*USDA Forest Service, San Diego State University: San Diego; 306–312.

Green MB, Bailey AS, Bailey SW, Battles JJ, Campbell JL, Driscoll CT, Fahey TJ, Lepine LC, Likens GE, Ollinger S V, et al. 2013. Decreased water flowing from a forest amended with calcium silicate. *Proceedings of the National Academy of Sciences of the United States of America* **110** (15): 5999–6003 DOI: 10.1073/pnas.1302445110

Gromet P, Silver L. 1987. REE variations across the Peninsular Ranges batholith: Implications for batholithic petrogenesis and crustal growth in magmatic arcs. *Journal of Petrology* **28** (1): 75–125

Grover B, Lamborn R. 1970. Preparation of porous ceramic cups to be used for extraction of soil water having low solute concentrations. *Soil Science Society of America Journal* **34** (4): 706–708

Hammond PB, Aronson AL. 1964. Lead Poisoning in Cattle and Horses in the Vicinity of a Smelter. *Annals of the New York Academy of Sciences* **111** (2): 595–611

Hatfield R, Stoner J. 2013. Magnetic Proxies and Susceptibility. In *Encyclopedia of Quaternary Science*, Elias S (ed.).Elsevier B.V.: Amsterdam; 884–898. DOI: http://dx.doi.org/10.1016/B0-44-452747-8/00312-4

Helvey JD, Patric JH. 1965. Canopy and litter interception of rainfall by hardwoods of eastern United States. *Water Resources Research* **1** (2): 193- DOI: Doi 10.1029/Wr001i002p00193

Hildemann L. 1991. Chemical composition of emissions from urban sources of fine organic aerosol. *Environmental Science & Technology* **25** (4): 744–759

Hillman AL, Abbott MB, Yu J, Bain DJ, Chiou-Peng T. 2015. Environmental legacy of copper metallurgy and mongol silver smelting recorded in yunnan lake sediments. *Environmental Science and Technology* **49** (6): 3349–3357 DOI: 10.1021/es504934r

Homer C, Huang C, Yang L, Wylie B, Coan M. 2004. Development of a 2001 national land-cover database for the United States. *Photogrammetric Engineering & Remote Sensing* **70** (7): 829–840 DOI: 10.14358/PERS.70.7.829

Hooper RP, Shoemaker C a. 1985. Aluminum mobilization in an acidic headwater stream: temporal variation and mineral dissolution disequilibria. *Science* **229** (4712): 463–5 DOI: 10.1126/science.229.4712.463

Huntington T, Hooper RP. 2000. Calcium depletion in a southeastern United States forest ecosystem. *Soil Science Society of America Journal* **64** (5): 1845–1858

Idriss K, Sedaira H, Ahmed S. 2009. of strontium and simultaneous determination of strontium oxide, magnesium oxide and calcium oxide content of Portland cement by derivative ratio spectrophotometry. *Talanta* **78** (1): 81–87 DOI: 10.1016/j.talanta.2008.10.044

Ingalls WR. 1916. The Donora Zinc Works. *Engineering and Mining Journal* **102** (15): 648–654

Isabelle PS, Fooks LJ, Keddy PA, Wilson SD. 1987. Effects of roadside snowmelt on wetland vegetation: an experimental study. *Journal of Environmental Management* **25** (1): 57–60

Jagoe C, Matey V, Haines T, Komov V. 1993. Effect of beryllium on fish in acid water is analogous to aluminum toxicity. *Aquatic toxicology* **24**: 241–256

Jaradat Q, Momani K. 1999. Contamination of roadside soil, plants, and air with heavy metals in Jordan, a comparative study. *Turkish Journal of Chemistry* **23**: 209–220

Jasinski SM. 2013. Phosphate Rock [Advance Release]. *United States Geological Survey Minerals Yearbook*: 56.1-56.9

Johnson DB, Hallberg KB. 2005. Acid mine drainage remediation options: A review. *Science of the Total Environment* **338** (1–2): 3–14 DOI: 10.1016/j.scitotenv.2004.09.002

Jones JA, Swanson FJ, Wemple BC, Snyder KU. 2000. Effects of roads on hydrology, geomorphology, and disturbance patches in stream networks. *Conservation Biology* **14** (1): 76–85 DOI: 10.1046/j.1523-1739.2000.99083.x

Jongman B, Ward PJ, Aerts JCJH. 2012. Global exposure to river and coastal flooding: Long term trends and changes. *Global Environmental Change* **22** (4): 823–835 DOI: 10.1016/j.gloenvcha.2012.07.004

Juice SM, Fahey TJ, Siccama TG, Driscoll CT, Denny EG, Eagar C, Cleavitt NL, Minocha R, Richardson AD. 2006. Response of sugar maple to calcium addition to northern hardwood forest. *Ecology* **87** (5): 1267–1280

Kabata-Pendias A. 2011. *Trace elements in soils and plants*. CRC Press: Boca Raton, FL. DOI: 10.1201/b10158-25

Kabir MI, Daly E, Maggi F. 2014. A review of ion and metal pollutants in urban green water infrastructures. *The Science of the Total Environment* **470**: 695–706 DOI: 10.1016/j.scitotenv.2013.10.010

Kapička A, Petrovský E, Ustjak S, Macháčková K. 1999. Proxy mapping of fly-ash pollution of soils around a coal-burning power plant: A case study in the Czech Republic. *Journal of Geochemical Exploration* **66** (1–2): 291–297 DOI: 10.1016/S0375-6742(99)00008-4

Karraker N, Gibbs J, Vonesh J. 2008. Impacts of road deicing salt on the demography of vernal pool-breeding amphibians. *Ecological Applications* **18** (3): 724–734

Kaste JM, Norton SA, Hess CT. 2002. Environmental Chemistry of Beryllium-7. *Reviews in Mineralogy and Geochemistry* **50** (1): 271–289 DOI: 10.2138/rmg.2002.50.6

Katzensteiner K, Glatzel G. 1992. Effects of air pollutants on mineral nutrition of Norway spruce and revitalization of declining stands in Austria. *Water, Air, and Soil Pollution* **61**: 309–322

Kaushal SS, Groffman PM, Likens GE, Belt KT, Stack WP, Kelly VR, Band LE, Fisher GT. 2005. Increased salinization of fresh water in the northeastern United States. *Proceedings of the National Academy of Sciences of the United States of America* **102** (38): 13517–20 DOI: 10.1073/pnas.0506414102

Kaushal SS, Likens GE, Utz RM, Pace ML, Grese M, Yepsen M. 2013. Increased river alkalinization in the Eastern U.S. *Environmental Science & Technology* **47** (18): 10302–11 DOI: 10.1021/es401046s

Kelly VR, Lovett GM, Weathers KC, Findlay SEG, Strayer DL, Burns DI, Likens GE. 2008. Long-term sodium chloride retention in a rural watershed: legacy effects of road salt on streamwater concentration. *Environmental Science & Technology* **42** (2): 410–5

Kennedy P, Gadd J, Moncrieff I. 2002. Emission factors for contaminants released by motor vehicles in New Zealand. *Prepared for the New Zealand Ministry of Transport and Infrastructure Auckland*

Kirchner J, Lydersen E. 1995. Base cation depletion and potential long-term acidification of Norwegian catchments. *Environmental Science & Technology* **29** (8): 1953–1960

Klimont Z, Cofala J, Bertok I, Amann M, Heyes C, Gyarfas F. 2002. Modeling particulate emissions in Europe. A framework to estimate reduction potential and control costs. In *IIASA Interim Report IR-02-076*International Institute for Applied Systems Analysis: Laxenburg, Austria.

Koryak M, Stafford L. 2001. Highway deicing salt runoff events and major ion concentrations along a small urban stream. *Journal of Freshwater Ecology* **16** (1): 125–134

Koryak M, Stafford L. 2002. Impacts of steel mill slag leachate on the water quality of a small Pennsylvania stream. *Journal of Freshwater Ecology* (August 2012): 37–41

Kozar MD, McCoy KJ, Britton JQ, Blake Jr. BM. 2012. Hydrogeology, Groundwater Flow, and Groundwater Quality of an Abandoned Underground Coal-Mine Aquifer, Elkhorn Area, West Virginia. *United States Geological Survey Bulletin* **B**-**46**: 1–103

Krám P, Hruška J, Wenner B, Driscoll CT, Johnson CE. 1997. The biogeochemistry of basic cations in two forest catchments with contrasting lithology in the Czech Republic. *Biogeochemistry* **37** (2): 173–202

Kumpiene J. 2010. Trace Element Immobilization in Soil Using Amendments. In *Trace Elements*

in Soils, Hooda P (ed.).Wiley: Chichester; 353–379.

Kunkle SH. 1972. effects of road salt on a vermont stream. *American Water Works Association*: 290–295

Labadia C, Buttle J. 1996. Road salt accumulation in highway snow banks and transport through the unsaturated zone of the Oak Ridges Moraine, southern Ontario. *Hydrological Processes* **10**: 1575–1589

Lagerwerff J, Specht A. 1970. Contamination of roadside soil and vegetation with cadmium, nickel, lead, and zinc. *Environmental Science & Technology* **4** (7): 583–586 DOI: 10.1021/es60042a001

Lake D, Ames N. 1857. *Map of Westmoreland County Pennsylvania*. William J. Barker: North Hector, New York.

Larssen T, Carmichael G. 2000. Acid rain and acidification in China: the importance of base cation deposition. *Environmental Pollution* **110** (1): 89–102

Lawrence GB, Sutherland JW, Boylen CW, Nierzwicki-Bauer SW, Momen B, Baldigo BP, Simonin HA. 2007. Acid rain effects on aluminum mobilization clarified by inclusion of strong organic acids. *Environmental Science & Technology* **41** (1): 93–8

Leighton H. 1927. *The Geology of Pittsburgh and its Environs: A Popular Account of the General Geological Features of the Region* (WJ Holland, ed.). Carnegie Institute Press: Pittsburgh, PA.

Lerner DN. 1986. Leaking Pipes Recharge Ground Water. *Groundwater* **24** (5): 654–662 DOI: 10.1111/j.1745-6584.1986.tb03714.x

Likens GE, Driscoll CT, Buso D. 1996. Long-term effects of acid rain: response and recovery of a forest ecosystem. *Science-AAAS-Weekly Paper Edition* **272**: 244–246

Los Angeles County GIS Data Portal. 2012. 2011 LA County Street Centerline & Address File Available at: http://egis3.lacounty.gov/dataportal/2011/12/09/2011-la-county-street-centerline-street-address-file/

Lowenthal DH, Zielinska B, Chow JC, Watson JG, Gautam M, Ferguson DH, Neuroth GR, Stevens KD. 1994. Characterization of Heavy-Duty Diesel Vehicle Emissions. *Atmospheric Environment* **28** (4): 731–743

Macdonald GM, Beukens RP, Kieser WE, Kitt DH. 1987. Comparative radiocarbon dating of terrestrial plant macrofossils and aquatic moss from the ' ice-free corridor' of western Canada. *Geology* **15** (9): 837–840 DOI: 10.1130/0091-7613(1987)15<837:CRDOTP>2.0.CO;2

Mahler BJ, Van Metre PC, Callender E. 2006. Trends in metals in urban and reference lake sediments across the United States, 1970 to 2001. *Environmental Toxicology and Chemistry* **25** (7): 1698–709

Mahowald N, Jickells TD, Baker AR, Artaxo P, Benitez-Nelson CR, Bergametti G, Bond TC, Chen Y, Cohen DD, Herut B, et al. 2008. Global distribution of atmospheric phosphorus sources, concentrations and deposition rates, and anthropogenic impacts. *Global Biogeochemical Cycles* **22** (4) DOI: 10.1029/2008GB003240

Mance G. 1987. *pollution threat of heavy metals in aquatic environments*.

Mason C, Norton S, Fernandez IJ, Katz L. 1999. Deconstruction of the chemical effects of road salt on stream water chemistry. *Journal of Environmental Quality* **28** (1): 82–91

Mattielli N, Petit JCJ, Deboudt K, Flament P, Perdrix E, Taillez A, Rimetz-Planchon J, Weis D. 2009. Zn isotope study of atmospheric emissions and dry depositions within a 5 km radius of a Pb-Zn refinery. *Atmospheric Environment* **43** (6): 1265–1272 DOI: 10.1016/j.atmosenv.2008.11.030

McDonald RA. 2009. Zinc Dithiophosphates. In *Lubricant Additives: Chemistry and Applications*, Rudnick LR (ed.).CRC Press; 29–43.

McElwaine AS. 2005. Slag in the Park. In *Devastation and Renewal: An Environmental History of Pittsburgh and Its Region*, Tarr JA (ed.).University of Pittsburgh Press: Pittsburgh, PA; 174–192.

McFee W, Kelly J, Beck R. 1977. Acid precipitation effects on soil pH and base saturation of exchange sites. *Water, Air, and Soil Pollution* **7** (3): 401–408

McPherson EG, Simpson JR, Xiao Q, Wu C. 2011. Million trees Los Angeles canopy cover and benefit assessment. *Landscape and Urban Planning* **99** (1): 40–50 DOI: 10.1016/j.landurbplan.2010.08.011

Meixner T, Fenn ME, Wohlgemuth P, Oxford M, Riggan PJ. 2006. N Saturation Symptoms in Chaparral Catchments Are Not Reversed by Prescribed Fire. *Environmental Science & Technology* **40** (9): 2887–2894

Metropolitan Transportation Commission. 2004. California Coast Available at: http://atlas.ca.gov/download.html#/casil/oceans

Metson GS, Hale RL, Iwaniec DM, Cook EM, Corman JR, Galletti CS, Childers DL. 2012. Phosphorus in Phoenix: A budget and spatial representation of phosphorus in an urban ecosystem. *Ecological Applications* **22** (2): 705–721 DOI: 10.1890/11-0865.1

Mielke HW, Gonzales CR, Smith M, Mielke PW. 1999. The urban environment and children's health: soils as an integrator of lead, zinc, and cadmium in New Orleans, Louisiana, USA.

Environmental Research **81** (2): 117–129

Mielke HW, Gonzales CR, Smith MK, Mielke PW. 2000. Quantities and associations of lead, zinc, cadmium, manganese, chromium, nickel, vanadium, and copper in fresh Mississippi delta alluvium and New Orleans alluvial soils. *The Science of the Total Environment* **246** (2–3): 249–59

Mielke HW, Laidlaw MA, Gonzales CR. 2010. Lead (Pb) legacy from vehicle traffic in eight California urbanized areas: Continuing influence of lead dust on children's health. *Science of the Total Environment* **408** (19): 3965–3975 DOI: 10.1016/j.scitotenv.2010.05.017

Miller AJ, Schuur EA, Chadwick O. 2001. Redox control of phosphorus pools in Hawaiian montane forest soils. *Geoderma* **102** (3): 219–237 DOI: 10.1016/S0016-7061(01)00016-7

Muller EK, Tarr JA. 2005. The Interaction of Natural and Built Environments in the Pittsburgh Landscape. In *Devastation and Renewal: An Environmental History of Pittsburgh and Its Region*, Tarr JA (ed.).University of Pittsburgh Press: Pittsburgh, PA; 11–40.

Muschack W. 1990. Pollution of street run-off by traffic and local conditions. *Science of the Total Environment* **93**: 419–431

Nabulo G, Oryem-Origa H, Diamond M. 2006. Assessment of lead, cadmium, and zinc contamination of roadside soils, surface films, and vegetables in Kampala City, Uganda. *Environmental Research* **101** (1): 42–52 DOI: 10.1016/j.envres.2005.12.016

National Cooperative Soil Characterization Database. 2012. No Title Available at: http://ssldata.nrcs.usda.gov/

National Weather Service. 2014. Pittsburgh Historical Snowfall Totals 1883 to Current Available at: http://www.erh.noaa.gov/pbz/thissnow.htm [Accessed 20 June 2015]

Navrátil T. 2000. Beryllium in Waters of Czech Forested Ecosystems and the Release of Beryllium from Granites. *Geolines* **12**: 18–40

Newbury RL, Belz DJ, Grubb RG. 1981. *Soil Survey of Allegheny County, Pennsylvania*. United States Department of Agriculture Soil Conservation Service.

Nicholls MA, Do T, Norton PR, Kasrai M, Bancroft GM. 2005. Review of the lubrication of metallic surfaces by zinc dialkyl-dithiophosphates. *Tribology International* **38** (1): 15–39 DOI: 10.1016/j.triboint.2004.05.009

NOAA National Climatic Data Center. 2014. Quality Controlled Local Climatological Data Available at: https://www.ncdc.noaa.gov/data-access/land-based-station-data/land-based-datasets/quality-controlled-local-climatological-data-qclcd [Accessed 5 June 2015]

Norrström AC, Bergstedt E. 2001. The impact of road de-icing salts (NaCl) on colloid dispersion

and base cation pools in roadside soils. *Water, Air, and Soil Pollution* **127** (1): 281–299

Nriagu JO. 2001. Arsenic Poisoning Through the Ages. In *Environmental Chemistry of Arsenic*, Frankenberger Jr WT (ed.).CRC Press: New York; 1–26.

Nriagu JO, Pacyna JM. 1988. Quantitative assessment of worldwide contamination of air, water and soils by trace metals. *Nature* **333** (6169): 134–139

Nriagu JO, Blankson ML, Ocran K. 1996. Childhood lead poisoning in Africa: a growing public health problem. *The Science of the Total Environment* **181** (2): 93–100

Ntziachristos L, Boulter P. 2003. Road vehicle tyre and brake wear Road surface wear. *Joint EMEP/CORINAIR Emission Inventory Guidebook* **B770** (1)

OEHHA. 2010. Risk Assessment - Soil and Soil Gas Available at: http://oehha.ca.gov/risk/chhsltable.html [Accessed 26 April 2016]

Ondov JM, Ragaini RC, Biermann AH. 1979. Elemental emissions from a coal-fired power plant. Comparison of venturi wet scrubber system with a cold-side electrostatic precipitator. *Environmental Science and Technology* **13** (5): 598–607 DOI: 10.1021/es60153a009

ONeill B, Bain DJ, Divers MT, Elliott EM. 2013. Identifying Slag Water Contributions to an Urban Stream. *American Geophysical Union Annual Fall Meeting Abstracts* **H21J–1201**: 1201

Onset. 2014. Soil Moisture Smart Sensor (S-SMx-M005) Manual

Ostendorf DW, Peeling DC, Mitchell TJ, Pollock SJ. 2001. Chloride persistence in a deiced access road drainage system. *Journal of Environmental Quality* **30** (5): 1756–1770 DOI: 10.2134/jeq2001.3051756x

Pacyna JM, Pacyna EG. 2001. An assessment of global and regional emissions of trace metals to the atmosphere from anthropogenic sources worldwide. *Environmental Reviews* **9** (4): 269–298 DOI: 10.1139/er-9-4-269

Page A, Ganje T. 1970. Accumulations of lead in soils for regions of high and low motor vehicle traffic density. *Environmental Science & Technology* **4** (2): 140–142

Pagotto C, Rémy N, Legret M, Le Cloirec P. 2001. Heavy metal pollution of road dust and roadside soil near a major rural highway. *Environmental Technology* **22** (3): 307–19 DOI: 10.1080/09593332208618280

Palmer CA, Oman CL, Park AJ, Luppens JA. 2015. The U.S. Geological Survey Coal Quality (COALQUAL) Database Version 3.0. *United States Geological Survey Data Series* **975**: 1–43 DOI: http://dx.doi.org/10.3133/ ds975

Palmer T, Räisänen J. 2002. Quantifying the risk of extreme seasonal precipitation events in a

changing climate. *Nature* **415** (6871): 512–514

PAMAP Program PA Department of Conservation and Natural Resources Bureau of Topographic and Geologic Survey. 2006. PAMAP Program 3.2 ft Digital Elevation Model of Pennsylvania Available at: http://www.pasda.psu.edu

Papadakis VG, Fardis MN, Vayenas CG. 1992. Effect of composition, environmental factors and cement-lime mortar coating on concrete carbonation. *Materials and Structures* **25** (5): 293–304 DOI: 10.1007/BF02472670

Parfitt R. 1989. Phosphate reactions with natural allophane, ferrihydrite and goethite. *Journal of Soil Science* **40** (2): 359–369

PennDOT. 2014. PennDOT Maintenance Stockpiles Honored for Salt Management, Storage

Pennsylvania. Dept. of Highways United States. Bureau of Public Roads. 1953. Report on the Penn-Lincoln Parkway

Pennsylvania Department of Environmental Protection. 2016. AML Polygons Feature Available at: http://www.pasda.psu.edu/uci/MetadataDisplay.aspx?entry=PASDA&file=AMLInventoryPolys2016_01.xml&dataset=459 [Accessed 15 October 2015]

Pennsylvania Department of Transportation, Bureau of Planning and Research GID. 2015. PennDOT - Pennsylvania Stateroads Available at: http://www.pasda.psu.edu [Accessed 25 August 2015]

Pennsylvania Department of Transportation Bureau of Planning and Research Geographic Information Division. 2016. PennDOT - Pennsylvania Traffic Counts Available at: http://www.pasda.psu.edu/uci/MetadataDisplay.aspx?entry=PASDA&file=PaTraffic2013_02.xml&dataset=56

Peñuelas J, Poulter B, Sardans J, Ciais P, van der Velde M, Bopp L, Boucher O, Godderis Y, Hinsinger P, Llusia J, et al. 2013. Human-induced nitrogen-phosphorus imbalances alter natural and managed ecosystems across the globe. *Nature communications* **4**: 2934 DOI: 10.1038/ncomms3934

Perakis SS, Sinkhorn ER, Catricala CE, Bullen TD, Fitzpatrick JA, Hynicka JD, Cromack K. 2013. Forest calcium depletion and biotic retention along a soil nitrogen gradient. *Ecological Applications* **23** (8): 1947–1961 DOI: 10.1890/12-2204.1

Pierson WR, Brachaczek WW. 1982. Particulate Matter Associated with Vehicles on the Road. II. *Aerosol Science and Technology* **2** (1): 1–40 DOI: 10.1080/02786828308958610

Piwinskii A. 1968. Experimental studies of igneous rock series central Sierra Nevada batholith, California. *The Journal of Geology* **76** (5): 548–570

Pizzuto JE. 2014. Long-term storage and transport length scale of fine sediment: Analysis of a mercury release into a river. *Geophysical Research Letters* **41** (16): 5875–5882 DOI: 10.1002/2014GL060722

Plantz PE. 2009. Self-paced Tutorial for Microtrac FLEX Software (Stepwise Approach to Learning and Understanding how to Use FLEX). *SL-AN-15 Rev C*

Powers SM, Bruulsema TW, Burt TP, Chan NI, Elser JJ, Haygarth PM, Howden NJK, Jarvie HP, Lyu Y, Peterson HM, et al. 2016. Long-term accumulation and transport of anthropogenic phosphorus in three river basins. *Nature Geoscience* (April): 1–5 DOI: 10.1038/ngeo2693

PRISM Climate Group Oregon State University. 2004a. 1971-2000 Normals Available at: http://prism.oregonstate.edu

PRISM Climate Group Oregon State University. 2004b. 1981-2010 Normals

Que Hee SS. 1994. Availability of elements in leaded/unleaded automobile exhausts, a leaded paint, a soil, and some mixtures. *Archives of Environmental Contamination and Toxicology* **27** (2): 145–153 DOI: 10.1007/BF00214256

Rabinowitz MB. 2005. Lead isotopes in soils near five historic American lead smelters and refineries. *The Science of the Total Environment* **346** (1–3): 138–48 DOI: 10.1016/j.scitotenv.2004.11.021

R Core Team. 2016. R: A language and environment for statistical computing.

Redling K, Elliott EM, Bain DJ, Sherwell J. 2013. Highway contributions to reactive nitrogen deposition: tracing the fate of vehicular NOx using stable isotopes and plant biomonitors. *Biogeochemistry* **116** (1–3): 261–274 DOI: 10.1007/s10533-013-9857-x

Reimer P, Bard E, Bayliss A. 2013. IntCal13 and Marine13 radiocarbon age calibration curves 0-50,000 years cal BP

Reinke G, Glidden S. 2010. Analytical Procedures for Determining Phosphorus Content in Asphalt Binders and Impact of Aggregate on Quantitative Recovery of Phosphorus from Asphalt Binders. *Journal of the Association of Asphalt Paving Technologists* **79**: 695–718

Reuss JO. 1977. Chemical and biological relationships relevant to the effect of acid rainfall on the soil-plant system. *Water, Air, and Soil Pollution* **7** (4): 461–478 DOI: 10.1007/BF00285545

Reynolds TS. 2002. *Stronger than a hundred men: a history of the vertical water wheel*. Johns Hopkins University Press: Baltimore, Maryland.

Rhoades EL, O'Neal MA, Pizzuto JE. 2009. Quantifying bank erosion on the South River from 1937 to 2005, and its importance in assessing Hg contamination. *Applied Geography* **29**

(1): 125–134 DOI: 10.1016/j.apgeog.2008.08.005

Riverside County Transportation & Land Management Agency. 2012. County Wide Active GIS Data Available at: http://www.rctlma.org/gisstore/p-39-county-wide-active-gis-data.aspx

Rodgers P, Soulsby C, Petry J, Malcolm I, Gibbins C, Dunn S. 2004. Groundwater-surface-water interactions in a braided river: A tracer-based assessment. *Hydrological Processes* **18** (7): 1315–1332 DOI: 10.1002/hyp.1404

Romero FM, Prol-Ledesma RM, Canet C, Alvares LN, P??rez-V??zquez R. 2010. Acid drainage at the inactive Santa Lucia mine, western Cuba: Natural attenuation of arsenic, barium and lead, and geochemical behavior of rare earth elements. *Applied Geochemistry* **25** (5): 716–727 DOI: 10.1016/j.apgeochem.2010.02.004

Rossi RJ, Bain DJ, Elliott EM, Divers MT, ONeill B. 2016. Hillslope Soil Water Flowpaths and the Dynamics of Roadside Soil Cation Pools Influenced by Road Deicers. *Hydrological Processes*

Rossi RJ, Bain DJ, Jenerette GD, Clarke LW, Wilson K. 2015. Responses of Roadside Soil Cation Pools to Vehicular Emission Deposition in Southern California. *Biogeochemistry* **124** (1): 131–144

Runge-Metzger A. 1995. Closing the cycle: obstacles to efficient P management for improved global food security. *Scope-Scientific Committee on Problems of the Environment International Council of Scientific Unions* **54**: 27–42

Russell MC. 2015. The Impact of Three Recent Coal-fired Power Plant Closings on Pittsburgh Air Quality: A Natural Experiment.Emory University.

Ryan P. 2014. *Environmental and low temperature geochemistry*. John Wiley & Sons: West Sussex.

Sadler R, Olszowy H, Shaw G, Biltoft R, Connell D. 1994. Soil and water contamination by arsenic from a Tannery Waste. *Water Air and Soil Pollution* **78** (1–2): 189–198

Schaberg PG, DeHayes DH, Hawley GJ, Murakami PF, Strimbeck GR, McNulty SG. 2002. Effects of chronic N fertilization on foliar membranes, cold tolerance, and carbon storage in montane red spruce. *Canadian Journal of Forest Research* **32** (8): 1351–1359 DOI: 10.1139/x02-059

Schnurrenberger D, Russell J, Kelts K. 2003. Classification of lacustrine sediments based on sedimentary components. *Journal of Paleolimnology* **29** (2): 141–154

Schrenk HH, Heimann H, Clayton GD, Gafafer WM, Wexler H. 1949. Air Pollution in Donora, Pa. Epidemiology of the Unusual Smog Episode of October 1948. Preliminary Report. In *Public Health Bulletin*1–173.

Schwartz J, Pitcher H, Levin R, Ostro B, Nichols AL. 1985. Costs and benefits of reducing lead in gasoline: final regulatory impact analysis. *Office of Policy Analysis* **EPA**-**230**-**05**

Seto KC, Fragkias M, Güneralp B, Reilly MK. 2011. A meta-analysis of global urban land expansion. *PloS one* **6** (8): e23777 DOI: 10.1371/ journal.pone.0023777

Shacklette HT, Boerngen JG. 1984. Element Concentrations in Soils and Other Surficial Materials of the Conterminous United States. *United States Geological Survey Professional Paper* **1270**: 1–105

Shanley JB. 1994. Effects of Ion Exchange on Stream Solute Fluxes in a Basin Receiving Highway Deicing Salts. *Journal of Environment Quality* **23** (5): 977 DOI: 10.2134/jeq1994.00472425002300050019x

Sharpley A, Jarvie HP, Buda A, May L, Spears B, Kleinman P. 2014. Phosphorus Legacy: Overcoming the Effects of Past Management Practices to Mitigate Future Water Quality Impairment. *Journal of Environmental Quality* **42** (5): 1308–1326 DOI: 10.2134/jeq2013.03.0098

Sharpley AN, Smith S, Jones O, Berg W, Coleman G. 1992. The transport of bioavailable phosphorus in agricultural runoff. *Journal of Environmental Quaity* **21** (1): 30–35

Shortle WC, Bauch J. 1986. Wood characteristics of Abies balsamea in the New England states compared to Abies alba from sites in Europe with decline problems. *IAWA Journal* **7** (4): 375–387

Shortle WC, Smith KT. 1988. Aluminum-induced calcium deficiency syndrome in declining red spruce. *Science* **240** (4855): 1017–1021 DOI: 10.1126/science.240.4855.1017

Siebenthal CE. 1915. Origin of the zinc and lead deposits of the Joplin region. *United States Geological Survey Bulletin* **606**: 1–283

Singh M, Jaques P a., Sioutas C. 2002. Size distribution and diurnal characteristics of particle-bound metals in source and receptor sites of the Los Angeles Basin. *Atmospheric Environment* **36** (10): 1675–1689 DOI: 10.1016/S1352-2310(02)00166-8

Smil V. 2000. Phosphorus in the environment: Natural flows and human interferences. *Annual Review of Energy and the Environment* **25** (1): 53–88 DOI: 10.1146/annurev.energy.25.1.53

Smith G, Moyer R. 1949. Cadmium recovery practice at the Donora zinc works. *Transactions of the American Institute of Mining and Metallurgical Engineers* **185** (6): 360–363

Smith V. 1998. Cultural eutrophication of inland, estuarine, and coastal waters. In *Successes, Limitations, and Frontiers in Ecosystem Science*Springer: New York; 7–49.

Snyder LP. 1994. 'The Death-Dealing Smog over Donora, Pennsylvania': Industrial Air Pollution,

Public Health Policy, and the Politics of Expertise, 1948-1949. *Environmental History Review* **18** (1): 117–139

Soil Survey Staff, Natural Resources Conservation Service, United States Department of Agriculture. 2013. Web Soil Survey Available at: http://websoilsurvey.nrcs.usda.gov/ [Accessed 1 June 2016]

Spencer MT, Shields LG, Sodeman D a., Toner SM, Prather K a. 2006. Comparison of oil and fuel particle chemical signatures with particle emissions from heavy and light duty vehicles. *Atmospheric Environment* **40** (27): 5224–5235 DOI: 10.1016/j.atmosenv.2006.04.011

Spikes H. 2004. The history and mechanisms of ZDDP. *Tribology Letters* **17** (3): 469–489 DOI: 10.1023/B:TRIL.0000044495.26882.b5

Spliethoff HM, Hemond HF. 1996. History of toxic metal discharge to surface waters of the Aberjona Watershed. *Environmental Science & Technology* **30** (1): 121–128

Steding DJ, Dunlap CE, Flegal AR. 2000. New isotopic evidence for chronic lead contamination in the San Francisco Bay estuary system: implications for the persistence of past industrial lead emissions in the biosphere. *Proceedings of the National Academy of Sciences of the United States of America* **97** (21): 11181–11186 DOI: 10.1073/pnas.180125697

Stoddard JL, Van Sickle J, Herlihy AT, Brahney J, Paulsen S, Peck D V., Mitchell R, Pollard AI. 2016. Continental-Scale Increase in Lake and Stream Phosphorus: Are Oligotrophic Systems Disappearing in the United States? *Environmental Science and Technology* **50** (7): 3409–3415 DOI: 10.1021/acs.est.5b05950

Strzyszcz Z, Magiera T, Heller F. 1996. The influence of industrial immissions on the magnetic susceptibility of soils in upper Silesia. *Studia Geophysica et Geodaetica* **40** (3): 276–286

Swank W. 1986. Biological control of solute losses from forest ecosystems. *Solute processes*

Swanson SM, Engle M a., Ruppert LF, Affolter RH, Jones KB. 2013. Partitioning of selected trace elements in coal combustion products from two coal-burning power plants in the united states. *International Journal of Coal Geology* **113**: 116–126 DOI: 10.1016/j.coal.2012.08.010

Tao F, Jiantong L, Bangding X, Xiaoguo C, Xiaoqing X. 2005. Mobilization potential of heavy metals: A comparison between river and lake sediments. *Water, Air, and Soil Pollution* **161** (1–4): 209–225 DOI: 10.1007/s11270-005-4284-9

The Office of the Pennsylvania State Climatologist. 2007. Washington County Airport Wind Rose Available at: http://climate.psu.edu/features/wind_roses/AFJwindrose.php [Accessed 29 October 2015]

Three Rivers Wet Weather. 2014. Historical Rain Gauge Data Available at:

http://web.3riverswetweather.org/trp:Main.hist_html;trp:

Törnqvist TE, de Jong AF, Oosterbaan WA, Van der Borg K. 1992. Accurate dating of organic deposits by AMS 14C measurement of macrofossils. *Radiocarbon* **34** (3): 566–577

Turekian K, Wedepohl K. 1961. Distribution of the elements in some major units of the Earth's crust. *Geological Society of America Bulletin* **72** (2): 175–192

Uchida T, Asano Y, Ohte N, Mizuyama T. 2003. Seepage area and rate of bedrock groundwater discharge at a granitic unchanneled hillslope. *Water Resources Research* **39** (1): 1–12 DOI: 10.1029/2002WR001298

Uhlenbrook S, Leibundgut C, Maloszewski P. 2000. Natural tracers for investigating residence times, runoff components and validation of a rainfall-runoff model. *IAHS Publication(International Association of Hydrological Sciences)* (262): 465–471

Ulrich B, Mayer R, Khanna P. 1980. Chemical changes due to acid precipitation in a loess-derived soil in central Europe. *Soil Science* **130** (4): 193–199

United Nations. 2014. World Urbanization Prospects: The 2014 Revision, Highlights. *Department of Economic and Social Affairs, Population Division* **ST/ESA/SER** (352)

United States Central Intellegence Agency. 2014. The World Factbook: Country Comparison: Roadways Available at: https://www.cia.gov/library/publications/the-world-factbook/rankorder/2085rank.html# [Accessed 23 June 2016]

United States Energy Information Administration. Power Plant Report. *Form EIA* **906**

United States Energy Information Administration. 2014. Annual Electric Generator Report. *Form EIA* **860**

United States Environmental Protection Agency. 1990. Clean Air Act Amendments of 1990. In *1st Congress (1989−1990)*United States Environmental Protection Agency: Washington, DC.

United States Environmental Protection Agency. 2002. Emission Inventory for 2002 Available at: https://www.epa.gov/air-emissions-inventories

United States Environmental Protection Agency Office of Transportation and Air Quality. 2008a. Average Annual Emissions and Fuel Consumption for Gasoline-Fueled Passenger Cars and Light Trucks. *EPA420* **F**-**08** (024): 1–6

United States Environmental Protection Agency Office of Transportation and Air Quality. 2008b. Average In-Use Emissions from Heavy-Duty Trucks. *EPA420* **F**-**08** (027): 1–6 DOI: EPA-420-F-08-027

United States Geologic Survey. 1954. Smithton Quadrangle, Pennsylvania. In *7.5 Minute Series*United States Department of the Interior, USGS: Reston, VA.

United States Steel Corporation. 1933. Thirty-First Annual Report of the United States Steel Corporation for the Fiscal Year Ended December 31, 1932

United States Steel Corporation. 1935. Thirty-Third Annual Report of the United States Steel Corporation for the Fiscal Year Ended December 31, 1934

United States Steel Corporation. 1937. Thirty-Fifth Annual Report of the United States Steel Corporation for the Fiscal Year Ended December 31, 1936

United States Steel Corporation. 1939. Thirty-Seventh Annual Report of the United States Steel Corporation for the Fiscal Year Ended December 31, 1938

Uunk E. 1991. Eutrophication of surface waters and the contribution of agriculture. In *Proceedings of the Fertilizer Society*Peterborough, United Kingdom; 56.

Vermillion B, Brugam R, Retzlaff W, Bala I. 2005. The sedimentary record of environmental lead contamination at St. Louis, Missouri (USA) area smelters. *Journal of Paleolimnology* **33** (2): 189–203 DOI: 10.1007/s10933-004-4078-x

Veselý J, Beneš P, Ševčí K. 1989. Occurrence and speciation of beryllium in acidified freshwaters. *Water Research* **23** (6): 711–717

Vighi M, Chiaudani G. 1987. *Eutrophication in Europe: the role of agricultural activities*.

Vossen P. 2006. Changing pH in Soil. *University of California Cooperative Extension* **11**: 1–2

Wang R, Balkanski Y, Boucher O, Ciais P, Peñuelas J, Tao S. 2015. Significant contribution of combustion-related emissions to the atmospheric phosphorus budget. *Nature Geoscience* **8** (January): 48–54 DOI: 10.1038/ngeo2324

Ward J, O'Connor K, Wei-Bin G. 1990. Phosphorus losses through transfer, runoff and soil erosion. In *Phosphorus Requirements for Sustainable Agriculture in Asia and Oceania*International Rice Research Institute: Manila, Philippines; 167–183.

Warren K. 1987. *The American Steel Industry, 1850-1970: A Geographical Interpretation*. University of Pittsburgh Press: Pittsburgh, PA.

Watson JG, Chow JC, Lowenthal DH, Pritchett LC, Frazier CA, Neuroth GR, Robbins R. 1994. Differences in the carbon composition of source profiles for diesel- and gasoline-powered vehicles. *Atmospheric Environment* **28** (15): 2493–2505 DOI: 10.1016/1352-2310(94)90400-6

Wilcock R. 1986. Agricultural run-off: a source of water pollution in New Zealand? *New Zealand*

Journal of Agricultural Science **20**: 98–103

Wilson JJ. 1962. *History of Sewickley Township*. Herminie, PA: Herminie, PA.

Wilson JM, VanBriesen JM. 2012. Oil and gas produced water management and surface drinking water sources in Pennsylvania. *Environmental Practice* **14** (4): 288–300

Xiao Q, McPherson EG, Ustin SL, Grismer ME, Simpson JR. 2000. Winter rainfall interception by two mature open-grown trees in Davis, California. *Hydrological Processes* **14** (4): 763–784 DOI: 10.1002/(SICI)1099-1085(200003)14:4<763::AID-HYP971>3.0.CO;2-7

Yun S, Choi B, Lee P. 2000. Distribution of heavy metals (Cr, Cu, Zn, Pb, Cd, As) in roadside sediments, Seoul Metropolitan City, Korea. *Environmental Technology* **21** (9): 37–41

Zhu Q, Nie X, Zhou X, Liao K, Li H. 2014. Soil moisture response to rainfall at different topographic positions along a mixed land-use hillslope. *Catena* **119**: 61–70 DOI: 10.1016/j.catena.2014.03.010